University of Technology, Graz

Geocentre Graz

Tectonics of the southeastern Bohemian Massif in Austria

by

Marlene Löberbauer

Submitted for the degree of

Master of Science

Supervisor

Ao.Univ.-Prof. Dr.phil. Harald Fritz

Graz, January 2017

EIDESSTATTLICHE ERKLÄRUNG

3

Ich erkläre an Eides statt, dass ich die vorliegende Arbeit selbständig verfasst, andere als die angegebenen Quellen/Hilfsmittel nicht benutzt, und die den benutzten Quellen wörtlich und inhaltlich entnommenen Stellen als solche kenntlich gemacht habe.

Graz, am……………………….   ……………………………………..

                                                          (Unterschrift)

STATUARY DECLARATION

I declare that I have authored this thesis independently, that I have not used other than the declared sources / resources, and that I have explicitly marked all material which has been quoted either literally or by content from the used sources.

Graz, ……………………………   ……………………………………..

              date   (signature)

Danksagung

Abstract

Investigations on structural geology as well as petrographic mineralogy were applied on the Moldanubian unit in the southeastern Bohemian Massif (Lower Austria) which represents an ancient orogenic root system. The Moldanubian unit is distinguished from tectonic hanging wall to footwall into the high-grade Gföhl Unit including the Raabs Serie at its bottom, the middle to high-grade Drosendorf Unit and the lower-grade Ostrong Unit. Detailed studies on the kinematic and rheology of the exposed Drosendorf Unit and the Gföhl Unit with the Raabs Serie were performed. The Drosendorf Unit is a continental terrane including metasedimentary units, the Raabs Serie is characterised by oceanic affinity and the granulites of the Gföhl Unit are derived from metamorphosed calc-alkaline magmatites, likely originated from island arcs.

Based on the results gathered by lattice preferred orientation studies performed on quartz, rheology observations and the occurrences of specific metamorphic mineral assemblages, three (maybe four) different metamorphic events can be concluded. The first metamorphic event is a granulite-facies deformation which influenced only the future granulites sampled from the Blumau Granulite Complex as well as from the Karlstein Schuppe. The second HT-metamorphic event is observed in the Drosendorf Unit, the Raabs Serie as well as the Gföhl Unit. The last LT-event caused retrograde mineral alterations and multiple shear senses with strike slip character.

Top-to-the NE flow at higher amphibolite facies conditions and lower grade deformation at tectonic boundaries are exhibited in the Drosendorf Unit. The Raabs Serie displays an overall top-to-the NE transport coeval to migmatisation overprinted by localized N-S strike slip zones. The granulites of the Blumau Granulite Complex are characterized by W-E coaxial flow with N-S internal folds. Gained data suggest that the different tectonic units took their current position comparably late in the Variscan history during flow along of localized mylonite zones and other young shear zones.

Key words: Moldanubian unit, Structural Geology, Kinematic, LPO

Zusammenfassung

Strukturgeologische und mineralogische Untersuchungen wurden in der moldanubischen Zone der südöstlichen Böhmischen Masse ausgeführt. Die moldanubische Einheit wird vom Hangenden bis zum Liegenden in die hochgradig metamorphe Gföhl Einheit (mit der Raabs Serie als Basis), in die hoch-bis mittelgradige Drosendorf Einheit und in die niedriggradige Ostrong Einheit gegliedert. Detaillierte kinematische und rheologische Untersuchungen der aufgeschlossenen Drosendorf Einheit und der Gföhl Einheit mit der Raabs Serie wurden unternommen. Die Drosendorf Einheit ist ein kontinentales Terrain mit metasedimentären Einheiten, die Raabs Serie charakterisiert sich durch ozeanischen Chemismus und die Granulite der Gföhl Einheit stammen von metamorphen kalk-alkalinen Magmatiten ab, welche sich in Inselbögen entwickelten.

Drei (vielleicht vier) metamorphe Ereignisse wurden basierend auf Resultaten, welche durch LPO – Studien von Quarzen, rheologische Untersuchungen sowie durch das Auftreten bestimmter metamorphen Mineralverbindungen gewonnen wurden, definiert. Das erste metamorphe Event besteht aus einer Granulite-faziellen Deformation, welche die zukünftigen Granulite, die in dem Blumau Granulite Complex und in der Karlstein Schuppe gesammelt wurden, überprägte. Das zweite HT-metamorphe Ereignis wurde in der Drosendorf Einheit, der Raabs Serie und in der Gföhl Einheit beobachtet. Die letzte LT-Metamorphose verursachte retrograde Mineralumwandlungen und viele Strike-slip Scherzonen.

Top-to-the NE flow unter höher-amphibolite-faziellen Bedingungen und niedriggradige Deformation wirkend an tektonischen Grenzen ist in der Drosendorf Einheit ersichtlich. Die Raabs Serie zeigt generell top-to-the NE Transport mit Migmatisierungen, welche durch vereinzelte Strike-slip Scherzonen überprägt sind. Die Granulite des Blumau Granulite Complex sind charakterisiert durch W-E coaxial flow mit N-S gerichteten internen Falten. Die in der Masterarbeit herausgefundenen Ergebnisse lassen vermuten, dass die tektonischen Decken ihre heutige Lage spät in der variszischen Entwicklung eingenommen haben. Diese Verlagerungen der Decken passierten vermutlich entlang von mylonitischen Zonen und anderen jüngeren Scherzonen.

Stichwörter: Moldanubische Einheit, Strukturgeologie, Kinematik, LPO

Table of content

List of figures

Introduction

As fascinating as young and living orogens are, they do have some disadvantages, especially if someone is interested in the heart of a mountain system. Despite the heavily erosion and the lack of fresh outcrops only old orogens give geologists the possibility to investigate the root of orogens.

The Bohemian Massif is a part of the European remnant of the vast and ancient Variscan orogen which stretched for several thousands of kilometres and sewed Gondwana as well as Laurussia together to one supercontinent called Pangea during the late Palaeozoic. After years of erosion the orogenic root system of the Bohemian Massif has been uncovered. Interactions of mantle and crust are unrevealed and now help to understand the development of massive orogens (Babuška and Plomerová, 2013).

The Moldanubian unit of the Bohemian Massif in particular, represents the crystalline heart of a fossil orogen. Past HP – geologic events which happened in the middle of lower crust can now be seen on the surface. However, many lithological contacts have disappeared during the emplacement of syn- to post collisional plutonic intrusions like the CBP (Central Bohemian Pluton) or the SBP (South Bohemian Pluton). The evolution of the Bohemian Massif was not a simple one, but has endured multiple deformation events. To unravel the different metamorphic events, a lot of petrological and new geochronological studies have been executed (e.g. Petrakakis, 1997; Friedl et al., 2004; Faryad et al., 2010; and more). In comparison to those geological investigations little has been done in a structural geological point of view.

The writer of this thesis wants to summarize the structural and kinematic features of the rocks found in the SE-Bohemian Massif. Maybe with these results new insights into the tectonic evolution of the Bohemian Massif can be gained.

Field excursions were executed in spring and autumn 2015. During fieldwork a geological profile from east to west was developed.

1. Geographical overview

The field area of this master thesis lies in the northern part of Lower Austria ("Waldviertel") between the villages Eibenstein (in the east) and Karlstein an der Thaya (in the west; figure 1). Most of the rock samples and structural studies applied on outcrops were executed and collected near to rivers, like the Thaya, because of the bad outcrop situation in the smoothly hilled "Waldviertel". The field area can be summarized in a rectangle reaching from the village Drosendorf in the east to the village Karlstein an der Thaya in the west, and about 7km north and south of the river Thaya.

From a geological point of view, the field area lies in the Moldanubian Unit of the SE-Bohemian Massif near the contact zone to the Moravo-Silesian Unit of the Brunia domain.
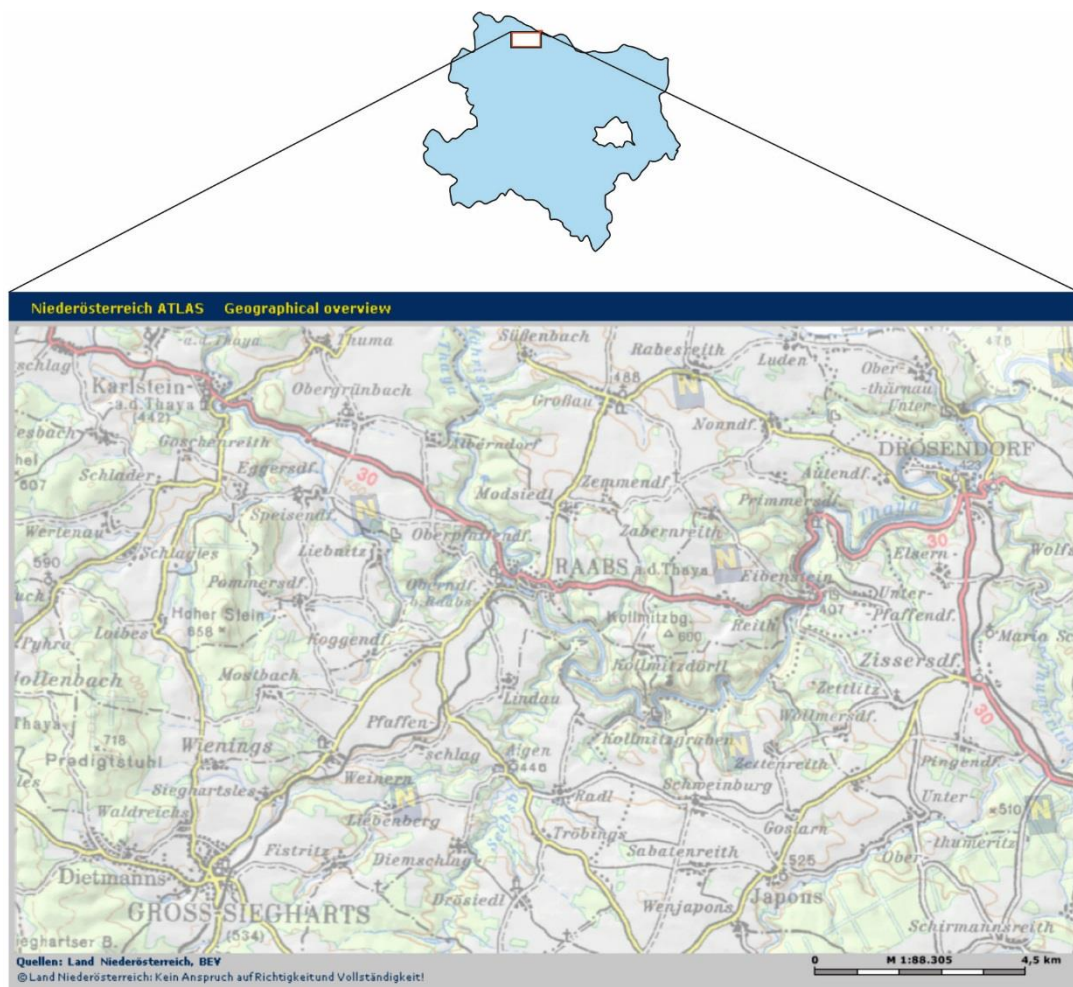
Figure 1 Geographical overview of the field area of the master thesis. (Land Niederösterreich, BEV, downloaded on the 21th November, 2016; © Land Niederösterreich)

2. Geological background

According to Kossmat (1927) the Bohemian Massif is subdivided into three parts. From north to south, they are the Saxothuringian domain, the Tepla – Barrandian and the Moldanubian domain. To the Southeast follows the Moravian domain as part of Brunia. The chosen field area lies in the SE – Bohemian Massif in the Moldanubian Unit. Here high pressure deformed – tectonic fragments meet with middle pressure deformed – nappes. Also an oceanic suture from the subducted Raabs Ocean can be found in this area and separates these two different metamorphosed tectonic nappes.

In Austria, the largest part of the Bohemian Massif is built up by the Moldanubian unit (e.g. Klötzli et al., 1999). This lithotectonic unit displays a wide variety of high-grade crystalline rocks. Mainly gneisses to migmatites but also quartzites and marbles, orthogneisses, amphibolites as well as deep-crustal rocks such as granulites, eclogites and peridotites can be found (Babuška and Plomerová, 2013). Variscan syn- to post-tectonic granitoide bodies have intruded the Bohemian Massif (Babuška and Plomerová, 2013) and changed the geological map to the view we know today.

From bottom to top the Moldanubian unit can be separated into the: Ostrong Unit, the Drosendorf Unit and the Gföhl Unit (including the Raabs Serie at its base; Racek et al., 2006; Petrakakis, 1997; Kotková, 2007; Fritz 1995). Only the last two units are exposed in the field area of this master thesis (figure 2).
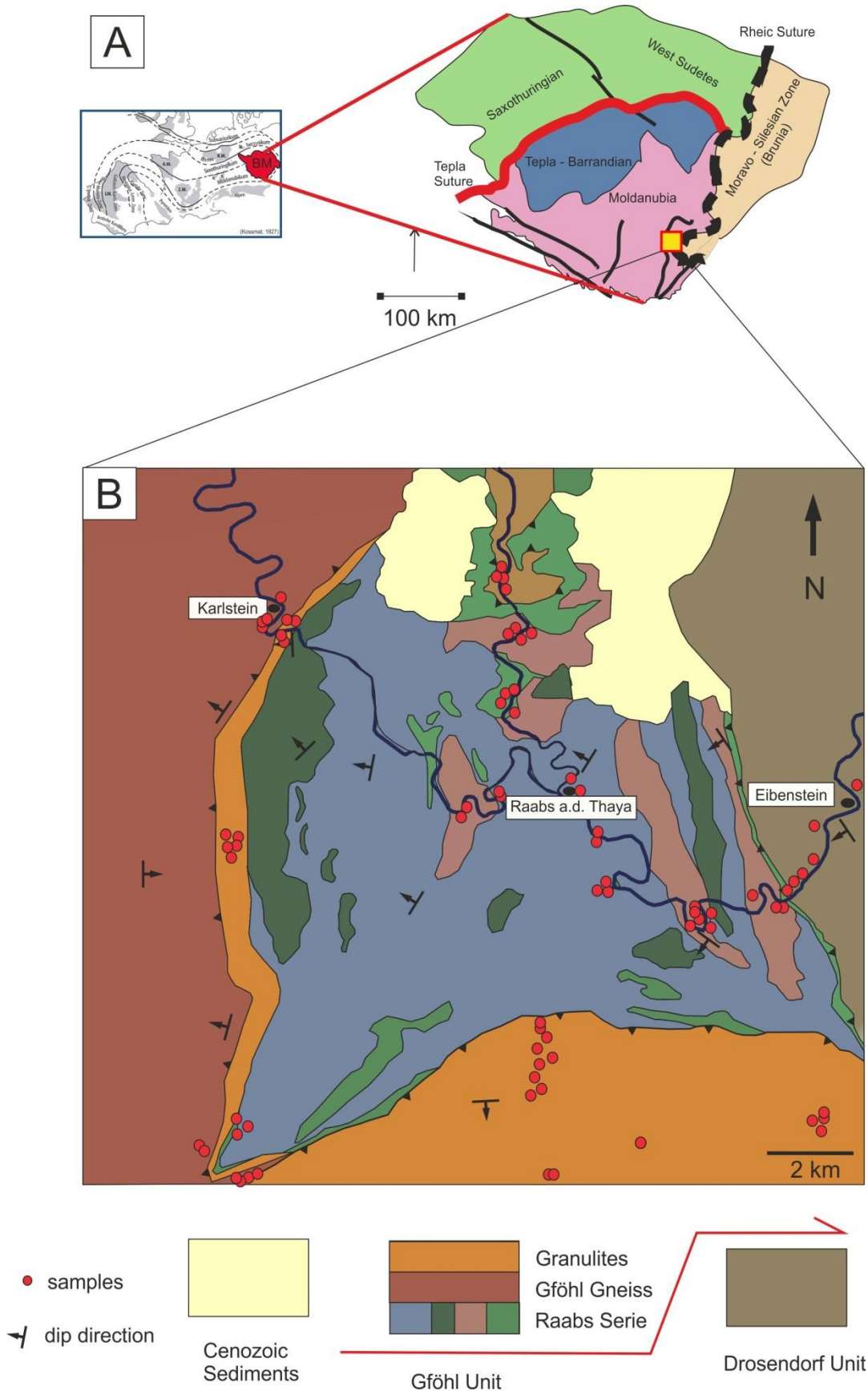
Figure 2 A:On the left side an overview of the European Variscan orogen is shown (after Kossmat, 1927), on the right side a schematic map of the Bohemian Massif is created (modified after Franke, 2000).
B: Geological overview of the field area (redrawn after sheet number 7 Gross-Siegharts by O. Thiele, © Geologische Bundesanstalt Wien, 1987)

2.1.   The lithotectonic of the Moldanubian nappes:

In this master thesis, a subdivision of the Moldanubian nappe system into three lithotectonic units is used (Klötzli et al., 1999; Fuchs and Scharbert, 1979). The subdivision is based on the different chronological and metamorphic evolution of each nappe unit (Klötzli et al., 1999). From the bottom of the Moldanubian nappe system to the top, they are as followed (figure 3):

1. The Ostrong Unit is the deepest unit exposed in the west of the Moldanubian Unit in Austria (Petrakakis, 1997) and includes polymetamorphic sediments of a late- to post-Cadomian active continental margin (Klötzli et al., 1999). Amphibolite-facies metamorphism influenced the Ostrong Unit (700°C and >4.5 kbar; Petrakakis, 1997). Occurrences of eclogite and spinel peridotite in this unit have led to a lot of discussion about the tectonic models of the Bohemian Massif during the Variscan orogeny (Babuška and Plomerová, 2013).

2. The Drosendorf Unit can be subdivided into a cover made of metasediments (quartzites, amphibolites, graphite schists, marbles and paragneisses) and a basement built up on orthogneisses like the Dobra gneiss and the Spitz gneiss (Friedl et al., 2004; Finger and Steyrer, 1995). The metasediments are assumed to be mainly of Palaeozoic age (Friedl et al, 2004; Finger and Steyrer, 1995) and lie on a ca. 2 Ga basement of crystalline rocks (Klötzli et al., 1999). There have been discussions about a correlation of the Dobra gneiss with the Moravian Bittesch gneiss because of the theory that the Dobra gneiss is a former Moravian Unit overthrusted in the Cadomian (Friedl et al., 2004; Finger and Steyrer, 1995).
    After Petrakakis (1997) the Drosendorf Unit experienced an amphibolite-facies metamorphic event with 7 − 9 kbar and temperatures of about 700 to 800°C.

3. The Gföhl Unit contains granulites at the top, the Gföhl gneiss and the Raabs Serie (at the bottom; Friedl et al., 2004). The granulites are characterised by its felsic chemistry and the occurrence of garnets and kyanites as well as by its

relics of HPHT – conditions of ca. 1000°C and 16 kbar (O'Brien and Carswell, 1993; Friedl et al., 2004). The Gföhl gneiss has an S-type granitic composition and has experienced partly migmatisation (Friedl et al., 2004). The protolith is mostly of acid magmatic origin and the age is Lower Palaeozoic, presumably Ordovician (Friedl et al., 2004; Klötzli et al., 1999). The Raabs Serie with its assemblage of amphibolites and paragneisses is assumed to represent an oceanic suture (Fritz, 1994; Fritz, 1995).
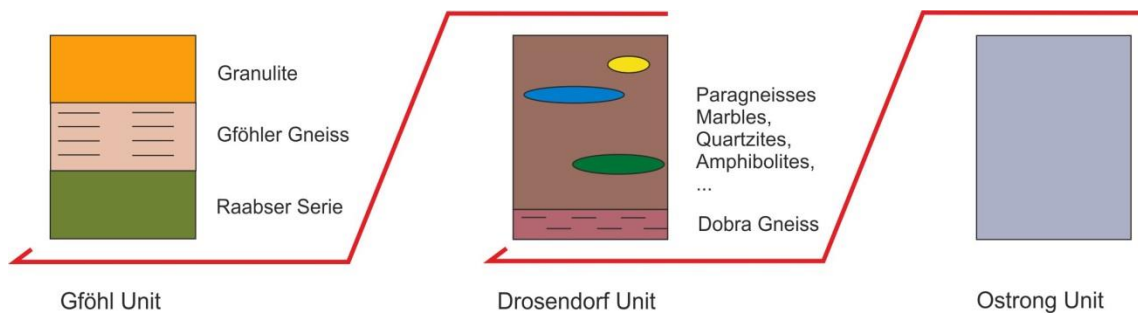
Figure 3 Tectonostratigraphy of the lithotectonic units in the Moldanubian (modified after Kotková, 2007; Racek et al., 2006; Petrakakis, 1997; Fritz, 1995)

2.2.   The Variscan Orogeny

The Variscan orogen is famous for being responsible for the formation of the supercontinent Pangea during the late Palaeozoic. It consists HP to UHP metamorphic rocks and was established during the Devonian to Carboniferous (Faryad 2011). Different models were proposed for the number of plates and oceans participating during the Variscan orogeny (e.g. Stampfli and Borel, 2002; Kroner and Romer, 2013). Despite the different tectonic models, it is generally agreed that microcontinents which separated from the northern margin of Gondwana during Early Palaeozoic and Devonian are the main components of the Variscan orogen (Finger and Schubert, 2015). As for the most important ocean that played a role during the Variscan orogeny, the Rheic Ocean is introduced (Nance et al., 2009).

2.2.1. The participating plates and oceans

The Variscan orogeny is characterised by the juxtaposition of allochthonous HP – metamorphic units of Late Devonian to Early Carboniferous metamorphic age next to autochthonous LP – metamorphic units derived from the Palaeozoic as well as Cadomian terranes (Nance et al., 2009).

During the early Ordovician the continent Avalonia separated from the South American part of Gondwana by opening the Rheic Ocean and collided with the continents Baltica and Laurentia around 450 Ma (Finger and Schubert, 2015; Nance et al., 2009; Stampfli and Borel, 2002). The northern part of the Variscan orogen in Europe is represented by the Avalonian continent and includes for instance the Moravian terranes as well as the Brunia domain of the SE – Bohemian Massif (Finger and Schubert, 2015).

Between ca. 370 – 330 Ma, the Rheic Ocean is closed by northward drifting of the micro-continent Armorica (Armorica-Liguria-Galatia in Stampfli et al., 2011; von Raumer et al., 2013) which separated from the northern margin of Gondwana during the Silurian (Stampfli and Borel, 2002; Nance et al., 2009). This is indicated by zircons which grew during magmatic activity in the realm of the future Bohemian Massif and exhibit ages of Upper Ordovician (Friedl et al., 2004).

Armorica is derived from the north - African part of Gondwana and builds up the main part of the central European Variscan orogen containing the Saxothuringian, the Tepla-Barrandian as well as the Moldanubian Units as an example (Friedl et al., 2004; Finger and Schubert, 2015; also known as Galatia in the work of Stampfli et al., 2011). According to Stampfli et al. (2011), the Moldanubian domain was part of the continent Liguria-Galatia (figure 4).

The suture of the Rheic Ocean can be followed throughout Europe (Iberian-Armorican arc, Lizard ophiolite in Britain, Sleza ophiolite in the Bohemian Massif and borders to the Moravo-Silesian Zone; Nance et al., 2009).
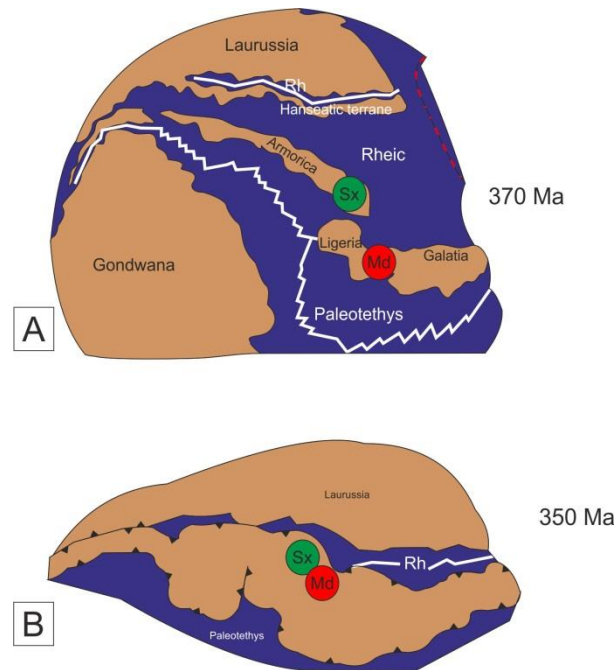
Figure 4 Simplified plate tectonic model during the Variscan orogeny (Stampfli et al., 2011; von Raumer et al., 2013). The location of the Saxothuringian (Sx) as well as the Moldanubian (Md) is located after the model of Stampfli et al., 2011.

2.2.2.   The Variscan orogeny in the SE - Bohemian Massif:

The Variscan orogeny in the Bohemian Massif is characterised by the collision of the Moldanubian blocks derived from Armorica with the Moravo – Silesian foreland of Brunia originated from Avalonia (Fritz, 1994). However, there are a lot of discussions about the real number of continental plates and oceans participating in the building of the Bohemian Massif (Schulmann et al., 2009; Babuška and Plomerová, 2013; Kroner and Romer, 2013; Stampfli et al., 2011).

According to seismic studies published in the paper by Babuška and Plomerová (2013), five different continental terranes were part of the evolution of the Bohemian Massif during the Variscan orogeny. Those were as followed: the Saxothuringian, the Sudetes, the Tepla-Barrandian, the Moldanubian as well as the Moravo-Silesian domain (Babuška and Plomerová, 2013).

Not only have several continental domains participated in the Variscan orogeny, but also multiple metamorphic events reworked the lithological units which took part during the Variscan. The most important metamorphic events are summarized below.

2.2.2.1.   The multiple metamorphic events

By focusing on the Moldanubian Unit, there have been several different metamorphic events during the Variscan orogeny (figure 5; Klötzli et al., 1999; Finger et al., 2007; Babuška and Plomerová, 2013). On the whole, three distinct metamorphic events characterised by complete different environmental conditions are presented. The associated plate tectonic models are examined in the next chapter.

The first HP – metamorphic event has been thoroughly discussed and seems to be limited to the Gföhl Unit only (Carswell and Jamtveit, 1990). After Petrakakis (1997) a metamorphic event with Pmax conditions should have happened before or at 370Ma. This corresponds with the model after Schulmann et al. (2009) which suggests subduction of the felsic granulite protolith under the Tepla-Barrandian crust at 380 Ma and therefore HP-conditions (Guy et al., 2011). The eclogite-facies metamorphism of the future granulites took place under conditions of 800°C – 900°C and ca. 3GPa (Faryad et al., 2010). Geochronological data also suggest for the occurrence of a HP to UHP event for around 370 Ma (Faryad et al., 2015).

Subsequently, granulite – facies metamorphism overprinted the future granulites at lower crustal levels (Cooke et al., 2000; Friedl et al., 2011; Schulmann et al., 2009). The timing of the granulite-facies metamorphism is still a matter of debate (between 370 Ma to 340 Ma; Schulmann et al., 2009; Anczkiewicz et al., 2007; Schulmann et al., 2005).
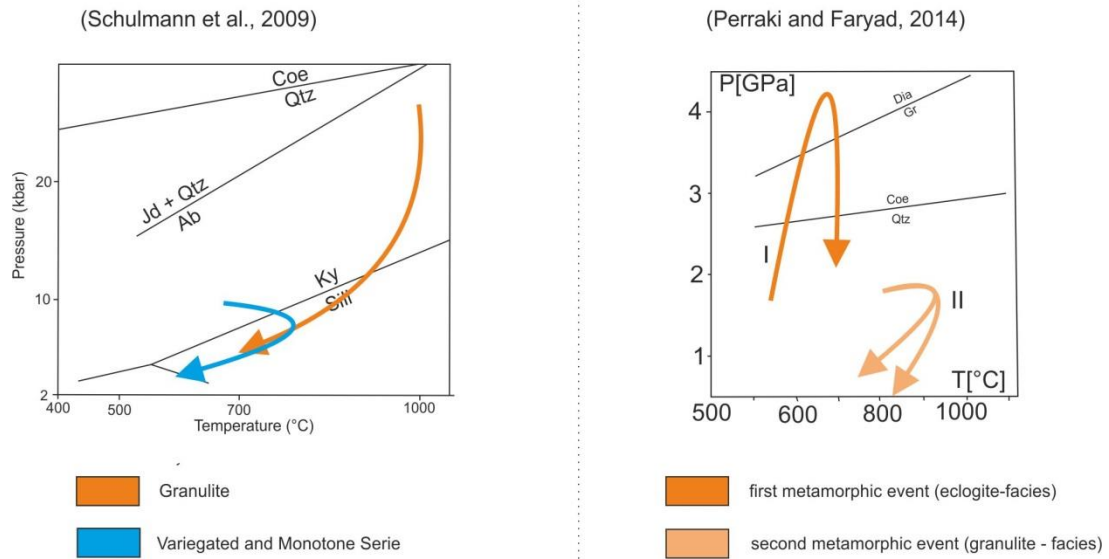
Figure 5 Two different PT-paths modelled for the evolution of the Moldanubian Unit.
The PT – diagram on the left side is presented in the paper after Schulmann et al. (2009) and displays the PT- evolution of the granulites (in orange) and of the Variegated as well as the Monotonous Serie (in Blue – Drosendorf Unit and Ostrong Unit). The granulites show a strong curving and retrograde path from nearly HP/HT conditions (ca. 340 Ma) to HT-MP to LP that was caused during the exhumation of the granulites. The Variegated and Monotonous Unit (equalling the middle crust of Schulmann et al., 2009) exhibit a reheating event after a MP/MT metamorphism by a subsequent exhumation.
The PT-diagram on the right side is modelled after the assumptions of Perraki and Faryad (2014) with data from Faryad (2010). In contrast to the PT-paths on the left side, the PT evolutionary path of the granulites (in dark as well as light orange) is divided into two events. The first event (I – in dark orange) represents the eclogite-facies metamorphism that the granulites have experienced. The second event (II – in light orange) characterizes the granulite – facies event. The findings of microdiamond and coesite are represented in the arc of the PT – path reaching into the diamond field.

Very famous in the Moldanubian unit is the tectonometamorphic overprint around 345 – 330 Ma which is also called the Moravo – Moldanubian Phase (Finger et al., 2007). This second metamorphic event influenced all of the Moldanubian units (Finger and Steyrer, 1995) under different stages of intensity (figure 6; granulite to amphibolite-facies; Faryad et al., 2015). The most extreme metamorphism dominated the Gföhl Unit and decreased towards lower structural units (Finger and Steyrer, 1995). During this metamorphic event, two important tectonic scenarios simultaneously took place: thrusting of the Moldanubian nappes onto Brunia and exhumation of HP-HT metamorphosed rocks, like the Gföhl Unit (Finger et al., 2007; Fritz and Neubauer, 1993). At ca. 340 Ma the Gföhl Unit, the Drosendorf Unit as well as the Ostrong Unit were placed on to each other during the Variscan orogeny (Friedl et al., 2004).

The last event is characterised by an LP-HT metamorphic overprint (330 – 315Ma). Maybe it was triggered by late Variscan delamination of mantle lithosphere and caused strong reheating of the western parts of the Moravo-Moldanubian regime and intrusion of voluminous granitic plutons in the crust (Finger et al., 2007 – Bavarian Phase).

After this event, cooling took place and lasted until 290 Ma (Klötzli et al., 1999).
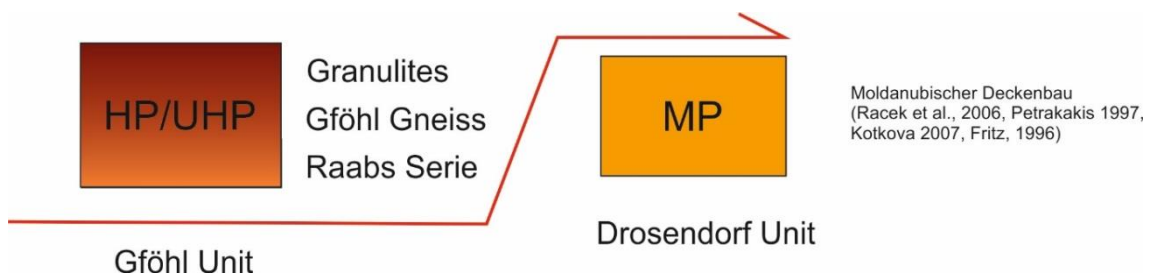
Figure 6 Degree of metamorphism of the lithological units exposed in the field area of the master thesis. High-grade rocks are embedded on lower-grade rocks.

Beside these three metamorphic events, numerous plutonic bodies intruded the Bohemian Massif throughout the Variscan. The occurrence and chemistry of these plutonic suites are interesting because of the connection to the plate tectonic movements during the Variscan orogeny (Žák et al., 2014; von Raumer et al., 2013). The different plutonic suites which intruded the Moldanubian are explained in chapter 2.4.

2.2.2.2.   Tectonic model considerations:

The writer of this master thesis favours a tectonic model that includes the westward subduction of a Gföhl Ocean under the Tepla-Barrandian Block and, more importantly, the westward subduction of the Raabs Ocean under the Moldanubian Unit (figure 7; Franke, 2000; Finger et al., 2007, Babuška and Plomerová, 2013). The preference of this model is evident since the author of this study works in a domain defined as Raabs Ocean.
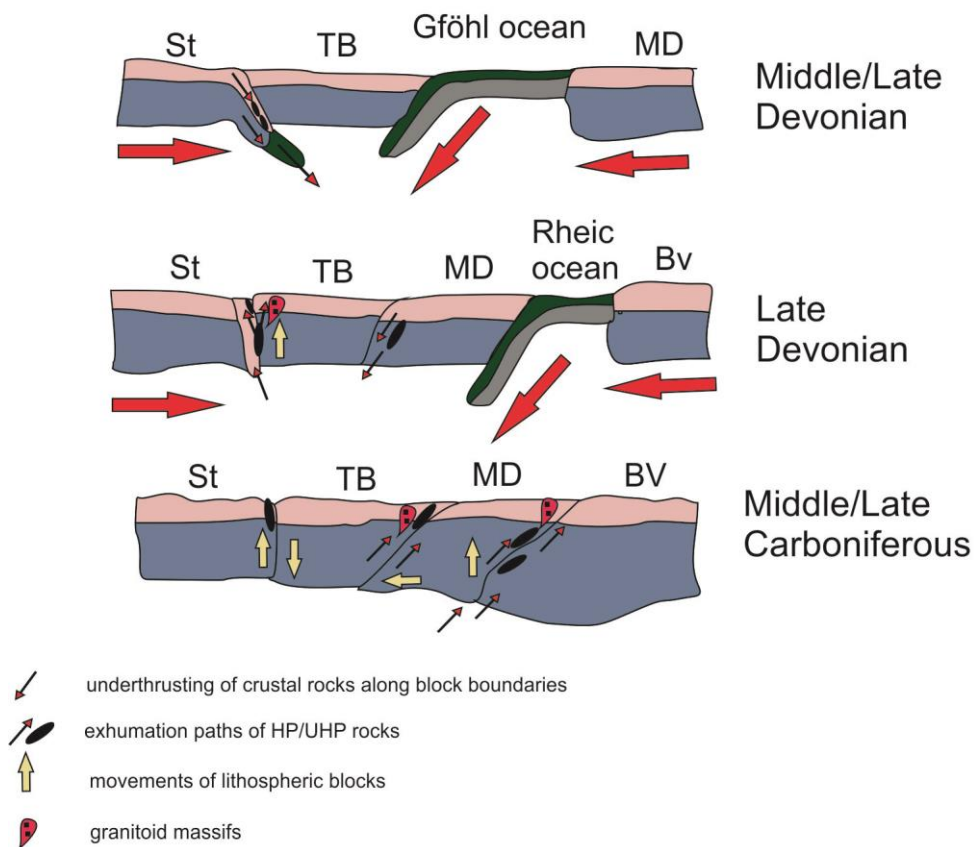
Figure 7 Plate tectonic model after Babuška and Plomerová (2013). Three oceans are part of the evolution of the Bohemian Massif. Exhumation channels enable the emplacement of lower crustal rocks into upper crustal regimes. St (Saxothuringian continent), TB (Tepla-Barrandian Block), MD (Moldanubian Unit), BV (Brunia).

To understand the location of today's lithotectonic units, the whole Bohemian Massif assemblage must be considered. In the suggested model after Babuška and Plomerová (2013) a bivergent subduction system under continental crust is presented. This model is based on anisotropic investigations executed on mantel data (Babuška and Plomerová, 2013).

The starting point in the model after Babuška and Plomerová (2013) is the eastward subduction of the first ocean (the Saxothuringian Ocean) under the Tepla-Barrandian block during the early Devonian (Schulmann et al., 2009). The felsic granulite protolith could have experienced eclogite-facies metamorphism during this plate tectonic event (Schulmann et al., 2009; Faryad et al., 2010). The later experienced granulite-facies metamorphism probably took place during the Visean (Schulmann et al., 2005) or maybe earlier (370 Ma Lu-HF and SM-Nd age; Anczkiewicz et al., 2007). In other models, the granulites are derived from felsic rocks from the Moldanubian unit which

are subducted westwards deep under the Tepla-Barrandian Block (Babuška and Plomerová, 2013).

This implies an ocean between the Tepla-Barrandian Block and the Moldanubian unit, the second ocean participating in the bivergent model, the so-called Gföhl Ocean sometimes also called the Moldanubian Ocean (Faryad et al., 2015). After the subduction and collision, buried continental crust, eclogites as well as peridotites is brought to the surface by exhumation channels (Babuška and Plomerová, 2013). Arguments for a Gföhl Ocean are the occurrences of eclogite and spinel peridotite in the Ostrong Unit (Babuška and Plomerová, 2013).

The Raabs Serie at the base of the Gföhl Unit represents an oceanic fragment separating the continental terranes of the Moldanubian in the west and Brunia in the east (Fritz and Neubauer, 1993). The Brunia terrane reacted probably as a rigid indenter during the Variscan collision (Klötzli et al., 1999). In tectonically view, the Raabs Serie as a representative of a former oceanic floor is sandwiched between the Gföhl Gneiss and Granulite terrane and the Drosendorf Unit (Fritz, 1995) and is the third ocean getting subducted during the Late Devonian (Babuška and Plomerová, 2013). However, it was likely a very small ocean and has barely reached the stadium of being called an ocean (Finger and Steyrer, 1995). The origin of the Raabs Ocean was caused probably by a back-arc extension phase (Finger and Steyrer, 1995).

After the multiple subduction of oceans, exhumation channels could have formed along the sutures of two continental plates. Because of these channels, buried HP – rocks and mantle slabs were transported to the surface (Babuška and Plomerová, 2013). This could be a possible model describing the processes that took place in the past of the SE-Bohemian Massif.

Returning back to the geological map of this master thesis, the location of the Raabs Serie is suspicious. It separates the Gföhl gneiss and granulite layer from the Drosendorf Unit. This special geological position suggests that the Drosendorf Unit was separated from the Gföhl gneiss and granulite nappe by an ocean. Especially by unravelling the tectonostratigraphic positions of the nappes into different independent continental terranes through balancing cross-section methods, it is difficult to add the Drosendorf Unit to the Moldanubian domain.

Recent considerations about the origin of the Drosendorf Unit have arisen (Finger et al., 2007; Finger and Steyrer, 1995). There are new tectonic model developments where the Drosendorf Unit is included into the Avalonian terrane (figure 8; Finger and Schubert, 2015). One of the first of these models is presented in the work of Finger and Steyrer (1995) where the Drosendorf Unit as well as the Moravian terrane are part of a passive continental margin of Brunia separated by the Raabs Serie from the Moldanubian Unit including the Ostrong Unit. This model is quite interesting for the right position of the Raabs oceanic suture and their emplacement above the Drosendorf Unit (Finger and Schubert, 2015). Additionally, the similar composition of the Dobra Gneiss with the Moravian Bittesch Gneiss is a strong argument for the belonging of the Drosendorf Unit to the Moravian Unit (Finger and Steyrer, 1995).
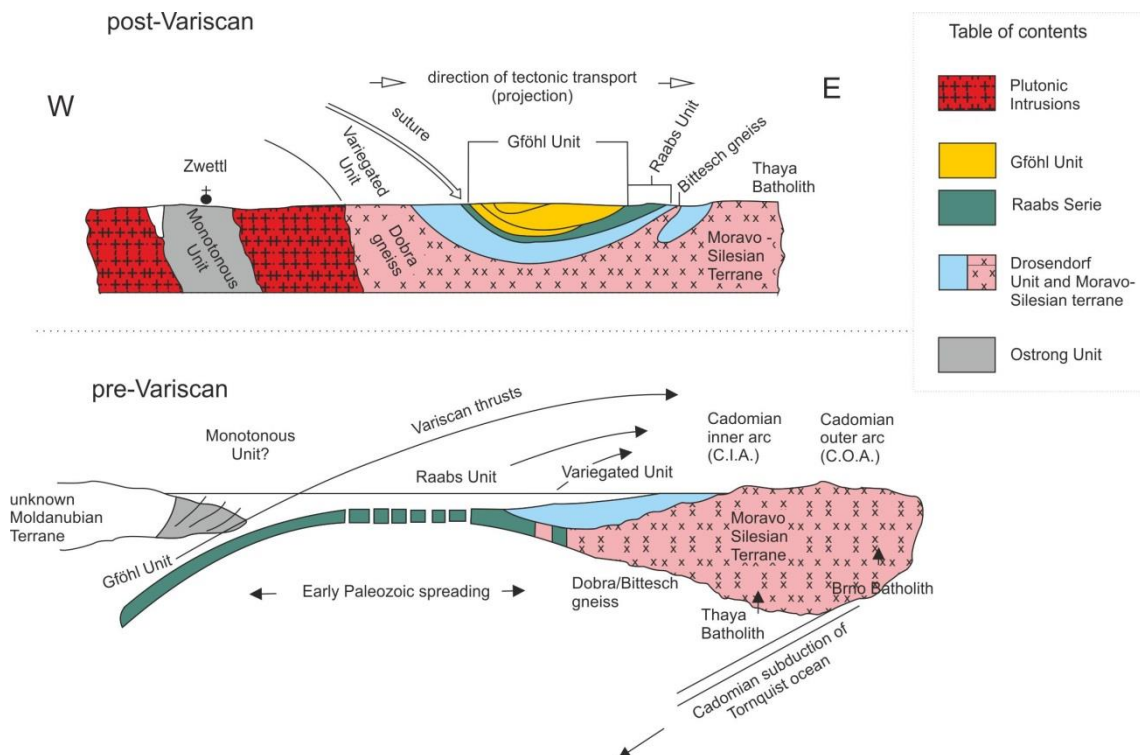
Figure 8 Tectonic model after Finger and Steyrer (1995).The Variegated Unit (metasedimentary cover of the Drosendorf Unit) represents a shelf regime of the Brunia continent. Together with the Dobra gneiss (basement of the Drosendorf Unit), the Bittesch gneiss and the Variegated Unit, they build a passive continental margin of the Brunia – Silesian terrane (Finger and Schubert, 2015). The active continental margin consists of a Moldanubian terrane, the Monotonous Unit (Ostrong Unit) and the exhumed Gföhl Unit. The ocean which got subducted between the Moldanubian unit (Armorica) and Brunia (Avalonia) is the Raabs Ocean.

As for their developing environment, the following assumptions can be made:

- The Ostrong Unit may be derived from an environment including trench and accretionary wedge sediments (Finger and Steyrer, 1995). However, the age of the sediments and the exact date of the eclogite-facies metamorphism is poorly constraint.
- The Drosendorf Unit consists of a wide variable lithological set of marbles as well as metapelites. Therefore, considerations about its origin or formation environment include a shelf regime with slope sediments (Petrakakis, 1997). Ages of basement rocks seem to be different. For the Dobra Gneiss (basement of Drosendorf Unit) a late Palaeoproterozoic protolith age was published, and for the Bittesch and Thaya Gneisses a late Neoproterozoic age is constraint (Klötzli et al., 1999). Nevertheless, age of basement provides no argument for the nature of sediments laying above.
- The Gföhl Unit is famous for its metamorphosed granitic rocks and could have been formed at an active continental margin (Petrakakis, 1997). However zircon ages suggest that these magmatic rocks were already formed in the Ordovician.
- The Raabs Serie represents a former ocean floor (Fritz, 1994). A plagiogranite-gneiss derived from this unit was dated at ca 428 Ma (Finger and von Quadt, 1995).

2.3.   Geological field overview and the kinematics of the Variscan Orogen

By studying the south-eastern border of the Bohemian Massif, the NW-SE trending belts of the lithological units such as the Ostrong Unit, the Drosendorf Unit and the Gföhl Unit are striking (figure 9 and 10; Guy et al., 2011). The NE – SW trending - protruding curve of the Brunia terrane with the Moravo – Silesian terrane in the east shows intense deformation (Guy et al., 2011).
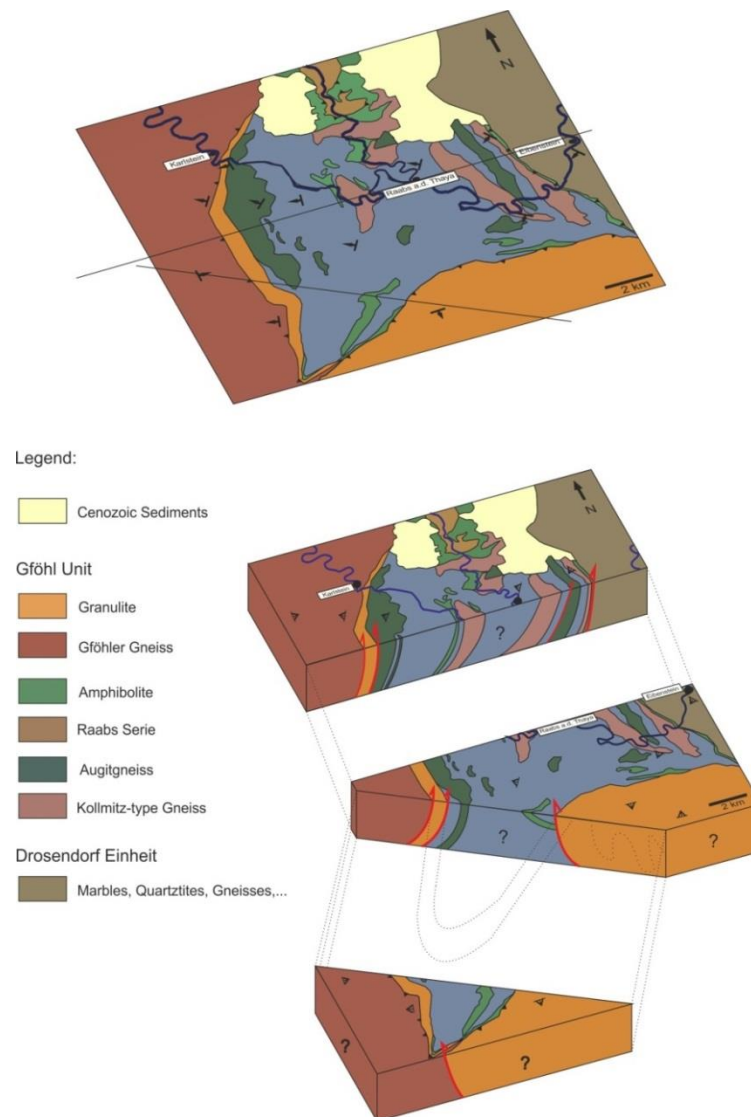
Figure 9 3D-Model of the geological map of the field area. In the model a distinct W-dipping trend of the Gföhl as well as the Drosendorf Unit is seen. Only in the near of lithotectonic boundaries is the dip of the nappes steeper (60 to 80°) than in the middle of the nappes (30 – 50°). The Blumau Granulite Complex in the south of the map displays internal steep N-S trending folds with W-E coaxial flow. The contact between the Raabs Serie as well as the southern granulite body is dipping to south with a steep inclination (70 to > 85°) and suggests existence of a probable later folding.

Through the thrusting of the Moldanubian unit over Brunia, an east-vergent structure is caused in the Gföhl Unit (Racek et al., 2006). This is coherent with the general agreement of transpressional transport into a NNE direction based on W-E compression seen in the south-eastern of the Bohemian Massif (Fritz and Neubauer, 1993; Fritz et al., 1996; Racek et al., 2006).

The lithological units in the Moldanubian Zone of Austria mostly strike NNE-SSW and dip ESE (Petrakakis, 1997). The flat foliation is folded into large antiforms (as indicated by the Drosendorf Unit) and small synforms (like the Gföhl Unit; Matte et al., 1990). After Fuchs (1991), the previously mentioned strike direction was caused by the collision of the Moldanubian units with the indenter of the Brunia terrane. A transpression zone was responsible for the bending of this area from E-W in Europe to NNE-SSW in Austria (Fuchs, 1991).

Other opinions are that a generally NNE-directed translation influenced nappe transport during the thrusting of the Moldanubian unit over the Moravian terrane of Brunia (Schulmann, 1990; Schulmann et al., 1995; Fritz and Neubauer, 1993).

After Matte et al. (1990) intense NW-SE stretching influenced the Moldanubian units by showing stretching lineation and boudinage structures.

(After Hasalova et al., 2008; Racek et al., 2006:)

Deformation event for the MD Unit	Structures	Plate tectonics
D1	Relict S1 foliation which is folded by	
D2	F2 (N-S trending folding axes) Steep S2 foliation	E-W compression, Thickening of crust; exhumation of HP-rocks
D3	Flat S3 foliation the granulites with mylonitic transposition; the Raabs Serie displaying mylonitic gneisses and the Drosendorf Unit exhibits development of sheath folds and strong N Lineation	Thrusting onto flat Brunia foreland (around 340Ma)
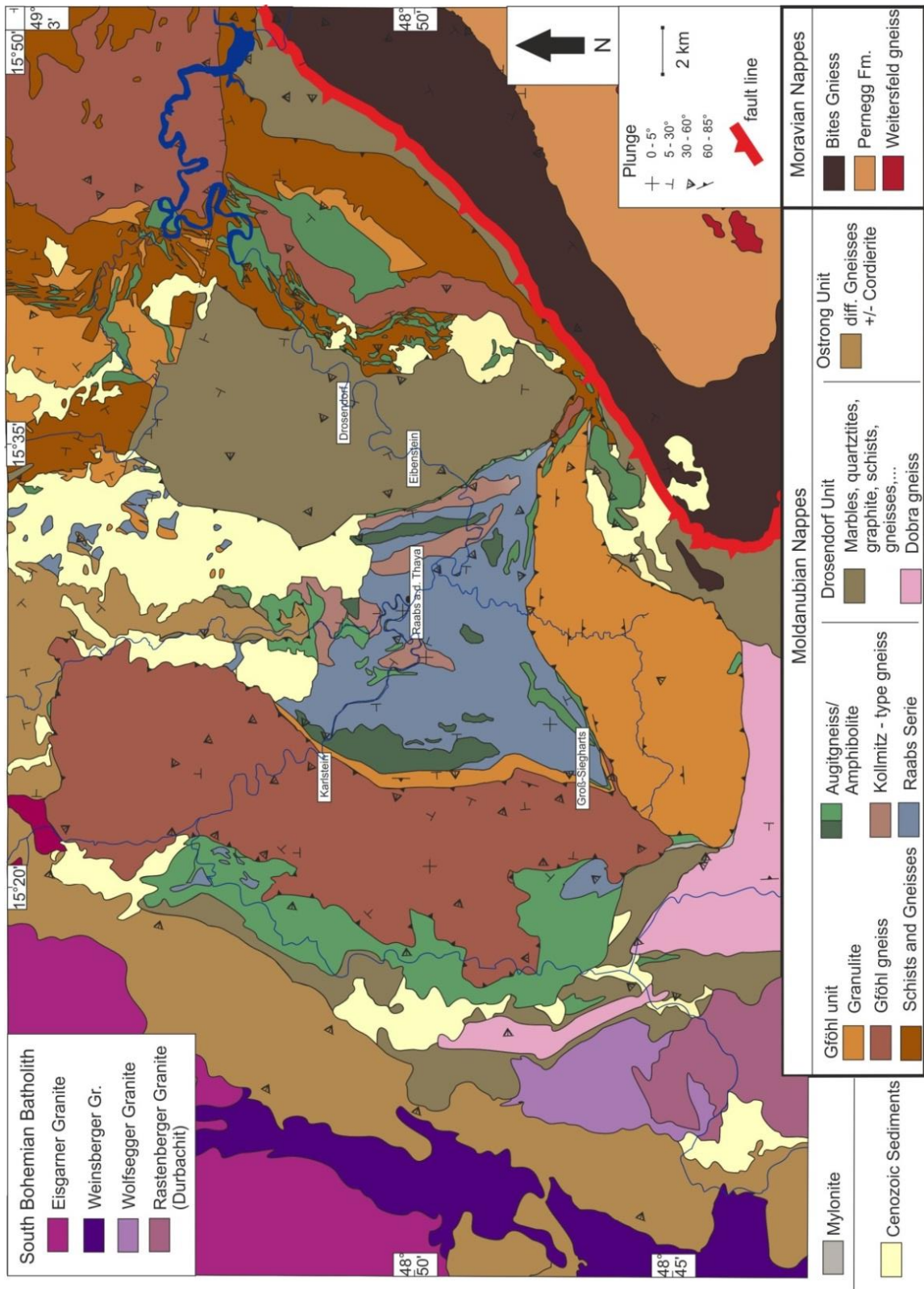
Figure 10 Geological map of the SE-Bohemian Massif. The map is drawn from the eastern boundary represented by the Moravo-Silesian terrane to the western boundary made by the plutonic intrusions (redrawn after sheet number 7 Gross-Siegharts by O. Thiele; number 8 Geras by R.Roetzel and G.Fuchs; number 20 Gföhl by G.Fuchs and E.Kupka; Geologische Karte Niederösterreich – Niederösterreich Nord© Geologische Bundesanstalt Wien, 1984, 1987, 2001, 2002.

2.4.   Zircon ages of the SE-Bohemian Massif

Several geochronological studies were applied on the samples of the Bohemian Massif (figure 11; Friedl et al., 1993; Friedl et al., 2004; Friedl et al., 2011; Neubauer and Handler, 2000; Košler et al., 2014; Klötzli et al., 1999; Finger and von Quadt, 1995; and references therein).

Zircons in a sample taken from the Kollmitz-type gneiss, Raabs Serie (ML19)	Zircon engulfed by a dark halo in a biotite, Raabs Serie (R55)
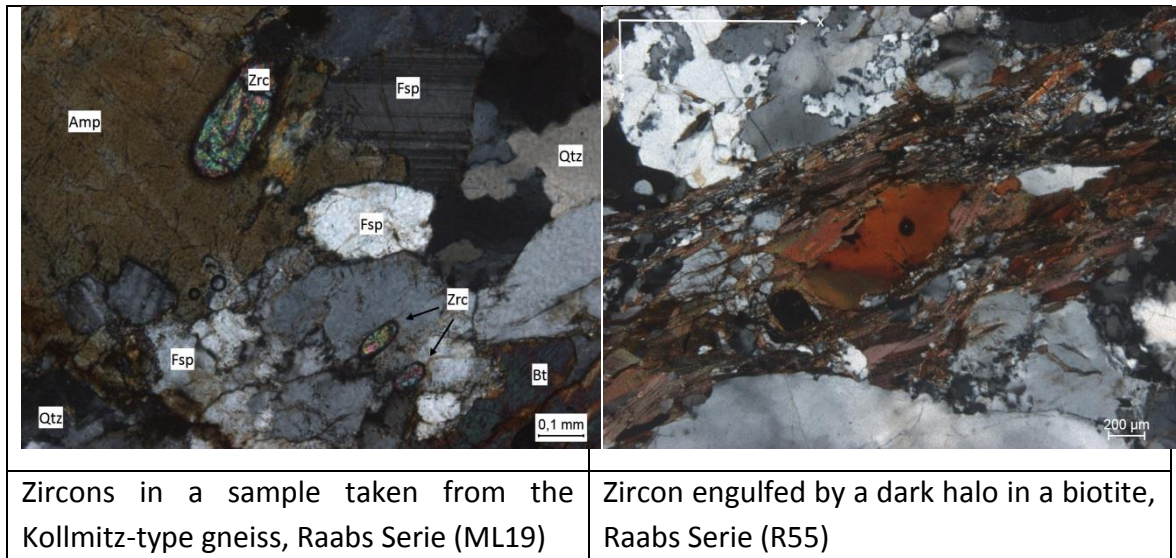
Theory is that the distinct zircon age distribution pattern represents a special paleo – environment. Therefore, lithotectonic units can be summarized to distinct continental terranes. Not only is the distribution pattern of ages important but also the evolution recorded in zircons. Zircons grow in magmatic regimes by crystallizing from a melt. As a result specific magmatic activities can be dated by the growth of a zircon. For instance cores of zircons are mostly developed during a magmatic event. Differences about rim growth during a magmatic or a metamorphic event are distinguished by the appearance of the rim layer. Magmatic oscillatory zoning of a rim is one of the examples for differentiating a developing regime.

Especially the exact timing of the Variscan metamorphism in the Bohemian Massif has been tried to date by studying the zircons (Friedl et al., 2011). If a zircon grows during a high-grade metamorphic event, it is generally accepted, that it is showing the date of the PT-event (Roberts and Finger, 1997). However, there have been cases where the zircons sampled from granulites, have post-dated the peak of pressure of a

metamorphism and therefore have shown, therefore, younger ages, because of melt infiltration (Roberts and Finger, 1997).
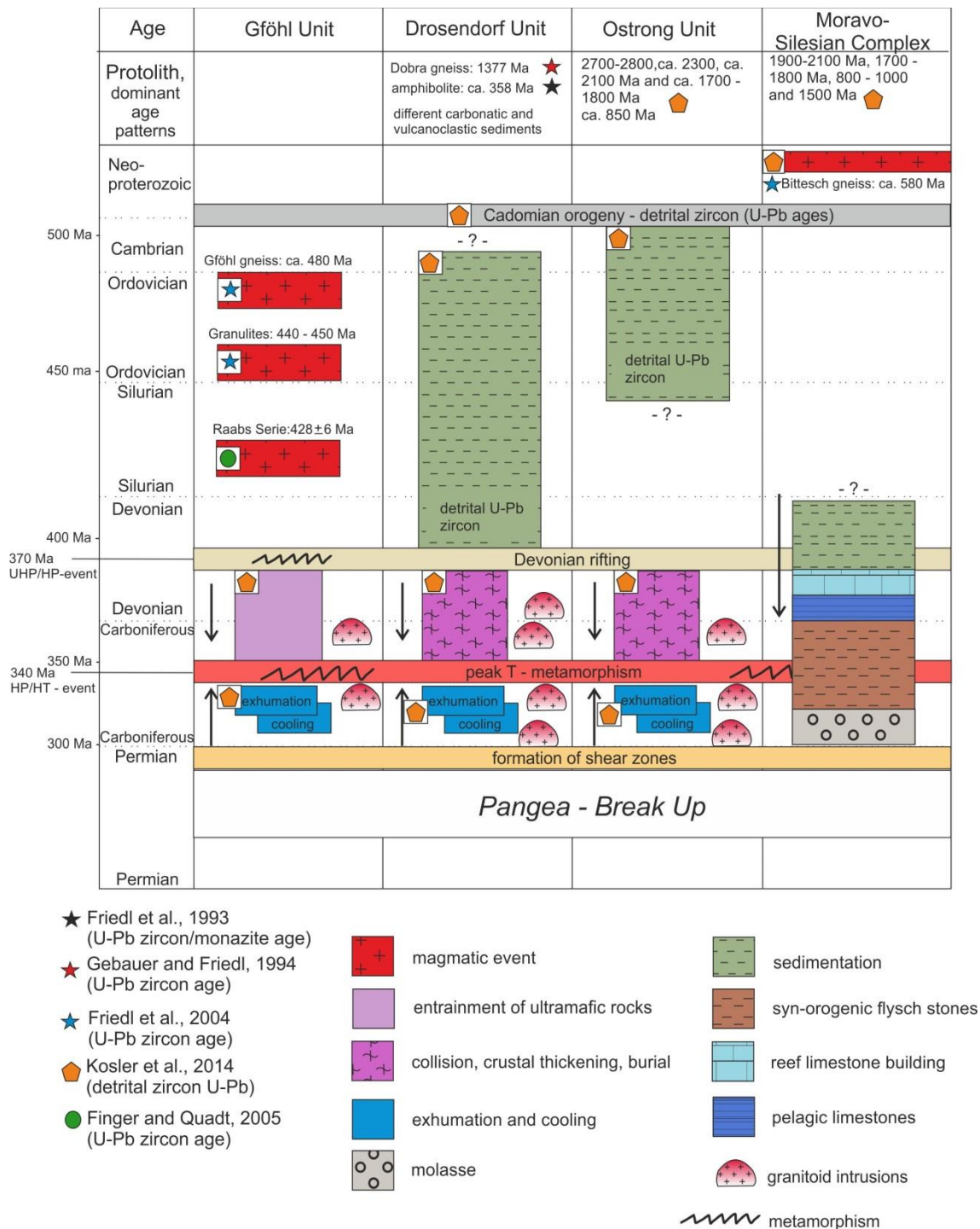
Figure 11 A simplified timetable with the deformation events of the individual lithotectonic units. The coloured rectangles exhibit major tectonic and metamorphic events. The smaller coloured rectangles display distinct evolutionary events. Summarized by published papers like: Košler et al., 2014; Friedl et al., 2011; Friedl et al., 2004; Friedl et al., 1993; Schulmann et al., 2005; Neubauer and Handler, 2000; Finger and Quadt, 1995 and Gebauer and Friedl, 1994.

The rocks derived from the Moldanubian unit display a typical distinct lack of zircon ages between 1.8 – 1.0 Ga which is taken as an evidence for ancestry from the North African part of Gondwana (Friedl et al., 2004). The Bittesch Gneiss of the Moravian-Silesian terrane contains zircons with inherited Mesoproterozoic and Early Palaeoproterozoic ages of ca. 1.2, 1.5 and 1.65-1.8 Ga, showing for instance derivation from the South American part of Gondwana (Friedl et al., 2004). The Dobra Gneiss as basement of the Drosendorf Unit with its age of ca. 1, 38 Ga (Gebauer and Friedl, 1994) is clearly exotic for the distribution of Moldanubian zircon ages and could indicate a relationship with the Moravian crust (Friedl et al., 2004).

Despite the protolith formation ages, most of the older zircons found in the Moldanubian part of the Bohemian Massif as well as the Moravo-Silesian terrane exhibit a Cadomian age (ca. 550 Ma). Additionally, the high numbers of Early Palaeozoic protolith ages indicate a strong magmatic activity during that time in the future Bohemian Massif (Friedl et al., 2004).

By studying the zircon ages shown in the table (figure 11), the lithotectonic units must be supplied by detritus of different sediments derived from separated source areas. A plate tectonic model which would locate the tectonic units all close together would not be possible by this data. Analyses of scarce detrital zircons depict that sedimentation in the Ostrong Unit stopped during the Ordovician or Lower Silurian whereas it continued in the Drosendorf Unit until the Devonian when Variscan Orogeny reworked the eastern part of today's Bohemian Massif (Košler et al, 2014).

During the Devonian, an extension-related phase influenced the continental configuration of the eastern realm of the Bohemian Massif (Schulmann et al., 2005). The subduction of the Saxothuringian Ocean beneath the Tepla-Barrandian Block and the emplacement of the granitic precursors of the granulites took place (Schulmann et al., 2005). This is maybe also indicated by the U-Pb and Pb-Pb data ages of 387 and 394Ma (Schulmann et al., 2005). The Devonian rifting and extension is also seen by the sedimentation of shallow water carbonates of the Moravo-Silesian terrane of Brunia (Schulmann et al., 2005; Košler et al., 2014). During that time the HP/UHP-event mentioned in the chapter 2.2.2.1 took possibly place (only seen in granulites; Klötzli et al., 1999).

Despite the different models concerning the exhumation of deep buried HP-rocks, collision as well as crustal thickening, HT-metamorphism and exhumation have happened around 340 Ma (U/Pb ages of zircons and Sm-Nd mineral ages; Košler et al., 2014; Schulmann et al., 2005; Neubauer and Handler, 2000). These ages are shown in nearly every lithological unit of the SE-Bohemian Massif (Košler et al., 2014).

The several plutonic intrusions are introduced in the next chapter.

2.4.1. Plutonism in the SE-Bohemian Massif

Several plutonic intrusions (figure 11) which are characterised by distinct chemistry and origin infiltrated the Bohemian Massif. The "first" intrusions (ca. 370 – 346 Ma) were calc-alkaline magmatic granitoids with magmatic-arc character (CBP – Central Bohemian Plutonic Complex) which developed above the subduction zone between the overriding Tepla-Barrandian Block and the sinking Moldanubian unit (Neubauer and Handler, 2000; Žák et al, 2014).

The next magmatic impulse (ca. 346-335 Ma) was characterised by emplacement of ultra-potassic Durbachites (e.g. Rastenberger Granodiorite; Žák et al., 2014). Those Durbachites are derived from an enriched mantle source and developed above subduction zones (von Raumer et al., 2013). Brunia (Avalonia continent) has started to get subducted westwards under the Moldanubian unit followed by melting of its subducted crust. Furthermore, the development of the Durbachites is favoured by a hot anomaly under the continental crust caused by a possible slab window or sinking of a subducted oceanic crust like the Rheic Ocean (von Raumer et al., 2013).

The waning stages of the Variscan orogeny in the south-eastern Bohemian Massif are accompanied by intrusions (ca. 340 – 310 Ma) of voluminous S-type granitic plutonic bodies (South Bohemian Pluton – SBP; Eisgarner Granite, Weinsberg Granite) which are enabled by diapiric upwelling of subducted crust (Neubauer and Handler, 2000; Žák et al., 2014). These granites crosscut the boundaries between different lithotectonic units and postdate the stacking of nappes (Neubauer and Handler, 2000). Through the ongoing collision of Gondwana and Laurussia multiple dextral shear zones crosscut the Bohemian Massif (e.g. Pfahl fault; 335-315 Ma; Žák et al., 2014). The last group

(around 300 Ma) has late-stage leucogranitic features and occurs in the near of strike-slip systems (Neubauer and Handler, 2000).

Triggered by N-S trending shortening processes major strike-slip systems have developed throughout the Bohemian Massif (Neubauer and Handler, 2000). The Permian is characterised by LP/HT – metamorphism and transtensional rifting processes (Neubauer and Handler, 2000).

3.   Analytical methods

The field research was executed in spring and autumn 2015, followed by thin-section preparation and microscopic study. The list including the thin-section samples can be found in the appendix.

It is important to study the microscale deformation mechanism that happened in minerals for determining the deformation regime in which the rock has formed. Specific dynamic recrystallization processes take place at distinct temperature ranges and can be used as a geothermometric tool (e.g. Kruhl, 1996; Law, 2014). However, old events are mostly overprinted and the last and youngest deformation events dominate the samples.

Before the deformation mechanism and their connection with their controlling factors like temperature as well as strain rate are presented, the tool for measuring the preferred lattice orientation of a mineral is shown. Analyses of textures applied on quartz by "G50 fabric analyser" give the first impression of the temperature realm in which the deformation of rocks occurred by presence of specific, temperature dependent glide systems. Also kinematic indicators can be shown by quartz c-axes girdles.

3.2.   Modified optical microscope

Before the measurements of the preferred orientation of quartz c-axes could be determined by a modified optical microscope, the occurrences of individual quartz domains in veins or scattered quartz minerals in the thin section had to be identified and classified for apparently different deformation mechanism by inspection of grain shape and grain boundary systematics. Under the microscope, certain quartz-rich areas are chosen und marked with a pen directly on the thin section.

With the modified optical microscope "G50 fabric analyser" the earlier marked areas of the thin-sections are analysed with alternating polarisation lights. The chosen area is separated into a mosaic and each small rectangle is analysed for quartz c-axis and saved by pictures in different polarisation lights (Wilson et al., 2007).

With the program "Crystal Imaging System G50 Fabric Analyser" the collected pictures are evaluated and quartz c-axes are determined in the scale of pixel points. An Excel-file is created which summarizes the entire quartz axes and can be plotted in the software "Fabric8". This program displays the data in form of a Schmidt net by using the data's plunge direction and dip angle. The finished plot is interpreted based on the preference of glide systems in quartz that are particularly dependent on the temperature and strain rate (Law, 2014). Also the kinematics, especially the shear sense direction, can be estimated if orientation of the sample is given (Passchier and Trouw, 2005)

3.2.1.   Deformation mechanism of mineral grains

Ductile rock deformation takes place in deep crustal levels by failure in the crystal lattice system of minerals (Passchier and Trouw, 2005). The damage made by this deformation is "healed" by recovery and recrystallization processes. The first one takes place in the lattice of the crystal like subgrain boundaries. The second one influences the grain boundaries and deals with the amount of dislocation density in neighbouring mineral grains (Passchier and Trouw, 2005). Atoms originated in the mineral with high dislocation density move to the neighbour with low dislocation density (Passchier and Trouw, 2005). Three major recrystallization mechanisms depending on increasing temperature and/or decreasing flow stress are summarized in figure 12: bulging (BLG), subgrain rotation (SGR) and grain boundary migration recrystallization (GBM; Passchier and Trouw, 2005). Especially at high temperatures, a healing process causes straightening of grain boundaries, the so-called grain boundary area reduction (GBAR; figure 13; Passchier and Trouw, 2005).
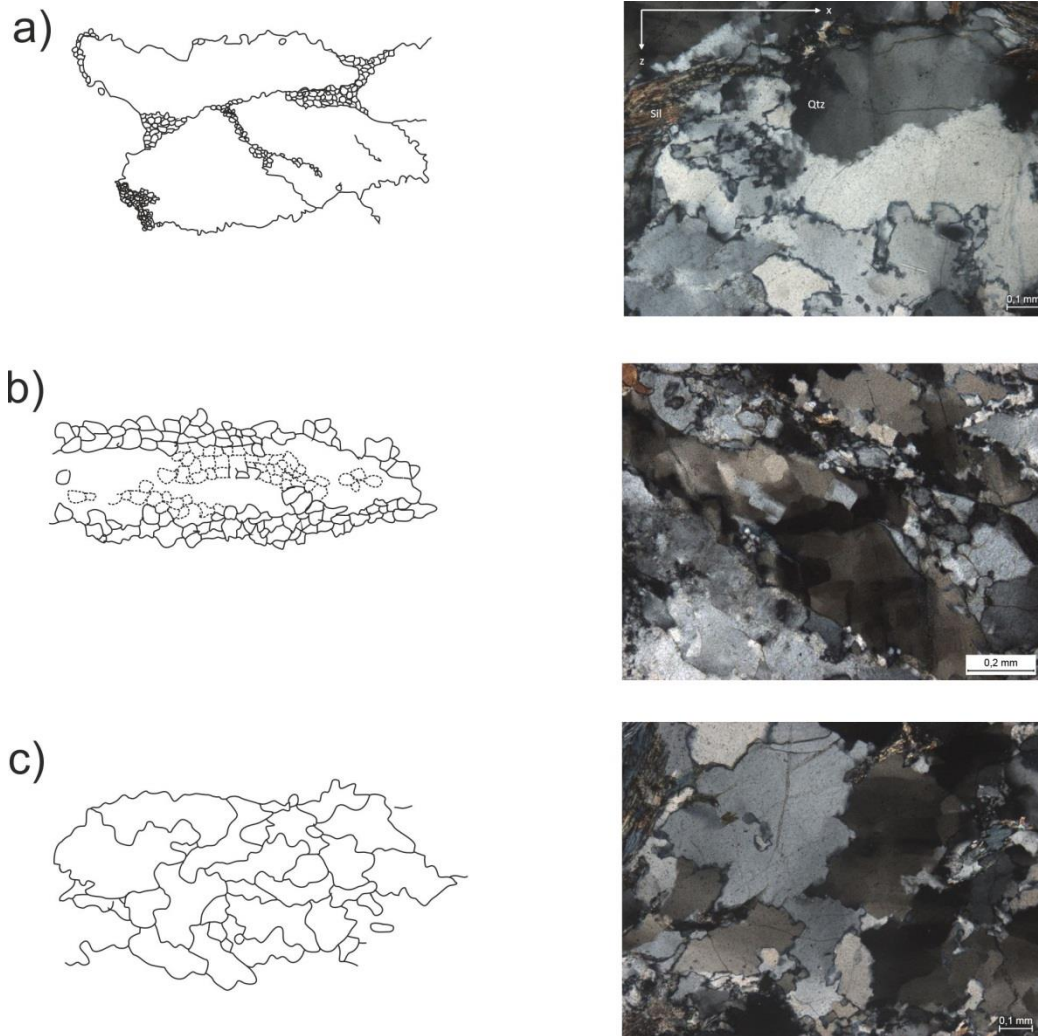
Figure 12 The three recrystallization processes shown with increasing temperature in quartzes on the left side (modified after Stipp et al., 2002) with pictures from thin samples of the study area on the right side.
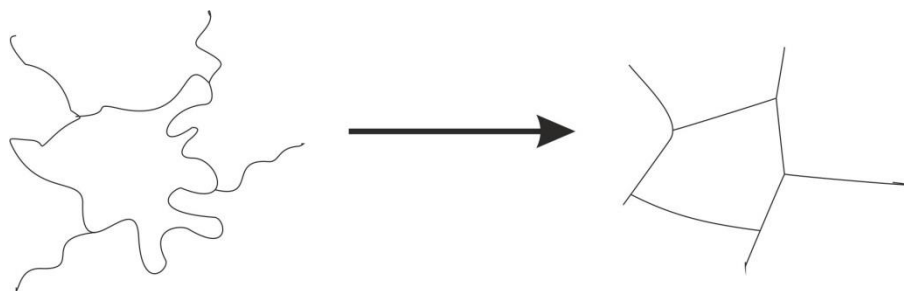
Figure 13 Grain boundary area reduction process by straightening of grain boundaries and growth of triple joints between mineral grains. Decrease of grain boundary energy is caused by the newly developed polygonal grains (Passchier and Trouw, 2005).

3.2.2. Quartz – thermometer

A simple geothermometer was introduced which allows a rough estimation of syn-tectonic temperatures from inspection of thin sections (Kruhl, 1996; Law, 2014). A premise is that the controlling factor which influences the recrystallization process is mostly temperature (Law, 2014). This connection between different subgrain recrystallizations and temperature can be used as a geothermometer (Kruhl, 1996). For example, prismatic grains will preferably form in low temperature regimes and chessboard pattern in quartz tends to form at higher temperatures (Passchier and Trouw, 2005).

In this master thesis, the grain boundary appearance of quartz and feldspar was used to estimate a temperature regime experienced by the investigated samples (figure 14).
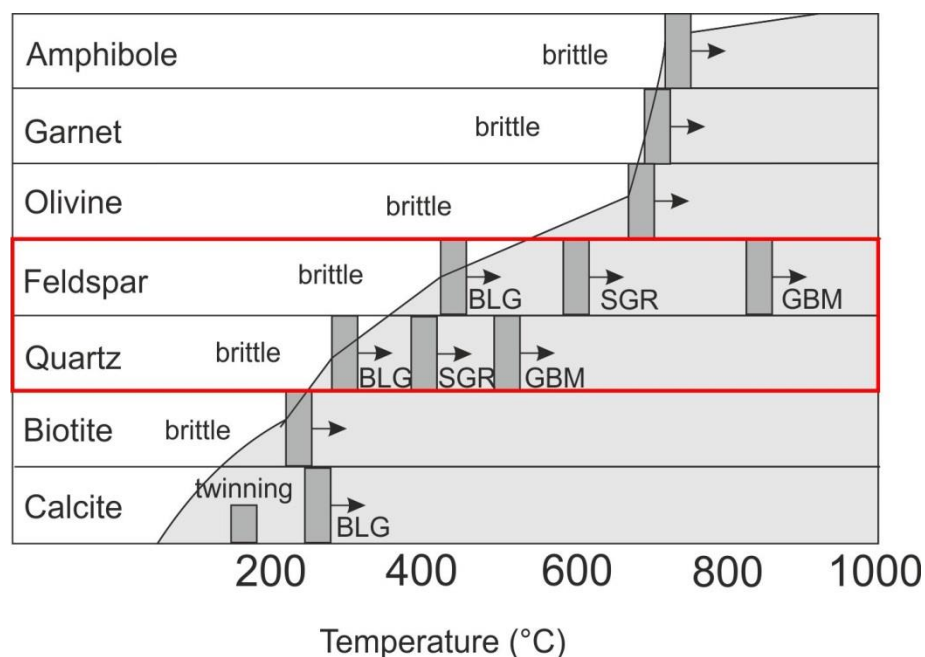
Figure 14 Different deformation mechanisms of alternate minerals for increasing temperature. The ornamented area displays the realm of crystaloplastic deformation. The bars indicate the type of recrystallization (modified after Passchier and Trouw, 2005). The red rectangle marks the used geothermometers.

Also the LPO pattern in quartz can be used as a geothermometer (Kruhl, 1998; Law et al., 2004). In this method a relationship between the c-axes opening angle and temperature was found (Kruhl, 1998). However, high strain rates may alternate the results (Okudaira et al., 1998). Nevertheless, according to Kruhl (1998) a temperature accuracy of ± 50°C can be achieved.

3.2.3.   LPO patterns of Quartz

The preferred orientation of a crystal's lattice is not accidental but follows a specific rule. This is called a "lattice preferred orientation", in short LPO. The opening angle of quartz c-axes changes with increasing temperature as mentioned in chapter 3.2.2 (figure 15; Law, 2014).
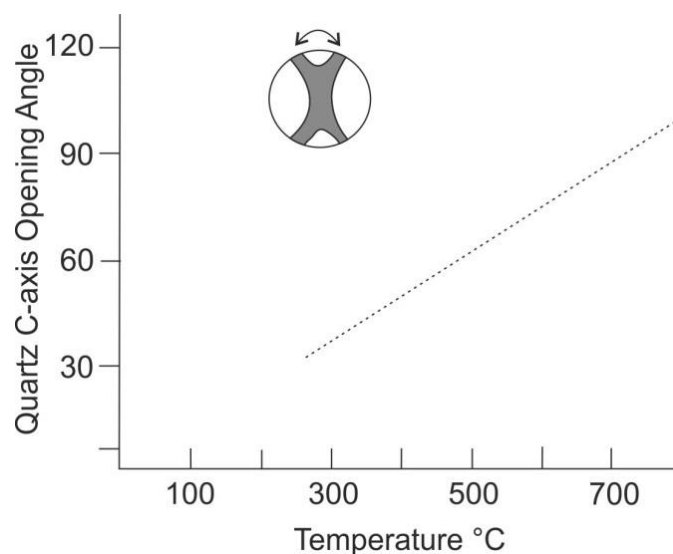
Figure 15 Diagram displaying the relationship of the c-axes opening angle and the deformation temperature. The angle will increase with the temperature (Law, 2014; Kruhl, 1998). Sometimes the high temperature part of the line (showing the linear connection between the temperature and the c-axes opening angle, here punctuated) shows strong steepening due to the quartz exhibiting an increasing size of opening angles to higher temperature (the cause of that is assumed to be the transition of low to high quartz form; Law et al., 2004).

Not only the opening angle of quartz - axes changes, but also the general topology of the LPO pattern is influenced by key factors such as temperature and strain rate. Also a distinction between coaxial and non-coaxial deformation has been made (figure 16).
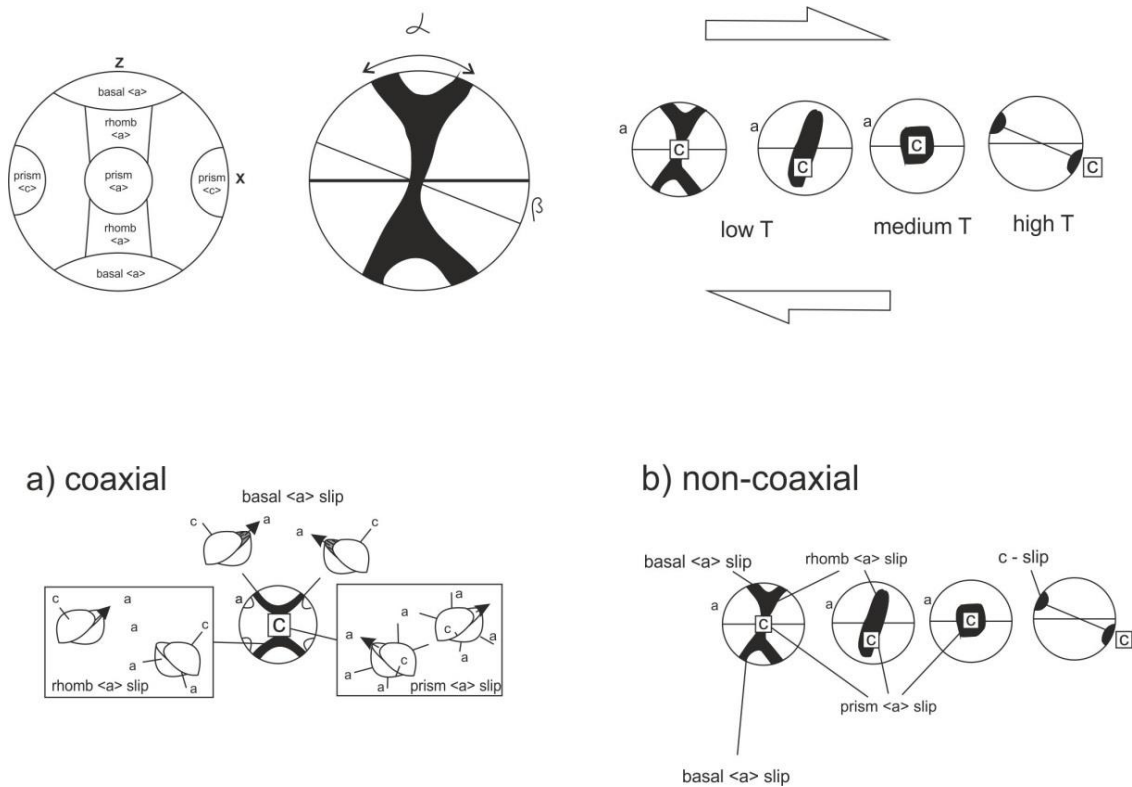
Figure 16 In the upper line on the left side, a sketch of the correlation of location of c-axes and slip systems in quartz is shown. Also the location of the c-axes opening angle α and the angle β between the fabric attractor as well as the line perpendicular to the girdle is indicated (modified after Schmid and Casey, 1986). In the upper line, on the right side, diagrams exhibiting the slip of a preferred c-axis due to increasing temperature is demonstrated.
In the bottom line, figure a depicts the active slip systems during coaxial flow. Figure b displays the pattern which will appear in a LPO-plot during non-coaxial flow and which slip systems will be active (Passchier and Trouw, 2005).

The most striking feature of coaxial plane strain deformation is that the girdle will not be inclined to the trace of foliation and a preference of slip of <a>-direction is given (Passchier and Trouw, 2005). On the other hand, the non-coaxial plane topology is characterised by the formation of new c-axes patterns with increasing deformation (Passchier and Trouw, 2005). Below temperatures of around 650°C, slip in directions of a-axes on basal, rhomb and prism planes are common (Passchier and Trouw, 2005). Above 650°C, slip in c-axes is dominant. Basal <a>-glide is preferred at low temperatures, prism <a>-slip and rhomb <a>-slip will become more dominant at higher temperatures (Passchier and Trouw, 2005). Prism <c>-glide characterises the very high temperature realm (Passchier and Trouw, 2005).

The quartz fabric can be used for shear sense determination. In non-coaxial deformation the slip of the <c> -and <a>- axes gets influenced and depicts an

asymmetry in their girdle appearance (Passchier and Trouw, 2005). This asymmetry is mostly characterised by inclination of their girdle in respect to the trace of foliation and indicating, therefore, the flow caused by deformation in the rock (Passchier and Trouw, 2005). However, shear sense determination should not exclusively depend on quartz fabrics, because complicated girdles and the influence of other minor flows in a rock can falsify the results.

3.2.4. Determination of pure shear or simple shear

A method to construct the flow geometry of rocks can be done by the plot which enables a connection between the angle β (angle between the foliation and the perpendicular to the central line of the girdle; figure 16) and finite strain called Rf for different mean kinematic numbers Wm (figure 17; Grasemann et al., 1999). This is important to indicate which different flow deformed the rocks throughout times (Grasemann et al., 1999). "Protected" quartz minerals can display older deformation events which are completely reworked by younger stages in other quartz minerals.
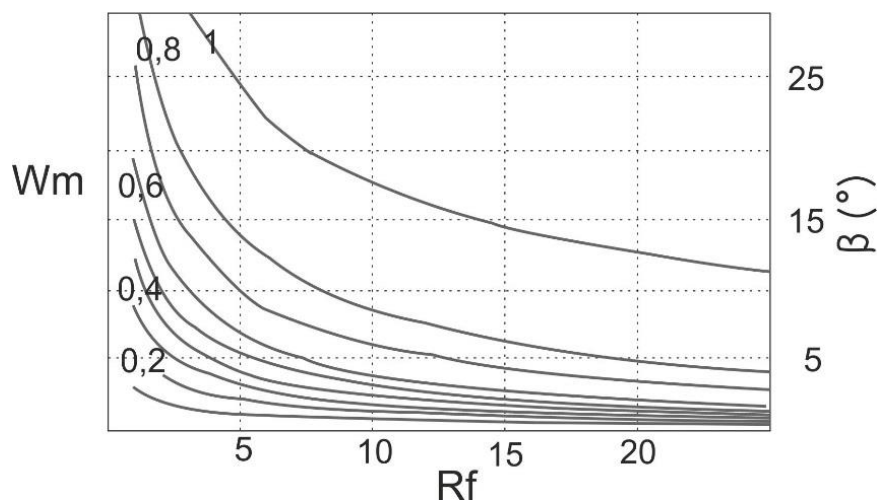
Figure 17 Diagram showing the relationship between the angle β, the mean vorticity number Wm and the finite strain Rf (Grasemann et al., 1999).

This method is especially efficient for low finite strain, since a good distinction for the kinematic number Wm can be made. If Wm is 1, simple shear takes place and if Wm is small (like 0) pure shear is the dominant flow. For high finite strain, this method is not very practicable, because of the Wm contours preferring to touch the abscissa and no

specific difference in the kinematic can be made (Grasemann et al., 2005). The absolute amount of Rf is in many cases hard to determine. However, if no very high strain domains are recognized in field or thin section, a value of Rf is assumed (for example 5<Rf<10).

3.3.   Software applied in this master thesis

Different computer programs were executed in this master thesis:

- ArcGIS (ArcMap 10.3)
- CorelDraw X7 (64-bit)
- Investigator G50 v5.9 Graz
- G50 fabric analyser
- Fabric8
- Nöatlas
  (http://atlas.noe.gv.at/webgisatlas/(S(dzh4bvumlragwpqynrtiignr))/init.aspx?karte=atlas_gst)
- Microsoft Office

4. The Drosendorf Unit:

In this master thesis the lowermost lithotectonic unit is the Drosendorf Unit (also known as Varied Series, Variegated series or Bunte Serie; Klötzli et al., 1999) which is characterised by its wide variety of different lithologies such as marbles, amphibolites, graphite schists, granitic orthogneisses, paragneisses, quartzites and others (Klötzli et al., 1999; Finger et al., 2007; Friedl et al., 2011). The Drosendorf Unit can be differentiated into a basement of Proterozoic age (Dobra gneiss) and a cover of metasediments of a presumed Palaeozoic age (Finger and Steyrer, 1995; Büttner and Kruhl, 1997). A passive continental margin is assumed to be the former depositional environment (Büttner and Kruhl, 1997).

In the investigated area, the Drosendorf Unit is tectonically overlain by the Raabs Serie in the west near the location of "Rollsteine" (figure 18). This master thesis uses the term Drosendorf Unit as a lithotectonic complex containing different lithologies in the Moldanubian part in Lower Austria (Fuchs, 1976; Finger et al., 2007). Paragneisses lie next to marble and quartzites. However, because of the vegetation and weathering, a direct contact is mostly not seen. The lithotectonic unit is named after the village Drosendorf in Lower Austria.
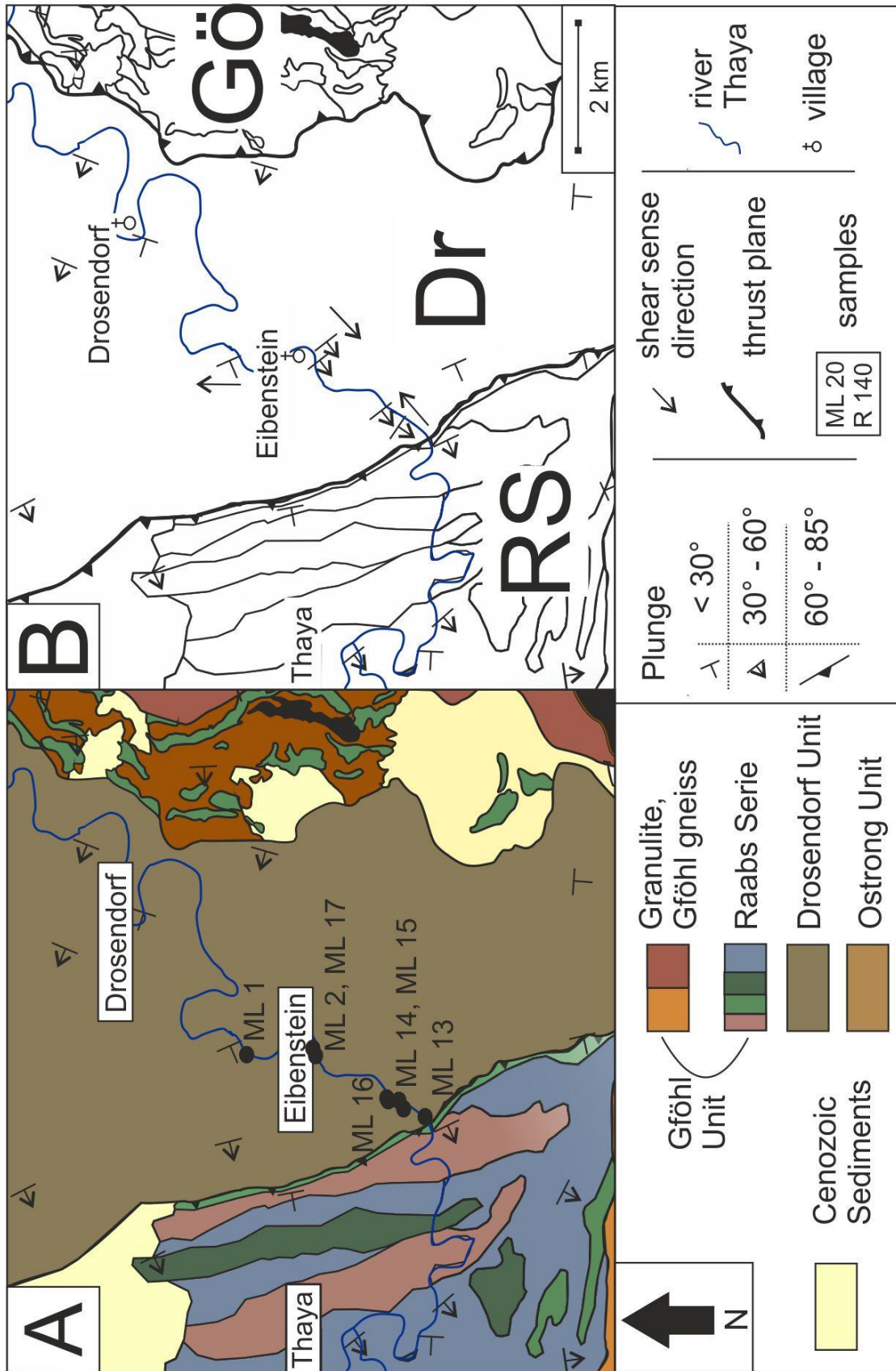
Figure 18 Geological map overview. Figure A on the left side shows the geological map with sample points. The Drosendorf Unit is coloured in light brown. Figure B on the right side displays the structural key points with the orientation data and shear sense directions. RS (Raabs Serie), Dr (Drosendorf Unit) and Gö (Gföhl Unit).

4.1.   Lithological Description

Former mentioned by the name "Varied Unit", this lithotectonic unit is characterised by a wide variety of different lithologies. Information about each lithology, thin section observation, interpretation of macro- and microstructural analyses as well as petrographic studies are pointed out in the next chapters.

The most noticeable feature of the Drosendorf Unit which differentiates it from the Gföhl Unit as well as the Raabs Serie, is the metamorphic layering that parallels lithological boundaries in any scale (Büttner and Kruhl, 1997).

4.1.1. Quartzite:

From a "macroscopic" point of view the outcrops appear not to be altered on the surface (figure 19). The spacing of foliation planes varies from very thin layered (mm) to thick layered (dm) parts. Striking are the reddish layers in the quartzite rocks, as well as the intercalations of dark amphibolite boudins with recrystallized strain shadows composed of feldspar and quartzes.

Figure 19 Quartzite outcrop ("Lazarus", south of the village Eibenstein near the river Thaya; Coordinates N 48.844266° E 015.577551°)

The sampled quartzites (ML 2, ML 16 and ML 17) contain minerals such as quartz, biotite, feldspar, tourmaline, rutile, zircon, amphibole, chlorite, and white mica. The two latter ones are mostly of secondary origin and show evidence of a retrograde metamorphism. The matrix consists of heterogranular grains containing mostly quartz. In some samples (like ML 16), titanite arises frequently together with amphibole, where the latter one has lost nearly its entire colour, due to the titan moving from amphibole to titanite.

ML 2 (X to SW); Equigranular grains with amoeboid grain boundaries deformed by GBM as seen from the left over grains. Comparable large grain size hints at low differential stress.	ML 16 (X to SW); Comparably smaller grains probably due to higher differential stresses. Bimodal grain size distribution of quartz with larger amoebidal grains and smaller grains showing slight shape preferred orientation and bulging grain boundaries. All this might be the result of polyphase deformation and/or displacement partitioning with localized high stress layers.
ML 17 (yz – cut; Y to SW); Matrix of equigranular grains showing GBM. Similar to thin section ML 2.	ML 17 (X to NW); fluid trails pervade the big quartz vein. The trails are deformed and crosscut the quartz grains. The quartz grains of the matrix display GBM.
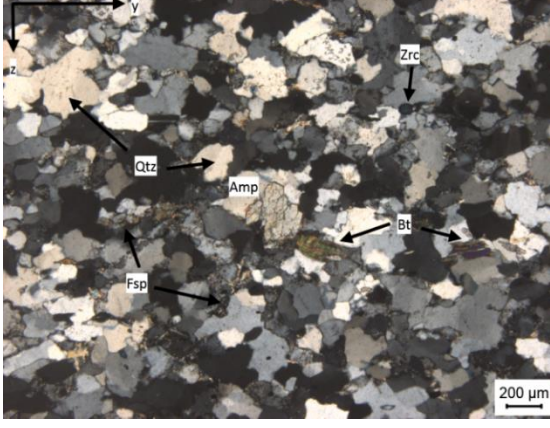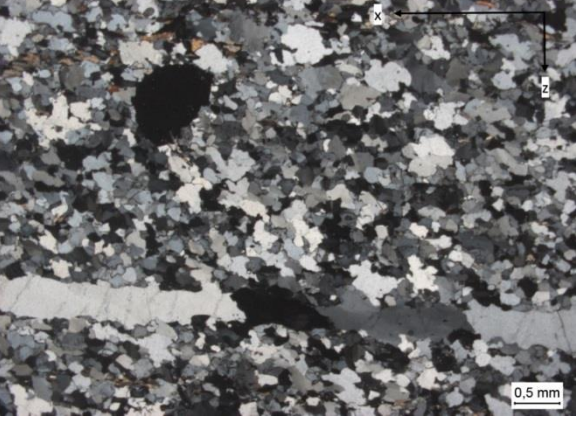
Noticeable are the tremendous amount of fluid trails especially in quartz grains which crosscut the grain boundaries. Saussuritization of plagioclase indicates retrograde deformation events and lower temperatures (Büttner and Kruhl, 1997).

All quartzite samples are characterised by grain boundary migration of quartz and some subgrain boundary recrystallization (ML 16). Principally quartz veins are characterised by subgrain rotation recrystallization which enables the formation of

smaller subgrains. Kinematic analyses are not easily applied here, due to the lack of any shear sense indicators throughout the thin sections. Therefore, mostly lattice preferred orientation and petrographic studies of mineral reactions are used for characterisation. Mild foliation is visible from aligned minerals such as biotite, amphibole and titanite.

Based on the samples thin sections, a decreasing grain size trend is observed from east (near Eibenstein) to west at the tectonic boundary between the Drosendorf Unit and the basis of the Gföhl Unit (Raabs Serie). Further, the shape of the grain boundary migration recrystallization follows this investigated trend changing from amoeboid in the east into more polygonal formed in the west. This trend may indicate an increase of temperature and flow stress from the interior of the nappe through the contact to the Raabs Serie in the west.

4.1.2. Marble

The outcrop of the marble location (figure 20) is very dark in appearance and is composed of parallel foliated layers and layers parallel to the shear zones which contain only mm to cm thick pieces of pulverized rocks. Small boudins of probably dolomitic carbonate are embedded in the rock layers and exhibit domino structures (Passchier and Trouw, 2005). Sense of shear derived from localized asymmetric boudins is to the SW.
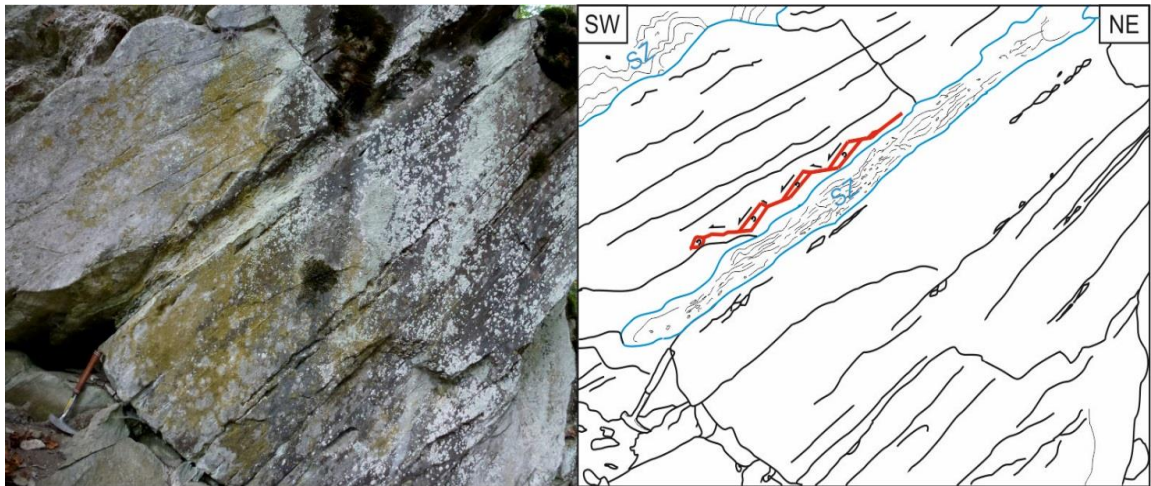
Figure 20 Marble outcrop. Red coloured are brittle structures of marble boudins that depict movement to SW. The outcrop is differentiated into intact segments and parts which are nearly completely sheared into small rock pieces.

This outcrop is quite interesting for being in the near of a tectonic boundary (Drosendorf Unit – Raabs Serie). The outcrop exhibits some brittle features such as the domino structures dipping to SW.

The marble thin section (ML 14) contains minerals such as calcite, zircon and tremolite.

	Deformation of calcite twinning lamella: In this thin section, a type II twinning lamella can be oberserved. Therefore temperatures for the latest deformation event of about 300°C are suggested (Passchier and Trouw, 2005)

ML 14
The grain size is very heterogeneous. Larger grains display twinning deformation mechanism type II twins. Smaller grains are free of twinning lamella and were deformed by grain boundary migration process. The section documents late stage low temperature deformation.

4.1.3.   Biotite-gneiss and – schists:

The outcrops of this lithological unit display strong alternating layering between dark (greenish, amphibole and biotite rich) and light (quartz as well as feldspar) layers. A change of the layer thickness between cm to dm is also seen. The lineation is characterised by shape preferred orientation of dark minerals like amphibole and/or biotite.

Through studying the thin sections (ML 1, ML 15) the following minerals can be distinguished: quartz, feldspar, biotite, zircon, plagioclase, chlorite (secondary), calcite (secondary), tourmaline, opaque phases and also amphibole as well as titanite (just in ML 15).

ML 1 (X to S)	ML 15 (X to SW)
The quartz grains show strong GBM in both samples. Well equilibrated texture between biotite, quartz and feldspar is dominant. It appears that feldspar deformed dynamically. Hence this section represents the high temperature part of the deformation history.	
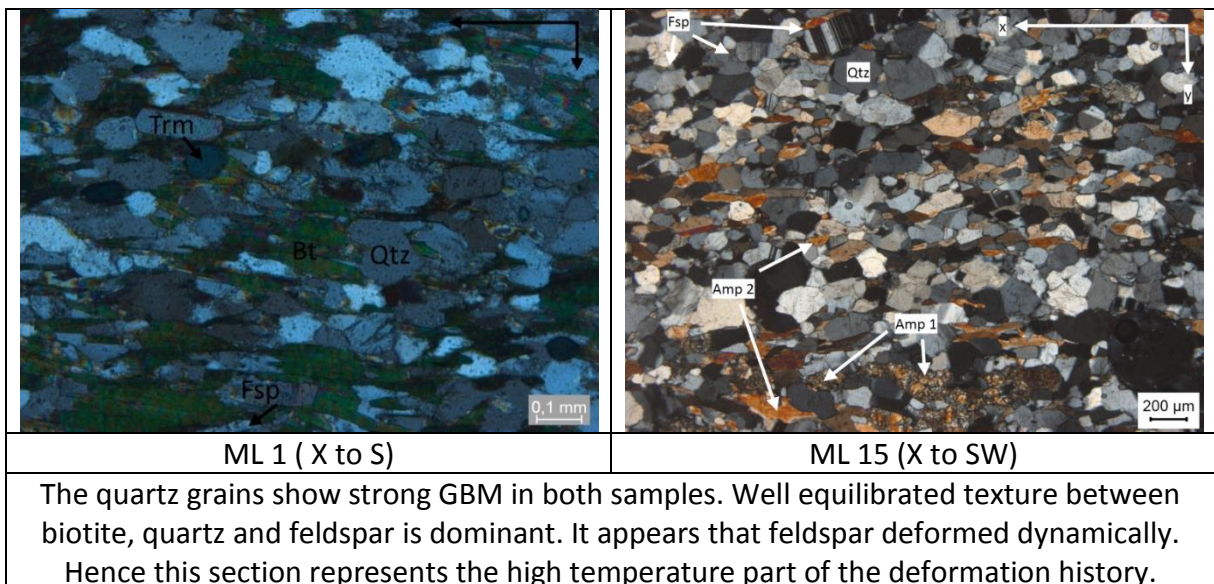
The most common mineral is quartz which exhibits grain boundary migration recrystallization and therefore indicates temperatures of more than 500 °C for the last deformation event (Passchier and Trouw, 2005).

The biotite is adjusted and parallel to the foliation. The quartz boundaries are not limited by the biotite, but they started to grow all around it and depict *window structures* (figure 21). Also the feldspar reacts partly dynamically and shows small BLG around its boundaries. This suggests temperatures exceeding 550°C.
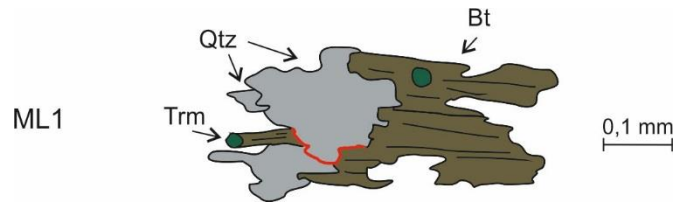
Figure 21 window structures of quartz grains between biotite.

Indications for retrograde metamorphism are displayed by saussuritization of plagioclase and brittle cracks throughout the thin section. Nevertheless, the rocks of this unit have experienced a hot deformation event, implied by feldspar grains which show bulging at their grain boundaries (temperature higher than 550°C; Passchier and Trouw, 2005). Additionally, deformation lamella occurring at the grain borders are seen.

Of importance is also the quite frequent occurrence of tourmaline in the thin section ML 1.

The thin section ML15, which is collected near of a tectonic boundary (Drosendorf Unit to Raabs Serie) indicates adjustments of biotite and amphibole to one direction although a shear sense direction is not displayed through the minerals. Mineral reactions of amphibole 1 to amphibole 2, as well as reaction of amphibole to biotite, occur in this sample. These chemical replacement reactions suggest transformation during cooler temperatures. Later brittle shear zones go through the thin section, indicating also a younger, brittle and therefore colder deformation event. On the other side, GBAR can also be seen in this thin section (ML 15), which is again an evidence for relict high to very high temperatures.

4.2. Structural geological investigations

The foliation data of the Drosendorf Unit displays a general W-dipping trend with stretching lineation dipping to W/SW (figure 22).
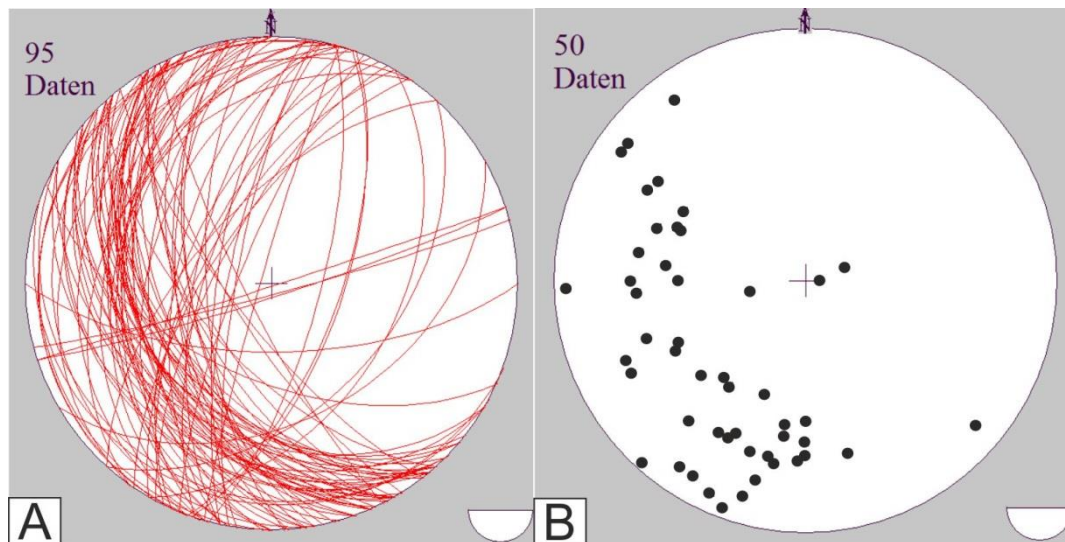
Figure 22 Orientation data of the Drosendorf Unit. A: Foliation data with an overall west-dipping trend. B: Lineation data with west-dipping trend indicated by stretching lineation.

Older deformation events exceed 550°C whereas younger events depict retrogression at ca-300-350°. Later brittle fracturing is probably associated with fluid flow (fluid inclusions and saussuritization). Additionally, flow stress increases towards tectonic boundary and here normal faults to SW are presented. Earlier shear is demonstrated as asymmetric boudins in top NE. On macroscale, layering of rheological different domains arises in development of manifold structures. A block diagram was modelled (figure 23) through investigating a quartzite outcrop.
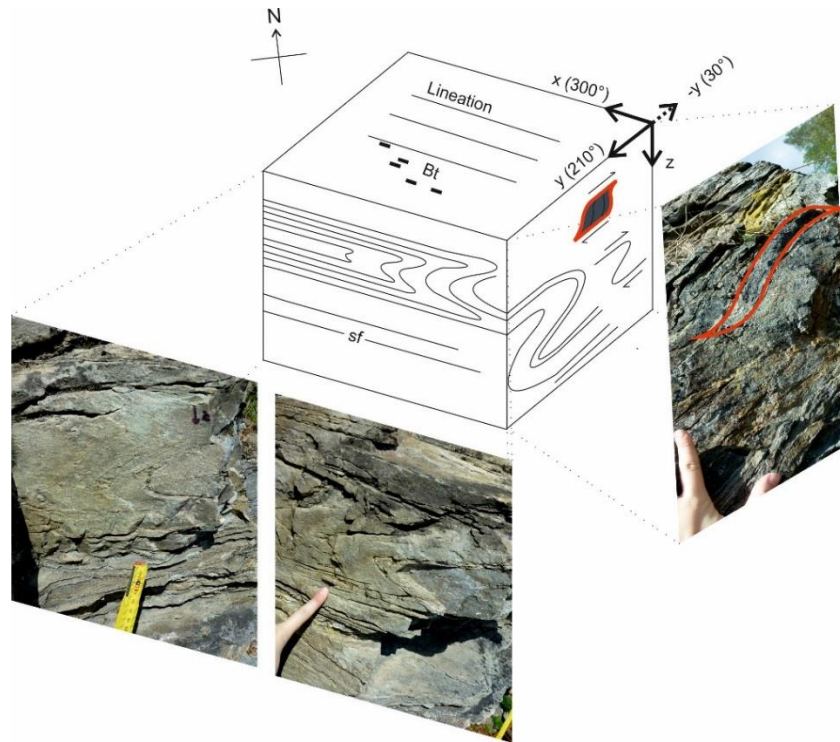
Figure 23 Blockdiagram based on the structures and textures seen in different sections of a quartzite outcrop. The xz section is parallel to the macroscopically visible main stretching lineation and perpendicular to the foliation (sf). Yz is perpendicular to the foliation as well to the lineation and xy is parallel to the foliation.

In the created block diagram the xz – cut depicts the foliation sf and the so-called "m"-folds. The foliation sf is refolded to nearly recumbent folds. The yz – cut displays "s"- and "z"-folds as well as sigmoidal bodies, like amphibolite boudins, incorporated into the softer lithologies. Those exhibit top to E displacement. The xy – cut shows stretching lineation (S to E) with a dip of 30 to 40 degree indicated by biotite minerals which grew orientated on the surface. Striking is that along the xz – cut no sigmoidal bodies or folds (excepted "m"-folds) appear.

A deformation evolutionary path is constructed and interpreted depending on the structures of the outcrop (figure 24). Different deformation events are presented. In chapter 4.5 a table, based on the structures observed in the field as well as under the microscope and the results gained through rheology studies of quartz, has been created.
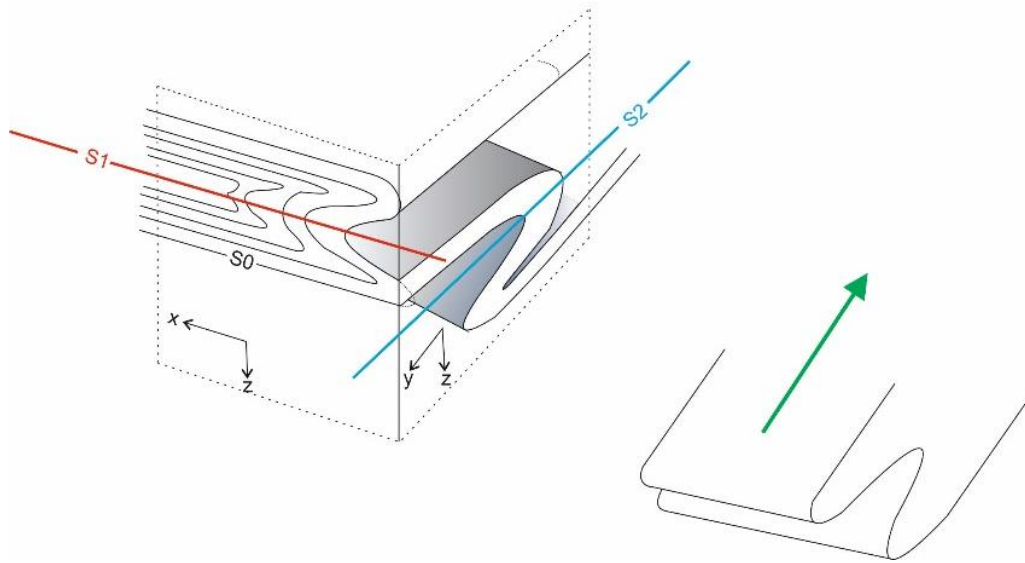
Figure 24 Structural evolutionary model interpreted on the appearance and occurrence of folds and sigmoidal bodies. Deformation mechanisms of the thin sections suggest deformation at temperatures exceeding 550°C.

No fabric asymmetries (shear senses) have been observed in the xz-section, but development of a strong foliation and isoclinal folds. The yz section displays asymmetric fabrics such as asymmetric boudins, sigmoidal quartz fishes and asymmetric folds. Shear senses derived from these structures is top NE.

An earlier deformation event is indicated by S0. Compressional deformation may have caused event S2. The latest deformation event show top to NE flow.

Folds display Ramsay type 2 interference pattern with a first isoclinal folding event with horizontal axial plane, probably associated with enhanced flattening geometry. This is overprinted by a second folding event with B-axes (F2 – S2) perpendicular to B-axes B1 (S1) and an inclined axial plane.

4.3.   Deformation and metamorphic reactions

In the following chapters, metamorphic mineral reactions and rheology as well as textures of quartz are analysed and presented. Specific mineral reactions take place at certain temperatures and pressure conditions and give hints at main metamorphose conditions as well as retrograde deformation processes.

Deformation happens on the scale of mineral grains and contains a huge number of different processes (Passchier and Trouw, 2005). This master thesis especially investigates and interprets the deformation history of quartz.

The quartz grains develop a strong tendency of orienting their mineral axes to a specific temperature status. Because of this tendency and the frequency of the most occurring mineral lattice axes, a specific temperature range can be estimated.

4.3.1. Metamorphic mineral assemblages and reactions

After Petrakakis (1997), peak temperatures of about 700 – 800°C and pressures of about 7-9 kbar were experienced in the Drosendorf Unit near the Danube valley. Some examples of mineral reactions are given in a small table below with rough estimates on temperatures and pressures. Since pressure-dependent reactions are rare, the pressure data shown in the table below are very rough estimations.

ML 15	Bt – Amp - Gneiss	Amp -> Bt	Retrogression to Ca. 500 – 650 °C, 4-7 kbar (?)
ML 2, ML 17	Quartzite	Bt -> Chl	Retrogression, 550 – 300°C; 3-6 kbar (?)
ML 2, ML 17	Quartzite	Ms growth	Retrograde 550 – 300 °C; 3-6 kbar (?)
ML 2, ML15, ML 16, ML 17		Plagioclase -> Saussuritization	Ca. 300°C; 2 – 6 kbar (?)

4.4.   Rheology of Quartz

The table below summarizes the microfabrics seen in the thin sections collected from the Drosendorf Unit. On the general, grain boundary migration recrystallization (GBM) is formed by most of the quartzes. Also subgrain rotation recrystallization (SGR) and to a lower extend bulging can be detected.

Because of the occurrence of those two types of dynamic recrystallization in the thin sections, high temperatures can be assumed (Passchier and Trouw, 2005).

Quartz (table modelled after Fritz et al., 2005)	Temperature increase →			Diffusion Disc quartz D Chessboard pattern Ch
	BLG U= undulatory extinction	SGR	GBM amoeboid - polygonal	
ML 1	X		XX	
ML 2			XX	
ML 15			XX	
ML 16		X	XX	
ML 17		XX	XX	Ch D

The occurrence of chessboard pattern displays dominating c-slip which is an indication for high temperatures (Büttner and Kruhl, 1997; Mainprice et al., 1986). Later retrograde overprinting may have recrystallized the quartz grains under lower – grade deformation mechanism like SGR and BLG (Büttner and Kruhl, 1997; Kruhl, 1996). Mostly an old and big quartz grain has been disintegrated to smaller new quartz grains displaying grain boundary migration recrystallization.

4.4.1. Textures of Quartz

The sample ML 1_matrix, ML 13 as well as ML 17 (lower temperature) display basal <a> glide and ML 15 as well as ML 16_matrix exhibit dominant prism <c> glide (figure 25). The preference for prism <c> glide indicate temperatures above 700 to 800 degrees. Younger events are displayed by LPO – girdles which are the result of a combination of basal <a>, rhomb <a> as well as prism <a> glide (ML 1_vein, ML 2_vein). The inclination of such girdles indicates shear sense direction. Only the quartz veins of the quartzites exhibit those typical LPO-girdles and display shear sense directions to N/NE. These colder events, indicated by basal <a> glide of quartz, may be related to a deformation event called D2 (see chapter 4.5.).
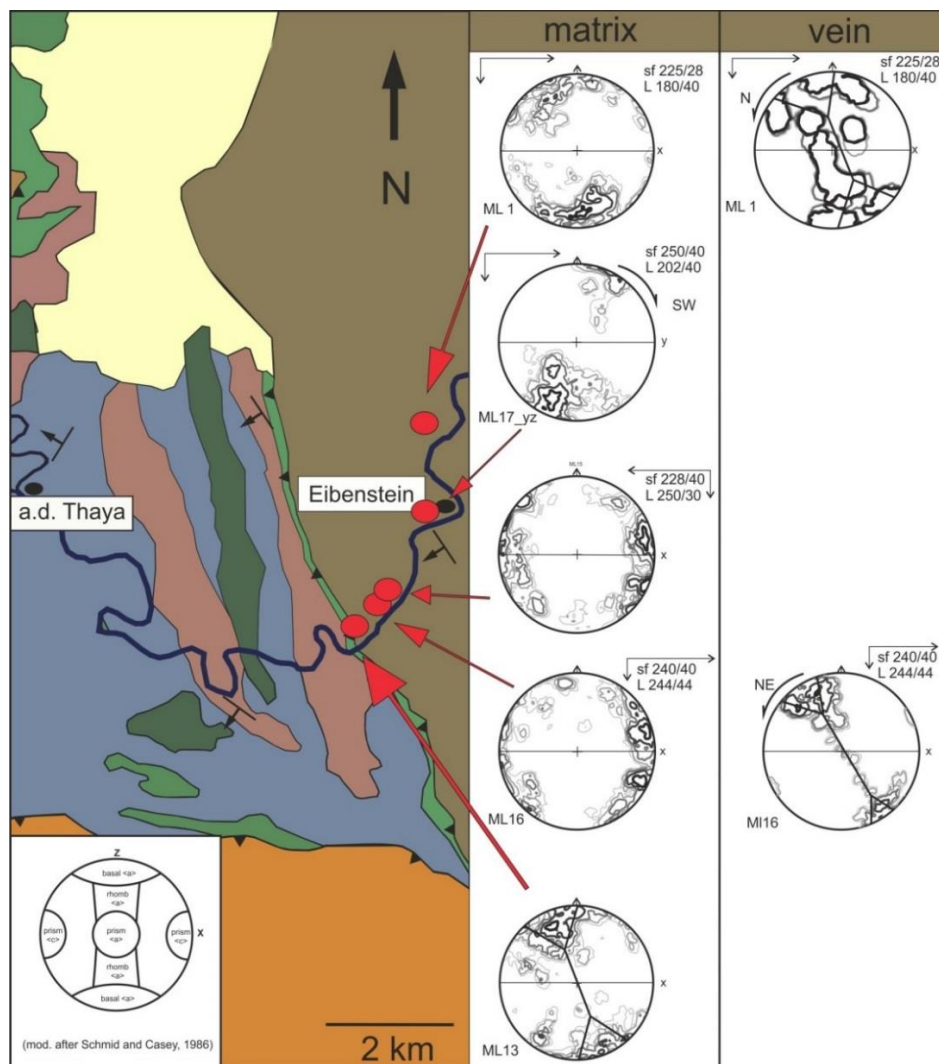
Figure 25 Geological map overview of the Drosendorf Unit. The red points are the locations of the collected samples with analysed LPO girdles of quartz. The table on the right side differentiates the LPOs of quartz into investigations of matrix grains and recrystallized vein grains. In the LPO-girdles observed in the veins, a shear sense direction to N/NE is indicated.

Especially temperatures above 600 degrees are common. Only younger recrystallized quartz veins display colder temperatures and show typical LPO quartz girdles. Furthermore, the quartz girdles depict a non-coaxial behaviour and indicate shear sense direction. The LT girdles give top N-NE displacement. However, one sample indicates shearing into a south-western direction.

In the figure 26 a trend to wide opening angles is seen which correlates with syn-tectonic temperatures.

sample	Lithology	Opening angle α	Temp.
ML 1_vein	Bt - gneiss	78°	600 - 650°C
ML 16_vein	Quartzite	55°	400 - 430°C
ML 13	Bt - gneiss	76°	600°C
ML 17	Quartzite	78°	600 - 650°C
ML 15	Bt – Amp - Gneiss	140°	>800°C
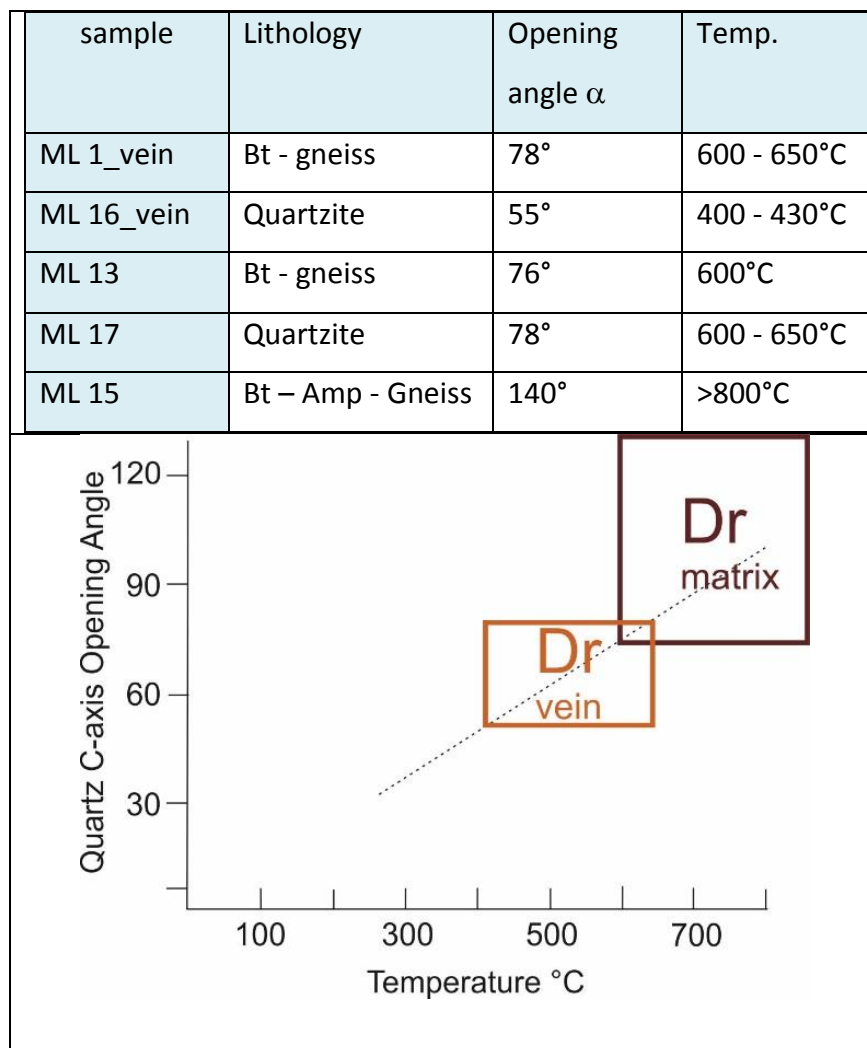
Figure 26 Opening angle of quartz c – axes (vertical axis) vs temperature (horizontal axis; modified after Kruhl, 1998; Law, 2014). The opening angles measured on the minerals from the Drosendorf Unit are summarized as rectangles. A differentiation of samples based on vein minerals (Dr vein) and matrix minerals (Dr matrix) is used. The recrystallized quartz vein minerals clearly show a tendency to lower temperatures than the quartz minerals from the matrix.

The opening angles of the quartz c-axes analysed in quartz can be used as a geothermometer (Kruhl, 1998; Law, 2014). Based on the wide opening angles, the rocks of the Drosendorf Unit lay strongly on the right side in the diagram after Kruhl (1998, figure 26). Opening angles estimated on the LPO quartz girdles taken from the matrix differentiate between 75° to 140° and temperatures between 600°C to more than 800°C can be assumed. The opening angles taken from the LPO quartz girdles investigated from the recrystallized quartz veins vary between 55° to 78° and conclude to temperatures of 400 to 650°C.

4.5.   Summary of the Drosendorf Unit

In summary, most samples display GBM, indicating syn-tectonic temperatures exceeding 500-600°C. Associated quartz textures with prism c glide event point to 600°C as lower limit of temperature during this deformation increment. Based on the data gained during this master thesis, three deformation events are suggested: D1, D2 and D3. The first deformation event is D1 where the high temperature evolved. Stretching associated with this deformation was NW-SE directed.

Subgrain rotation and rare bulging is associated with overprinting of a younger event (D2 or D3). During the subsequent deformation event, the foliation S1 (originated in D1) was refolded to recumbent isoclinal folds with horizontal axial plane. This may be D2 and shows low to middle temperatures.

The last folding event (D3) trends seemingly to NE which would correlate well with the deformation structures of small folds and sigmoidal boudins. Finally, semiductile to brittle structures parallel to the tectonic boundaries crosscut earlier formed fabrics.

On the basis of the results gained during this master thesis, a table has also been created:

D1	D2	D3
HT-deformation	LT-deformation	LT-deformation (ca. 330°C)
Coaxial flow	Top to NE flow	Normal faulting
	Thrusting over Gföhl Unit	

5. Raabs Serie:

The base of the Gföhl Unit consists of the migmatic Raabs Serie (figure 27) and represents a former ocean floor (Fritz, 1995), also known as the Raabs Ocean which was part of the Rheic Ocean (Finger and Steyrer, 1995; Schulmann et al., 2009). This Raabs Ocean was not a big ocean, but a continental rift which just touched the oceanization (Finger and Steyrer, 1995). Age data of a plagiogranite-gneiss from the Raabs Serie suggests ages of about 425 Ma and is assumed to represent a rifting event during the Palaeozoic (Finger and von Quadt, 1995). Over time, the ocean got subducted under the Moldanubian Unit which led to the final collision of the Moldanubian unit with Brunia (Finger and Steyrer, 1995). During the convergent movement between Brunia and the Moldanubian unit calc-alkaline magmas were generated and incorporated into the Raabs Serie (Fritz, 1995).

According to Racek et al. (2006) the base of the migmatic Raabs Serie is formed by an anatectic gneiss, the so-called Kollmitz-type gneiss, which also shows a migmatic fabric. Below the anatectic gneiss an eclogite layer is located, which should be exposed near the tectonic boundary to the Drosendorf Unit (more information in the publication of Racek et al., 2006). Bt – grt – gneisses make up the most of the lithology from the migmatic Raabs Serie. The samples of the Raabs Serie are characterized by melanosome layers with occurrences of garnet and biotite as well as leucosome parts consisting of quartz and feldspar. Migmatisation created sharp rheology contrasts between "soft" melt and "strong" mafic layers. Therefore, deformation within the Raabs Serie is melt-enhanced deformation with melt portions moving into tensional domains such as boudin necks or tension gashes. In the scale of thin section minor dynamic crystal fabrics are visible.
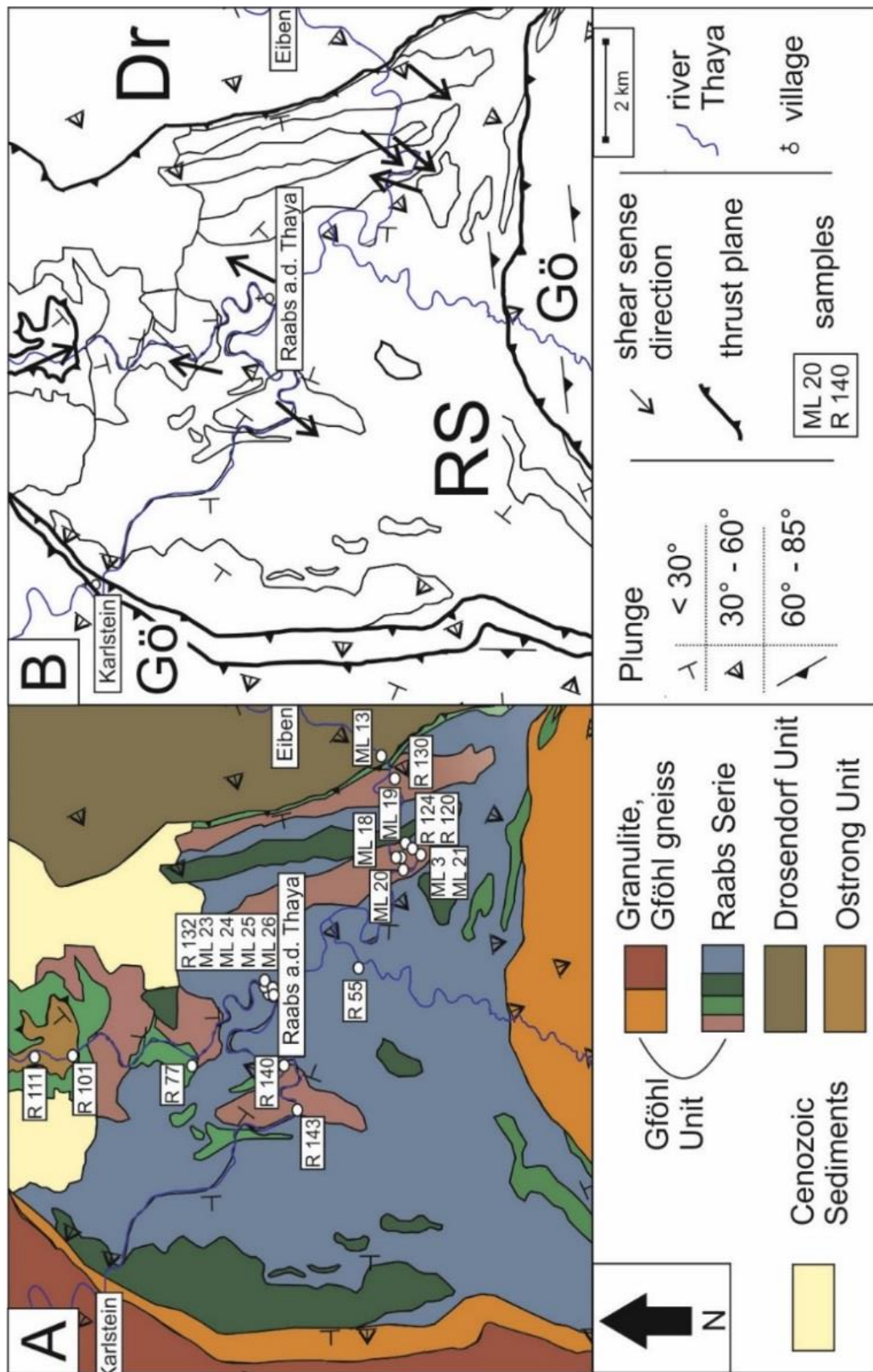
Figure 27 Geological overview of the Raabs Serie surrounded to the east by the Drosendorf Unit and to the west as well as to the south by the Gföhl gneiss and granulites. A: Geological map with sample points and plunge as well as orientation data. B: Structural geological overview map.

5.1.   Thin section description:

A prominent feature appearing throughout the thin sections of the migmatic Raabs Serie are the typical migmatic mineral layering and the occurrences of "augen" – structures. The minerals feldspar and garnet have strain shadows of biotite and recrystallized quartz (figure 28). The matrix consists of feldspar and elongated disc – shaped quartzes, which disintegrate into smaller polygonal quartz grains due to dynamic recrystallization processes. Noticeable are the lower temperature processes such as core mantle structures and SGR processes which enable the crystallization of smaller quartz grains due to stress differences in the crystal lattice. Fluid trails, which crosscut quartz minerals and even penetrate the grain boundaries of neighbouring minerals, are also observed in the thin sections of the Raabs Serie.

Other minerals embedded in the quartz matrix are big feldspar grains, biotite, garnet, sillimanite, apatite, zircon, titanite, mica as well as secondary chlorite. Striking are the features of brittle deformation and mineral reactions which occur in feldspar or the latter is a part of it. Myrmekitisation of quartz and plagioclase arises similar to worm – like shapes. Deformation lamella reaching from the rim of the feldspar mineral into its core are quite frequent and indicate high stress sites (Passchier and Trouw, 2005). The surface of the feldspar grains is disfigured by flame-shaped albite lamella and retrograde processes like saussuritization.

Through investigating the thin sections, hot deformation characteristics of the mineral appearances can be summarized (figure 28). The quartzes display grainboundary migration recrystallization and subgrain rotation crystallization (see chapter 5.3.1.). Even feldspar grains show bulging in their grain boundaries, which suggests temperatures of more than 550°C (Passchier and Trouw, 2005).

Several cracks are running through the thin sections and are filled with orange minerals, presumably Fe – oxides, or recrystallized quartz with mica, indicating also younger and cooler deformation events.

ML 18 "Kollmitz – type Gneiss"	ML 19 "Kollmitz-type Gneiss"
ML 23 Raabs Serie	ML 24 Raabs Serie
ML 25 Raabs Serie	R 55 Raabs Serie
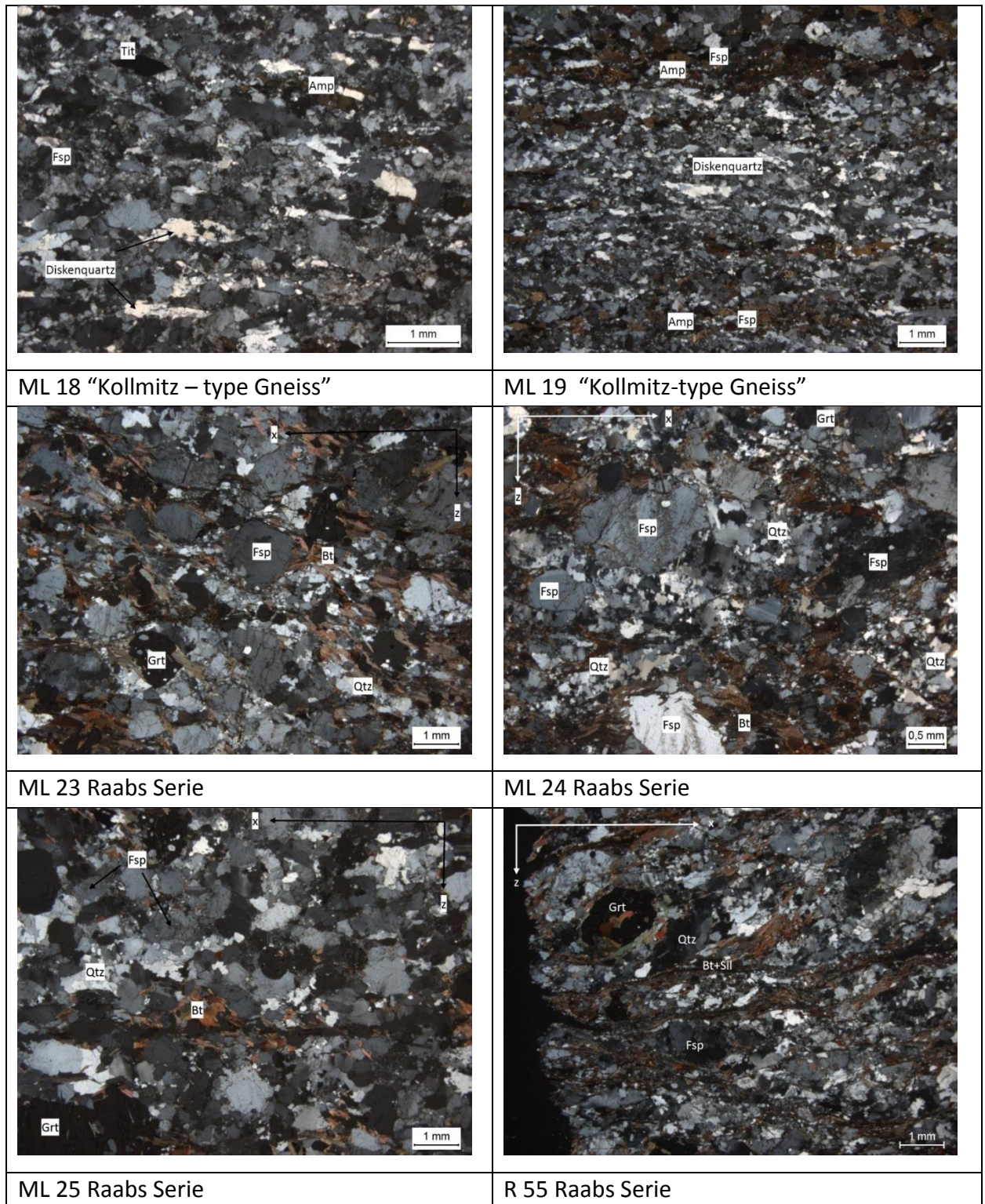
Figure 28 Thin section examples collected from the Raabs Serie. The first two (ML 18 and ML 19) are taken from the Kollmitz – type gneiss which protrudes from the Raabs Serie in the east. The gneiss is characterised by strong retrograde features such as emplacement of biotite or garnet by chlorite and saussuritization of feldspar. Nevertheless disc-shaped quartzes as a relict of hot temperature deformation are detected. Quartz shows GBM features and in parts (ML 19 centre) high strain domains with smaller grain size due to enhanced differential stress and probably cooler temperatures.

The migmatic Raabs Serie samples (ML23, ML 24, ML 25 and R55) depict "fresher" structures. In a matrix consisting of recrystallized smaller quartz grains and feldspar, big feldspar grains, biotite, garnet, sillimanite and other minerals are embedded.

The thin sections of the Kollmitz-type gneiss (ML 13, ML18 – ML 21) appear to be more altered than the samples from the Raabs Serie (ML 23 – 26). The plagioclase of the Kollmitz-type samples exhibits strong saussuritization. Chlorite which replaces biotite and/or garnet in these samples is frequent.

In contrast, the thin sections made of the Raabs Serie display nearly fresh structures with highly migmatized features. This suggests a "lower-grade" tectonic contact between the migmatic gneisses of the Raabs Serie and the Kollmitz –type gneiss (figure 29).

ML13: myrmekite (Plagioclase and quartz)	R55: stress lamella in feldspar
R143: flame shaped dissolution structures in feldspar	R143: bulging characteristics at the contact zone between two feldspars

| ML13: saussuritization of plagioclase | R55: fibrolithic sillimanite with bigger sillimanite microlithons |
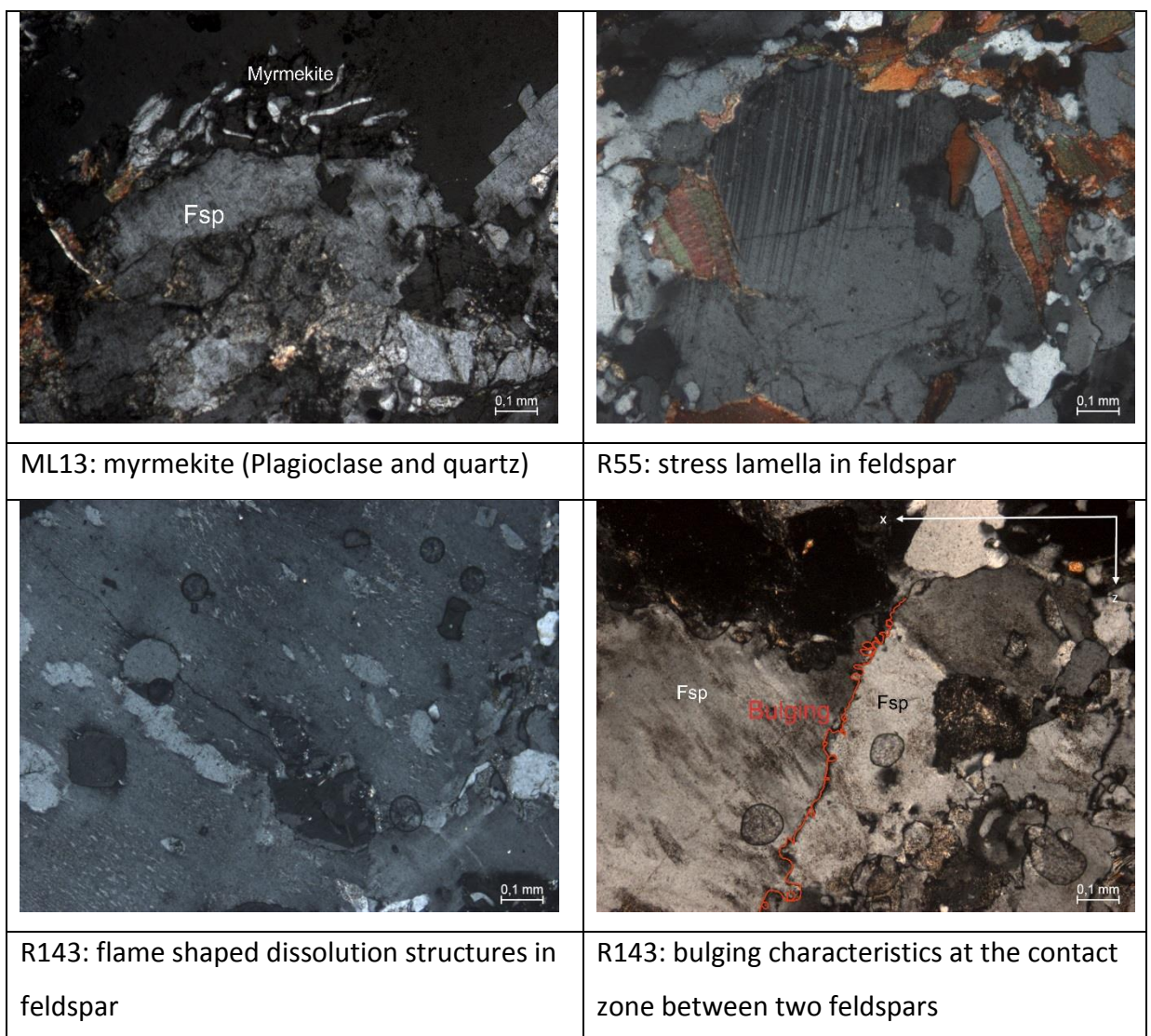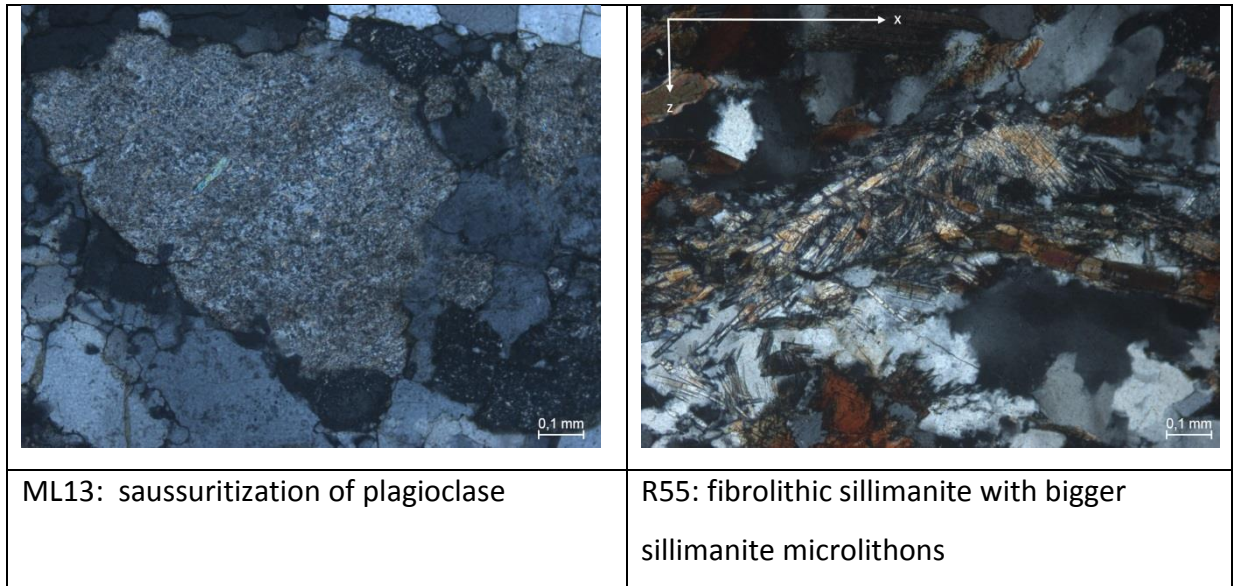
Figure 29 Metamorphic mineral reactions caused by distinct deformation conditions.

5.2.   Structural geological investigations

On either microscale or macroscale, the Raabs Serie displays typical migmatic characteristics. Distinct dark layers alternate with light layers and are deformed together in complicated fold structures. Boudins of amphibolite or feldspar together with quartz are embedded in the migmatic rocks.
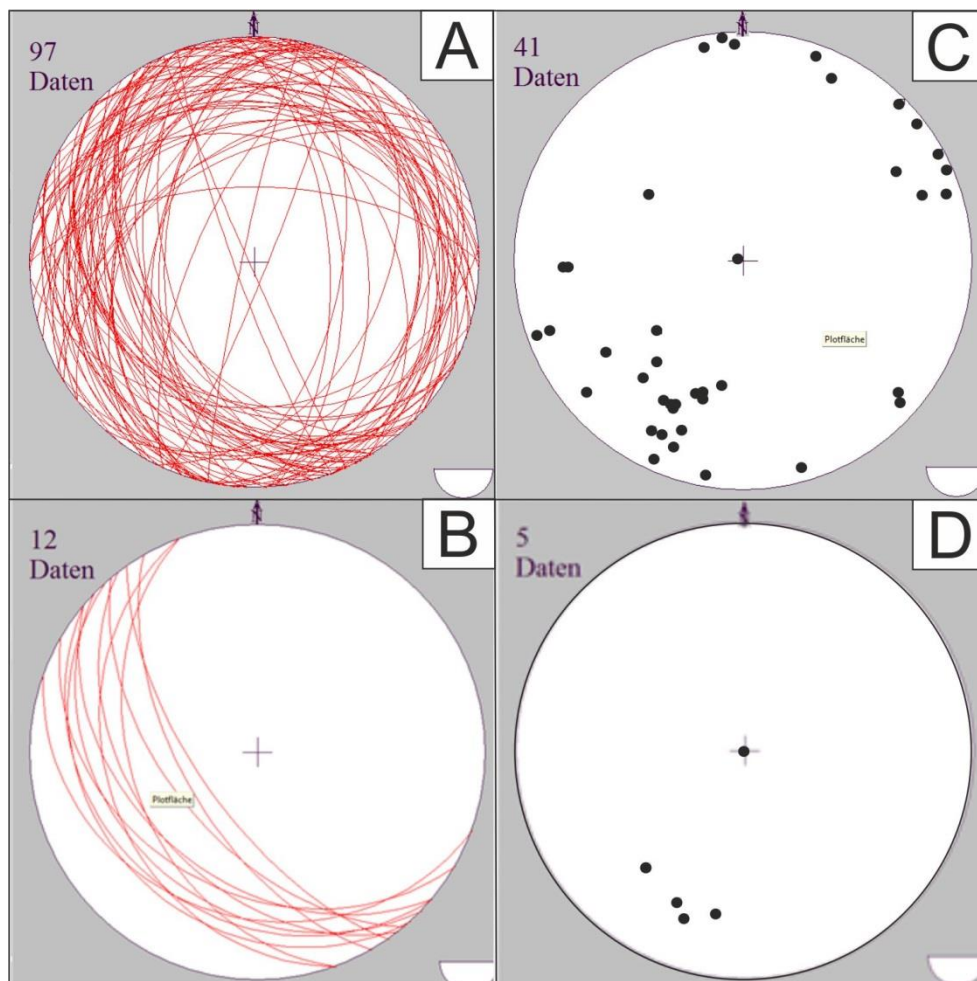
Figure 30 Foliation and stretching lineation of Raabs Serie (A, C) and Kollmitz-type gneiss (B, D)

A block diagram was constructed and summarizes the structural geological features that are detected in the field.

The xz – cut is characterised by the foliation sf and elongated boudins. The amphibolite boudins are very fine grained and may represent former lava flows (Finger and Steyrer, 1995). The strike of the foliation from NW to SE and a dip to W/WSW could be

investigated. Exceptions of the former are measurements of foliation which dip to E or NE (figure 30). Some of these results were gathered near of strongly folded sections. Intriguing is the tendency of fold structures being only visible in the yz – cut. Those folds are characterised by complicated multiple folding features. Normally a big and dark melanosome is surrounded by thinner parts of leucosome layers which include secondary folds (figure 31), but melt infiltrations are folded together with the gneisses und suggest melt enhanced deformation. Therefore, the migmatisation of the Raabs Serie and its folding has happened during similar time.
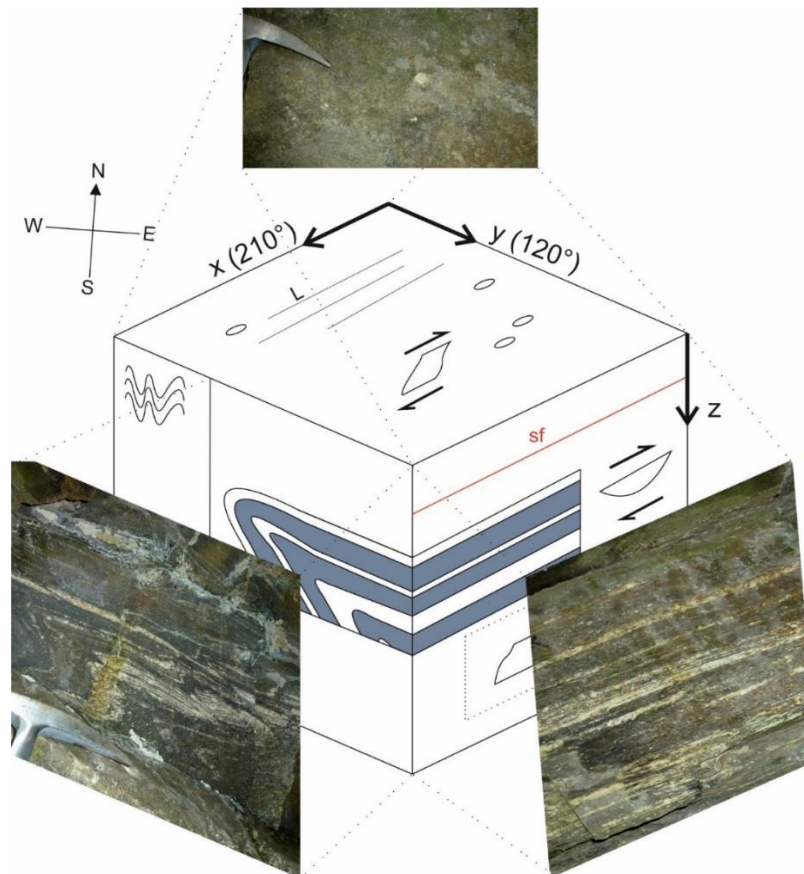
Figure 31 Blockdiagram of the migmatic Raabs Serie with in-situ taken pictures

The xy – cut shows minerals, such as garnet or feldspar, protruding from the surface by making small knobs of varying size (some millimetres to 1 cm). The lineation has a strong SW trend. Seldom lineations are pointing to northern or south-eastern directions. It is more likely that the feldspar and quartz recrystallized along the movement direction and both formed stretching lineations together.

Based on the information gathered from the outcrops, a transport movement to NE is suggested. This assumption would correlate well with conclusions in existing papers (such as: Racek et al., 2006; Fritz, 1996).
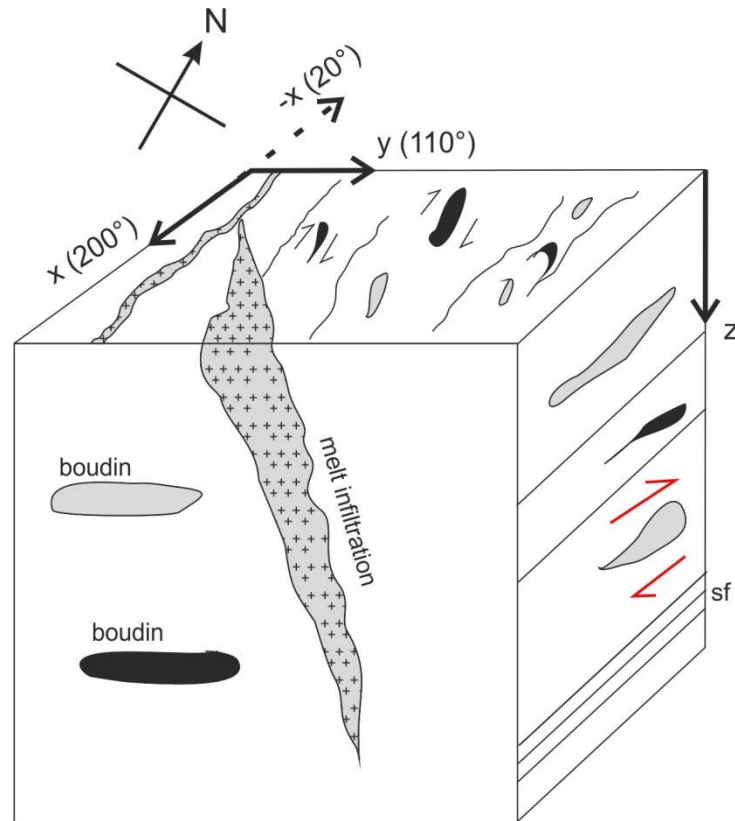
Figure 32 Block diagram of the Kollmitz-type gneiss

A second block diagram with the information gathered by studying outcrops in the Kollmitz-type gneiss is constructed (figure 32). It is very similar to the block diagram of the migmatic Raabs Serie. However some differences can be noted.

Light coloured melt infiltrations of coarse grained minerals such as feldspar arise quite frequently while crosscutting the lithology. Mostly they are not folded like in the typical migmatic Raabs Serie but crosscut the foliation which suggest melt infiltrations after migmatisation.

The stretching lineation is distinctly pronounced by sigmoidal dark mineral bodies and elongated grow of feldspar or biotite, which show a strike-slip movement.

Nevertheless, the Kollmitz-type gneiss likewise to the Raabs Serie shows lateral movement to northeast. Also the foliation shows a strong W/WSW dipping orientation.

5.2.1. Structural investigation of folds

The detected folds on the yz-cuts of the outcrops vary between rare symmetric folds and mostly asymmetric folds. In the majority of cases axial planes of folds dipping in to western direction are observed (figure 33). Scarce are the exposed folds which dip into other directions.

fold limbs
fold axis surface
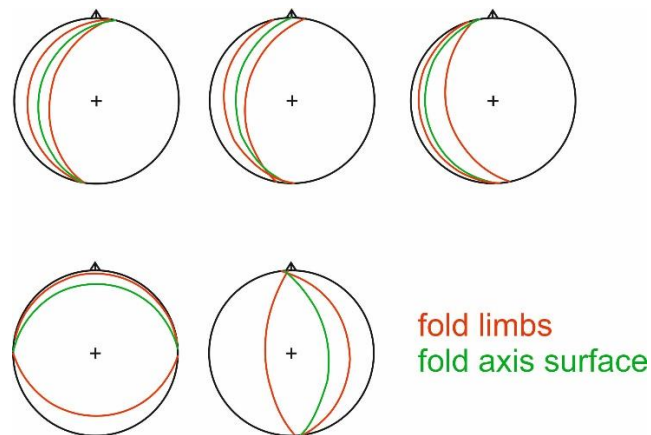
Figure 33 Representation of the folds measured from an outcrop near the village Raabs an der Thaya

The migmatic behaviour of the rocks from the Raabs Serie is marked by the layering of lighter and darker mineral layers which are complicatedly folded. Melt infiltrations made of coarse-crystallized feldspar and quartz grains are embedded into the folds or intersect the fold axis (figure 34). Additionally garnet occurs with varying size (some millimetres to 1, 5 cm) preferably in the near of the fold axis.

The occurrences of mafic boudins in the Raabs Serie are quite frequent and suggest an extensional deformation event. Also the kinematic flow can be interpreted by studying the elongation as well as the inclination of the boudins and the minerals which flow around them (figure 35). A NE-flow is interpreted by the found boudins of the Raabs Serie.

Figure 34 Migmatic rocks from the Raabs Serie. Highlighted is the layering of dark and light sections. The small red circles are garnets. The garnet prefers to grow in the fold hinge and seems to develop during the deformation. In the left section of the picture a fold axis with garnet growth is drawn. Light melt infiltrations are folded together with the rocks of the Raabs Serie.

Figure 35 Amphibolite-boudin in the Raabs Serie. Recrystallized feldspar is found around the mafic boudin. Stretching occurred between NE-SW. Flow to NE direction is suggested by studying the elongated minerals around the boudin in the field. Boudins are quite frequent in the Raabs Serie and suggest a past extensional regime.

5.2.2. Microstructures

From the microstructural point of view, typical "augen – structures" are formed by garnet or feldspar grains with strain shadows build-up by biotite or recrystallized quartz (figure 36). The strain shadows of these "augen – structures" indicate shear sense direction towards NE.
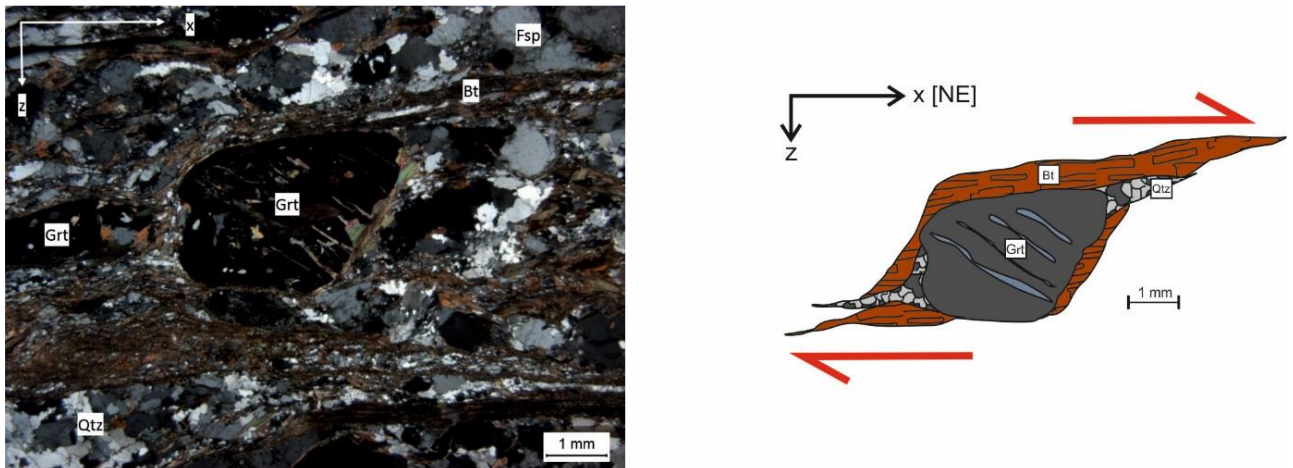
Figure 36 Thin section R77 exhibiting garnet with a strain shadow consisting of biotite and recrystallized quartz grains. On the left side a picture of the thin section is shown. The right side displays the highlighted sheared grain with strain shadows. Parallel tension gashes filled with biotite in the garnet depict a maximal stress regime (from upper left to lower right). Shear senses indicate top to NE.

Sigmoidal bodies of amphiboles or titanites are developed during shear deformation and are also markers for the direction of the shear sense. Striking are the shear zones which are build-up by a combination of fibrolithic sillimanite, sillimanite microlithons as well as biotite and stretch through the thin section. These mineral shear zones can also form typical SC – textures (figure 37).
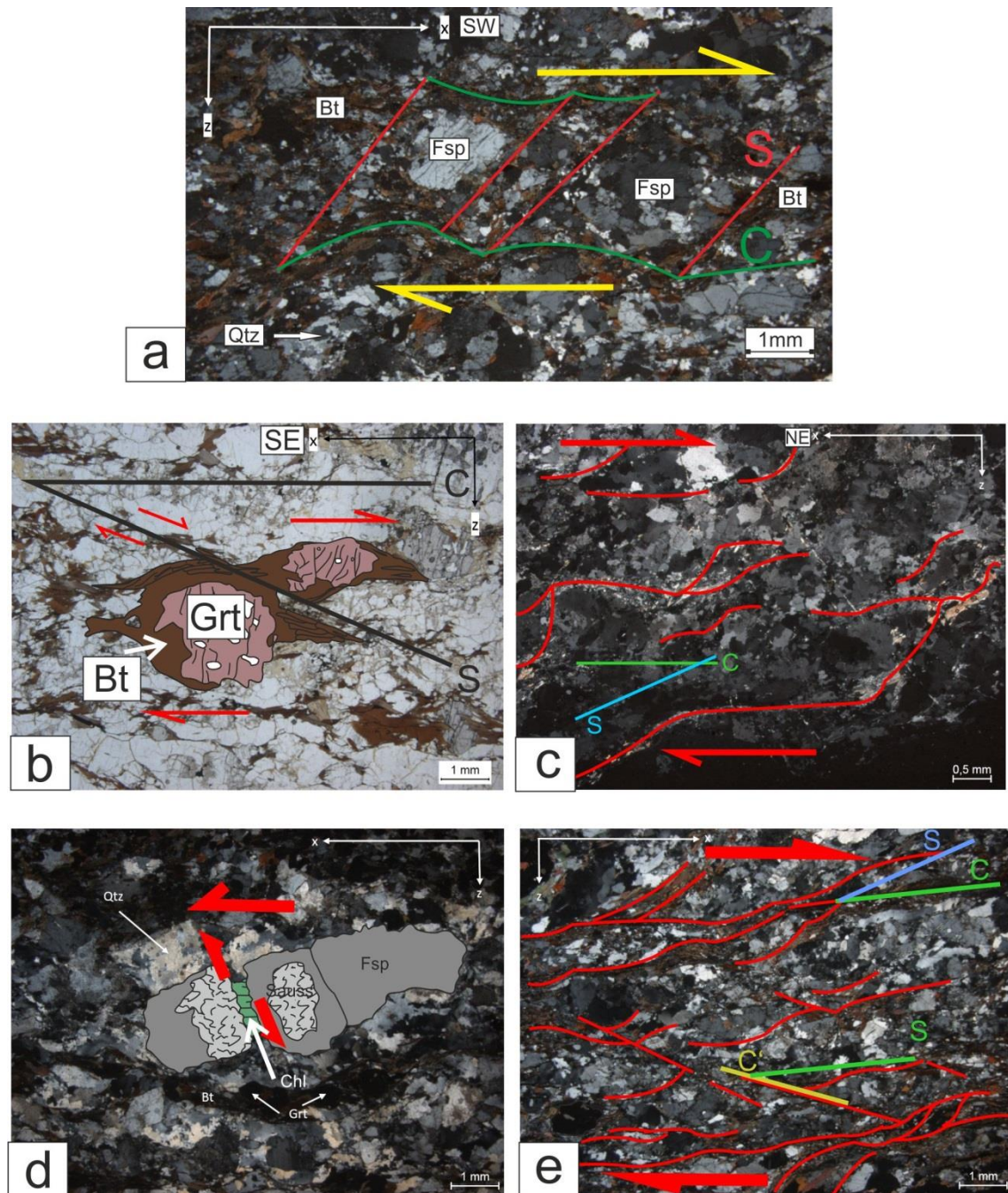
Figure 37 Typical kinematic indicators seen in thin sections.

a: SC-textures are displayed by recrystallized quartz and biotite around bigger feldspar grains. Shear sense is top to SW.

b: Sketch of microstructures from a Grt-Bt gneiss. Asymmetric strain shadows of biotite around garnet define an SC fabric coevally with localized extensions-type shears (c´). Shear sense is NW.

c: Higher temperature fabric cut by localized shear zones is indicated by extreme grain size reduction of quartz and change of deformation mechanisms from GBM to SGR. Shear sense of SW is also seen by the oblique tension gashes. This represents a later deformation event.

d: Synthetic microfaults in feldspar indicate shear sense direction. Lower-grade temperature shear zone with tension gashes filled by chlorite in feldspar.

e: Lower-temperature fabric with SC fabric and c' fabric shear sense are exhibited.

5.3.   Deformation and metamorphic reactions

Specific metamorphic mineral assemblages hints at their environment during development. Therefore relict pressure and temperature conditions can be estimated and help to understand the deformation history of rocks. However, several metamorphic events influence and rearrange minerals and the rock itself by obscuring the rocks real P-T evolutionary path and all the deformation events it has seen.

The samples of the Raabs Serie have experienced partial melting processes and other metamorphic events (Fritz, 1995) such as colder strike-slip deformation events. High temperature metamorphism can be seen throughout the samples. Nevertheless, a later low-temperature deformation event reworked some of the mineral structures and enabled retrograde mineral metamorphism as seen in the microstructures of the thin sections. This low-temperature event might be caused by localized shear zones.

5.3.1.   Metamorphic mineral assemblages and reactions

A distinction between a hot – temperature and a low – temperature metamorphism is suggested. Relicts of the hot – temperature event are garnets (grown during migmatisation), disc – shaped quartzes with chessboard patterns and grainboundary migration recrystallization as well as the occurrence of sillimanite and bulging occurring along the rims of feldspar grain boundaries.

Implications for a low – temperature event are bulging characteristics of quartz boundaries, transformation of biotite to chlorite and the saussuritization of feldspar. A list of low grade metamorphic mineral reactions is given below.

ML 19, R 124; ML 20,	Grt -> Chl	Ca. 300 – 550°C, 3-6kbar (?)
ML 13, R 143, R 120, R 132, ML 20, ML 21, R 140, R 77	Bt -> Chl	Retrogression, 550 – 300°C; 3-6 kbar (?)
ML 13, R 130, ML 20, R 132,	Ms growth	Retrogression, 550 – 300°C; 3-6 kbar (?)
ML 13, ML 18, ML 19, R 124, R 55, R 143, R 132, R 140, R 77	Plagioclase -> Saussuritization	Ca. 300°C; 2 – 6 kbar (?)

5.4.   Rheology of Quartz

Grainboundary migration recrystallization (GBM) with lobate boundaries, diffusional grain boundaries and to a lesser extent subgrain rotation recrystallization (SGR) dominate the rheological structures found in the quartzes in the thin sections (figure 38). Occasional disc-shaped quartz occurs in the thin sections as indicator of temperatures higher than 600°C. These elongated quartzes exhibit very often chessboard patterns and disintegrate through dynamical recrystallization processes like SGR to smaller subgrains. Occasionally, relict and big quartz grains decay to smaller polygonal quartzes forming so called "quartz ribbons" (Passchier and Trouw, 2005).

Also colder deformation events influenced the samples and so bulging (BLG) is also described here. Especially in shear zones crosscutting the thin sections, recrystallization has occurred and the quartzes show bulging and undulatory extinction.
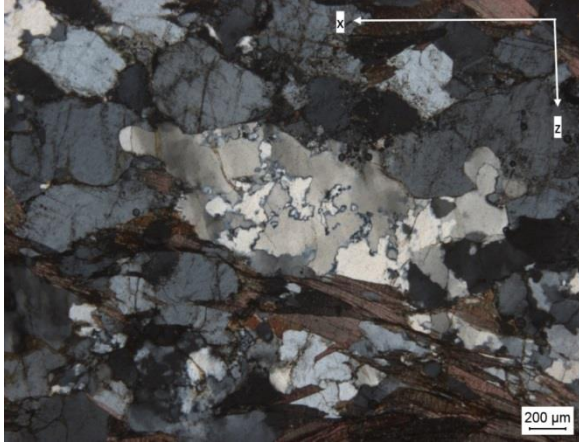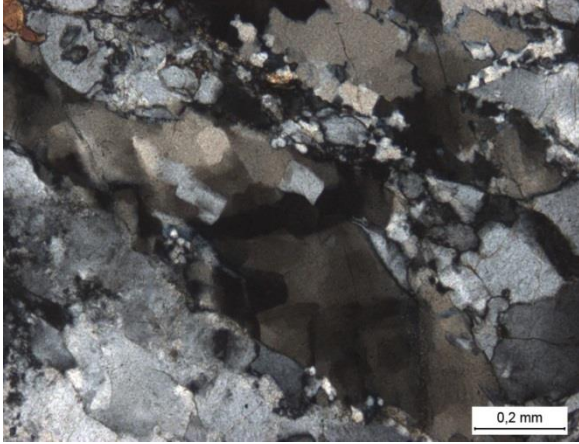
An elongated big quartz grain decays to smaller quartz grains by diffusion as well as GBM. Also BLG occurs around the new grain boundaries (ML 23).	Chessboard pattern in a quartz grain (ML 18) indicating higher temperatures (> 600° C; Mainprice et al., 1986)

| A big quartz grain has decayed to polygonal ribbon quartzes (ML 13) | Bulging of quartzes with undulatory extinction (R55) |
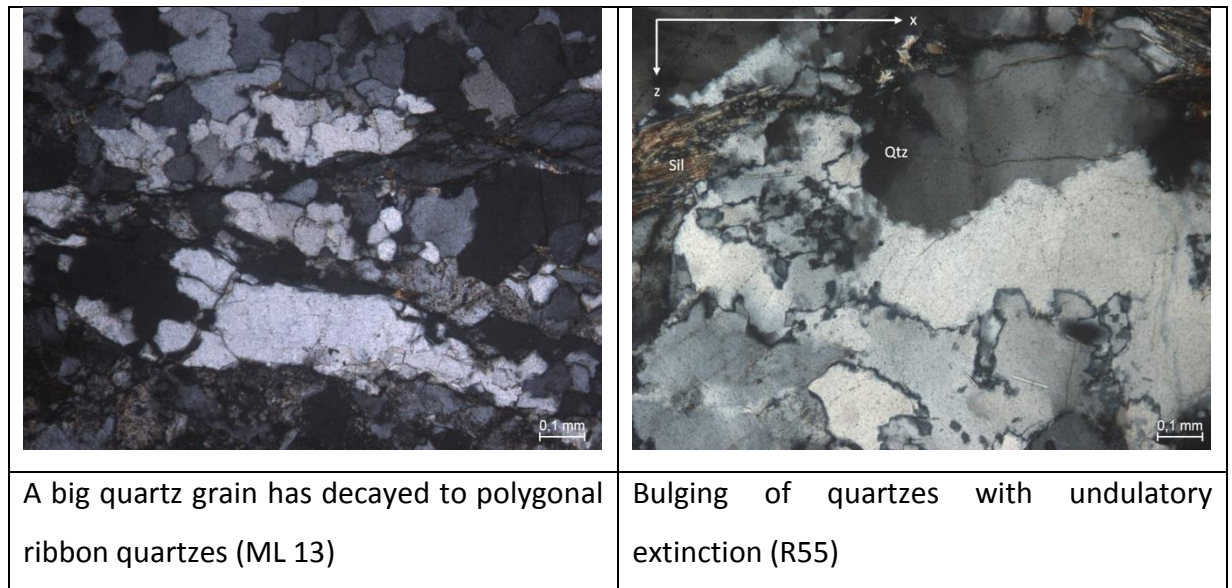
Figure 38 Rheology characteristics of quartz depending on temperature and pressure.

A table displaying the distribution of the rheological features of quartz in the thin sections of the Raabs Serie is shown below. Mostly GBM with amoeboid or polygonal structures together with SGR is shown by the quartz grains.

Quartz (table modelled after Fritz et a., 2005)	BLG U= undulatory extinction	SGR	GBM amoeboid - polygonal		Diffusion Disc quartz D Chessboard pattern Ch
ML 13			X		
R 130		X		X	
ML 18	X	X		XX	Ch D
ML 19		XX	XX		Ch D
ML 20		XX	X		Ch D
ML 21			XX		D
R 120	X	X		XX	Ch
R 55	X u		X		Ch
R 143	X	X		XX	
R 132	X u			XX	
R 140				XX	

R 77		X	X		
R 111			XX		Ch
ML 23		X		X	Ch
ML 24	X	XX	XX		D
ML 25		XX		XX	
ML 26	X	X	XX		
ML 3		X		XX	Ch

The samples collected from the Kollmitz-type gneiss (ML13 – ML21) are characterised mainly by SGR and relict chessboard pattern in quartzes. Therefore, generally lower temperatures or higher strain rate during deformation are depicted. The other samples of the Raabs Serie show polygonal grainboundary migration and to a lesser extent subgrain rotation recrystallization. The sample R111 is taken from the Ostrong Unit near of the boundary to the Raabs Serie and displays grainboundary migration recrystallization with chessboard pattern.

To sum it up, the dominant deformation mechanism characterising the Raabs Serie is a melt enhanced HT – metamorphic deformation whereas the Kollmitz-type show a lower- temperature event. The latter one has experienced a HT- deformation event as indicated by rare occurrences of chessboard pattern in quartz but it is completely overprinted by a colder and younger deformation event as indicated by retrograde minerals such as chlorite as well as the preference of lattice <a> slip systems in quartz. This result suggests that a possible younger shear zone influencing the Kollmitz-type gneiss has occurred. As indicated in the geological map (figure 27), a strike-slip system may be the cause for the low-temperature overprint in the Kollmitz-type gneiss.

5.3.1. Textures of Quartz

Lattice preferred orientations measurements on quartz were executed on selected samples. There are two different types of LPO patterns that can be seen in the Raabs Serie. The first one shows colder structures with small opening angles in the girdles and characterizes the colder younger deformation event. This includes a combination

of basal <a>, rhomb <a> and prism <a> - glide systems. The second one displays wide opening angles and also prism <c> - glide, which are relics of a higher temperature regime (figure 39). Others exhibit fabrics that are not indicative for any solid state deformation and may represent poorly oriented quartz axes formed during the melt enhanced deformation process.
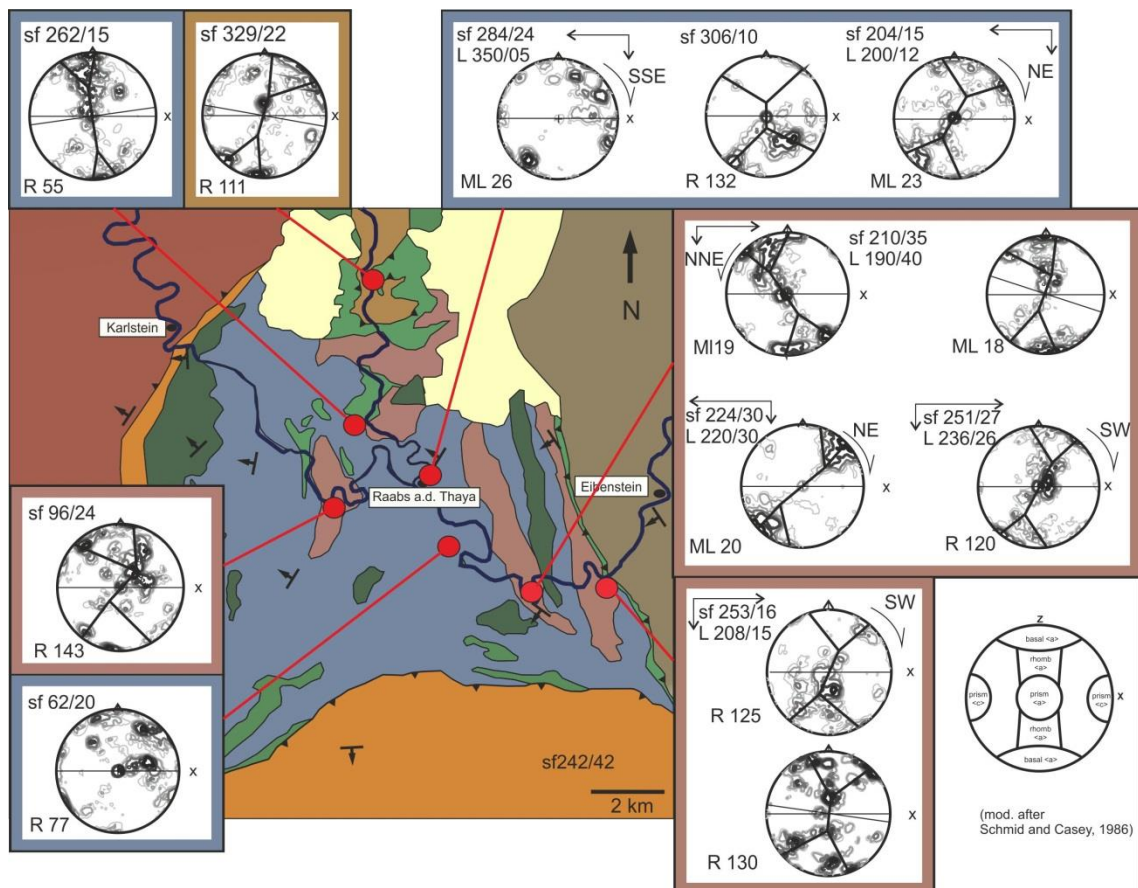
Figure 39 Geological overview map with sample points and studied LPO patterns of quartz. The colour of the frames around the LPO girdles represents the geological lithology (as in Figure 2).

The LPOs measured on the Kollmitz-type samples (in the figure 39 with pink frames) depict typical girdles with narrower opening angles than those measured in the migmatic gneisses of the Raabs Serie and further oblique single girdles. Deformation close to simple shear is suggested by the oblique girdles of the Kollmitz samples and shows movement top to NE but also SW.

However, the LPO – girdles of quartz studied from the migmatic samples collected in the Raabs Serie (in the figure 39 with blue frames), indicate wide opening angles – if a girdle is even detected and to a minor extent LT-fabrics. It appears that pure shear

deformation influenced the Raabs Serie, because of the mostly straight appearance of the LPO girdles.

sample	Lithology	Opening angle α	Temperature
ML 18	Kollmitz –type	68°	540°C
ML 19	Kollmitz –type	67°	540°C
ML 20	Kollmitz –type	50°	410°C
ML 23	migmatic Raabs Serie	98°	780°C
R 55	migmatic Raabs Serie	58°	470°C
R 111	Ostrong Unit	68°	540°C
R 120	migmatic Raabs Serie	88°	700°C
R 125	migmatic Raabs Serie	88°	700°C
R 130	migmatic Raabs Serie	87°	700°C
R 132	migmatic Raabs Serie	106°	800°C
R 143	migmatic Raabs Serie	65°	530°C

Quartz c-axes opening girdles measured on the samples taken from the Kollmitz-type gneiss show angles varying between 50° to 68° degree and therefore suggest temperatures of 400 to 540°C. The migmatic Raabs Serie rocks display wider opening angles of 58° to more than 100° and suggest temperatures ranging from 470°C up to 800°C with majority in the high temperature range close to 700°C . A sample from the Ostrong Unit underlying the Drosendorf Unit as well the Raabs Series was also observed and indicates temperatures of about 540°C.

sample	Lithology	Opening angle β	Rf
ML 18	Kollmitz –type	18°	5 - 10
R 111	Ostrong Unit	10°	5 - 10
R 130	migmatic Raabs Serie	8°	5 - 10
R 55	migmatic Raabs Serie	8°	5 - 10
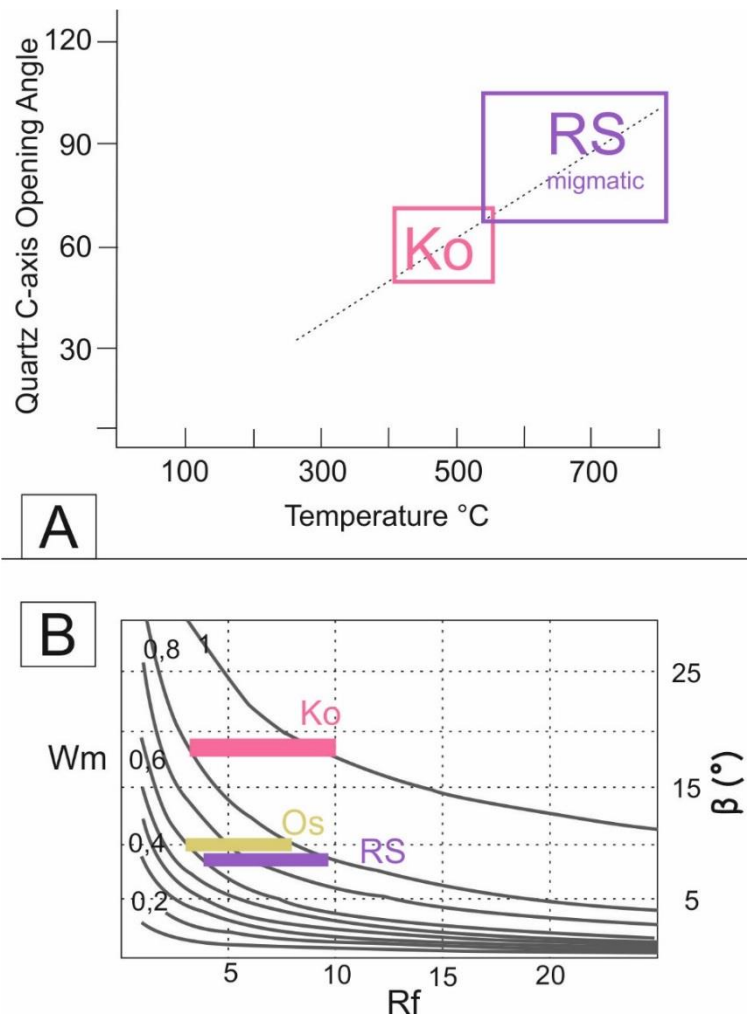
Figure 40 A: Diagram quartz c-axes opening angle vs temperature. The textures of quartz can be used as geothermometers. B: Diagram finite strain Rf vs angle β for different kinematic vorticity numbers. The main statement of this diagram is the occurrence of simple shear or pure shear for different samples at varying strains (modified after Grasemann et al., 1999).

Another method to reconstruct the deformation of rocks can be done with the plot Rf (finite strain) vs β for different kinematic vorticity numbers called Wm (figure 40; Grasemann et al., 1999). A deformation strain Rf of 5 – 10 is assumed.

The vorticity can be read directly from the diagram. Kollmitz-type gneiss samples exhibit higher vorticities than the rocks from the Ostrong Unit and the migmatic Raabs Serie. The highest β angles are found in the Kollmitz-type gneiss and suggest a Wm between 0, 9 to 1 for low to middle finite strains (Rf 5-10). A nearly complete simple shear flow is assumed because of these data.

On the other side, the Raabs Serie as well as the Ostrong Unit depict for the same finite strain numbers a much lower kinematic vorticity (0,6 – 0,8). Therefore, for this unit sub-simple shear to simple shear is suggested (Grasemann et al., 1999).

5.5.   Summary of the Raabs Serie

The Raabs Serie as the remnant of a small oceanic basin plays an important role in the plate tectonic configurations of the south-eastern Bohemian Massif. Also after the subduction of the Ocean and the incorporation of its rocks into the Moldanubian nappe system, deformation and metamorphism still took place.

In this master thesis, a special focus is given to the difference of the migmatic Raabs Serie and the Kollmitz-type gneiss. Further, the kinematic development of the Raabs Serie has been studied thoroughly. An analysis of the whole kinematic model of the field area as well as the Bohemian Massif will be given at the end, in chapter 7 (Results and Interpretation).

The Raabs Serie displays melt enhanced HT-deformation and LPO girdles of quartz c-axes with wide opening angles. The deformation is additionally influenced by extensional flow within the migmatic Raabs Serie as indicated by boudins and shear sense kinematics.

The first deformation event (D1) associated with migmatic layering was accompanied by coaxial NE-SW stretching. Melt enhanced deformation also characterized this deformation event. Shortly after, still at migmatic conditions, the migmatic layering was refolded and manifold to NE shear folds developed (D2). The last deformation event D3, which is suggested here, is a cold displacement event which caused strike slip zones to develop in the Raabs Serie. During general retrogression and cooling, localized shears developed variable senses of shear but generally combined to strike slip and normal faulting during this event.

The Kollmitz-type gneiss within the Raabs Serie shows relict HT-deformation and a dominant low-temperature deformation. Based on kinematic data obtained by micro- and macrostructures, a strike-slip shear zone also influenced this unit.

6.   Granulites of the Gföhl Unit:

In this master thesis, the granulites of the Blumau Granulite Complex are investigated through thin section analysis and observations of LPO patterns applied on quartz grains. The granulites experienced in general HP/HT conditions of lower crustal levels (Schulmann et al., 2009) and have encountered a complicated multi-stage evolution (Friedl at al., 2011). After their high-grade metamorphism, they underwent rapid exhumation (Finger et al., 2007). The protolith of the granulites, a calc-alkaline felsic magmatic body of Ordovician age (Friedl et al., 2011), experienced presumably an eclogite – facies metamorphism (at 800 – 900°C and ca. 3 GPa; Faryad et al., 2010) and was reworked by a subsequent granulite – facies metamorphism (at ca. 1000°C and 1.6 GPa; Cooke et al., 2000; Friedl et al., 2011).

After Franěk et al. (2006), the South Bohemian granulites (figure 41) represent a part of the "Gföhl" granulites which are derived from a lower crustal origin. The most common rock type of the granulites is the so called "Weißstein" with granitic composition consisting of garnet, kyanite, mesoperthitic K-feldspar as well as quartz (Friedl et al., 2011). Because of the exhumation of the Gföhl Unit and the subsequent emplacement onto the Drosendorf Unit, strongly mylonitic fabric overprinted the granulites and low temperature deformation influenced the appearance of these rocks (Friedl et al., 2011).
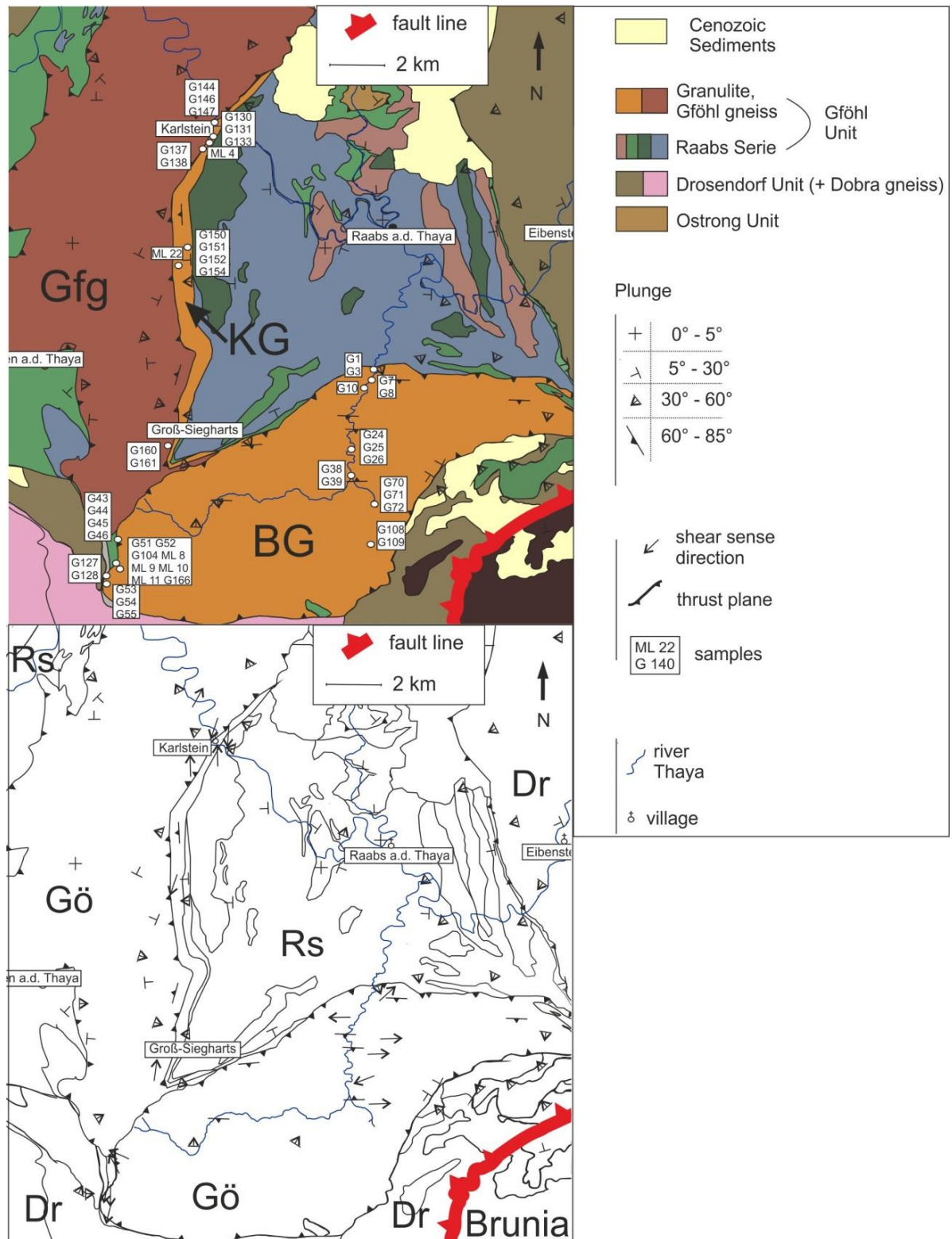
Figure 41 Geological overview of the Gföhl Unit with its granulites and the Gföhl gneiss. The upper picture shows a geological map with sample points and foliation data. The lower picture is a structural geological overview map with arrows as markers for shear sense direction. BG (Blumau Granulite Complex); Gfg (Gföhl gneiss); KG (Karlstein Granulite Schuppe); Gö (Gföhl Unit); Rs (Raabs Serie); Dr (Drosendorf Unit)

6.1.   Thin section description:

Three different types of granulites based on their appearance are introduced in this master thesis. The overall mineralogy of the granulites consists of a matrix build up by feldspar as well as quartz and inclusions of garnet, kyanite, sillimanite, spinel, zircon, rutile, biotite, chlorite (retrograde) as well as dark opaque phases.

First, there is the typical "Weißstein" which has a matrix completely composed of elongated quartz grains (disc-shaped quartzes) as well as recrystallized feldspar and entrapments of garnet, kyanite, sillimanite, zircon, rutile, biotite, chlorite (retrograde transformation of biotite) as well as dark opaque phases (figure 42). A special feature is the occurrence of ring – shaped garnets with inclusions of quartz or feldspar. This granulite is a typical HT-granulite
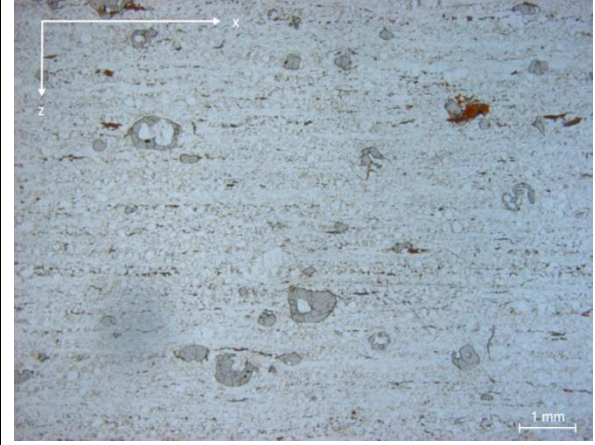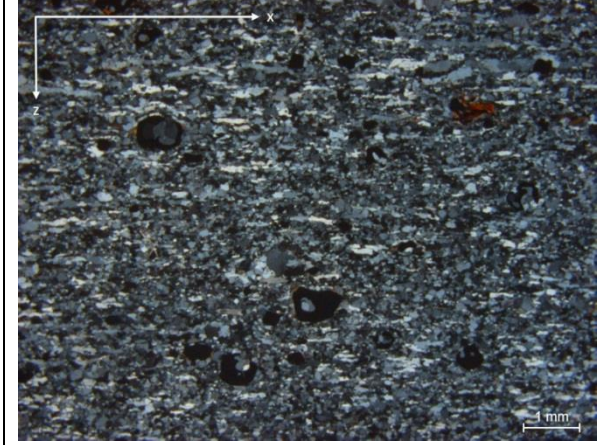
HT-granulite ("Weißstein") with non-polarized filters. Ring-shaped garnets are embedded in a matrix containing quartz and feldspar (G133)	HT-granulite ("Weißstein") with polarized filters. The disc-shaped quartzes are elongated parallel to the foliation (G133).
HT-granulite: Disc-shaped quartzes are slowly decaying to smaller subgrains (G157)	HT-granulite with retrograde features as indicated by the appearance of biotite (G 10)
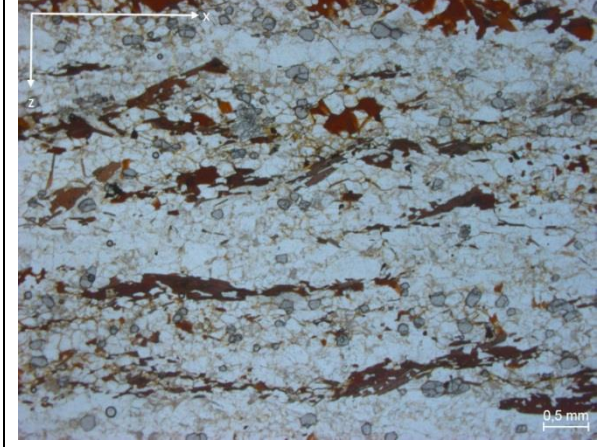
HT-granulite with ring – shaped garnets and biotite surrounded by a matrix made of quartzes and feldspar (G7)	HT-granulite: garnet with biotite strain shadows (G133)
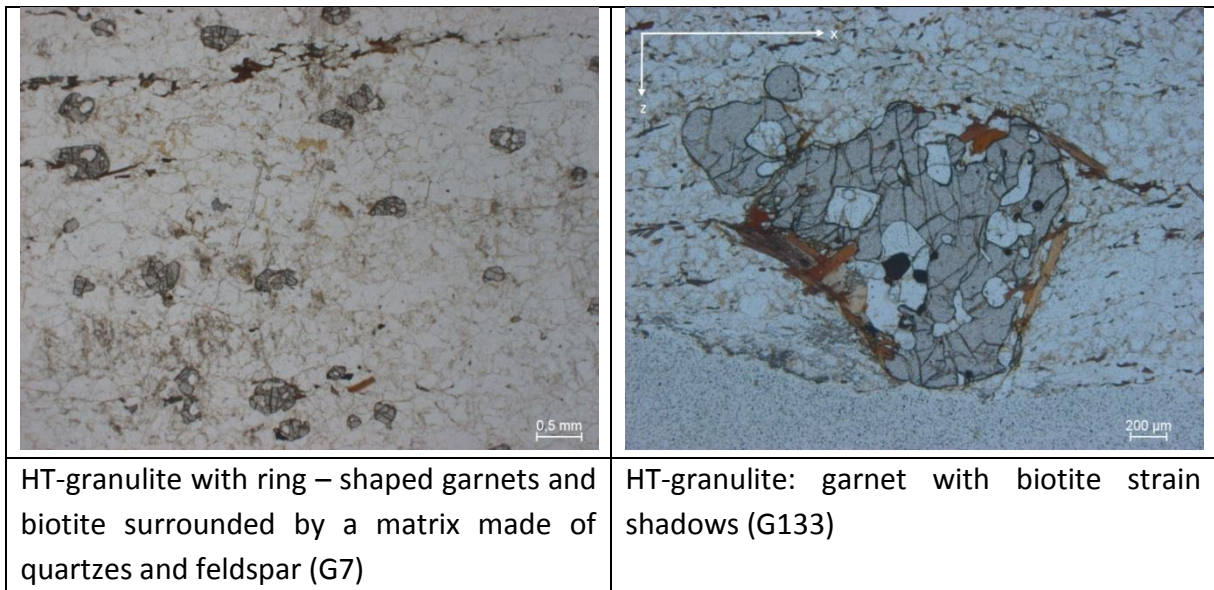
Figure 42 Thin section pictures of HT-granulites.

The second type is characterised by mylonites and folded mylonites represented by layers of very fine grained quartz as well as mica (presumably biotite) which are sometimes disrupted by recrystallized quartz veins. Big feldspar grains with twinning lamella display "augen-structures" with strain shadows consisting of recrystallized quartz grains. These "ultramylonites" are mainly located in the near of shear zones or lithotectonic boundaries (figure 43).

Ultramylonite with strongly folded quartz and feldspar veins (G166).	Ultramylonite with stronger and less strong mylonitized layers. Younger quarzitic veins crosscut the foliation (ML12).

| Ultramylonites: Big feldspar grains showing sigmoidal structures and strain caps (G 166) | Mylonite: Shear band with completely mylonitic biotite minerals and big feldspar grains (G160) |

Figure 43 Thin sections of LT-mylonitic granulites with biotite-quartz shear zones.

The third type of granulites is intensively overprinted by a LT-deformation event and exhibits typical low temperature features like bulging of quartzes and brittle structures in feldspar grains (e.g. bookshelf structures; figure 44). Occasionally, cataclasite zones are detected in the samples. Chlorite and biotite enclose garnet and may build strain shadows indicating the shear sense direction. The typical characteristic of this type of granulite are the big grains of brittle feldspar and garnet displaying "augen-structures" which are surrounded by small recrystallized quartz grains and biotite as well as mica. Also mylonitic features appear in these rocks. Biotite, sillimanite and quartz and/or feldspar are completely sheared to unrecognizable small grains.
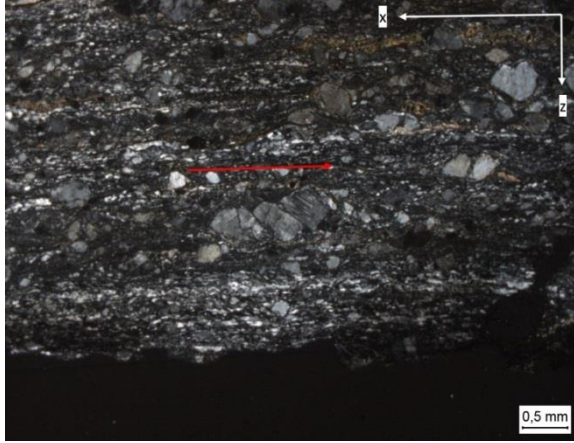
LT granulite: Brittle structures observed in feldspar grains and small recrystallized quartzes with bulging (G43) are depicted in this sample. The elongated feldspar grains exhibit synthetic shear bands.	LT granulite: Bookshelf-structure of a feldspar grain indicating shear sense direction (G54)
LT-granulite with mylonitic shear bands (G147)	LT-granulite with "augen"-structures made by sigmoidal garnets and mylonitic shear bands (G144)
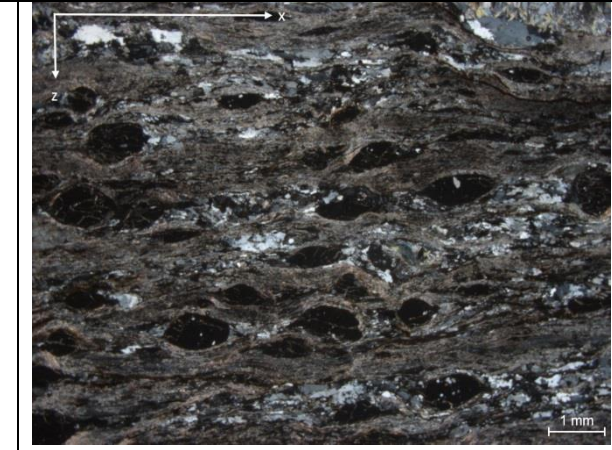
Figure 44 Thin sections of LT- granulites with mylonitic biotite-quartz shear zones.

6.2.   Structural geological investigations

The foliation of the granulites derived from the Karlstein Schuppe as well as the Blumau Granulite Complex is characterised by a wide variety of dipping directions. On the overall, there is a tendency to WSW and ENE dip direction (figure 45). However two major trends are seen. One set shows WSW – ENE orientation of planes and WSW – ENE lineations. These results are representative for data collected in the main bodies such as the Blumau Granulite Complex. Another set displays N – S trending planes and lineations which are seen in the margins of the Blumau Granulite Complex as well as the Karlstein Schuppe.
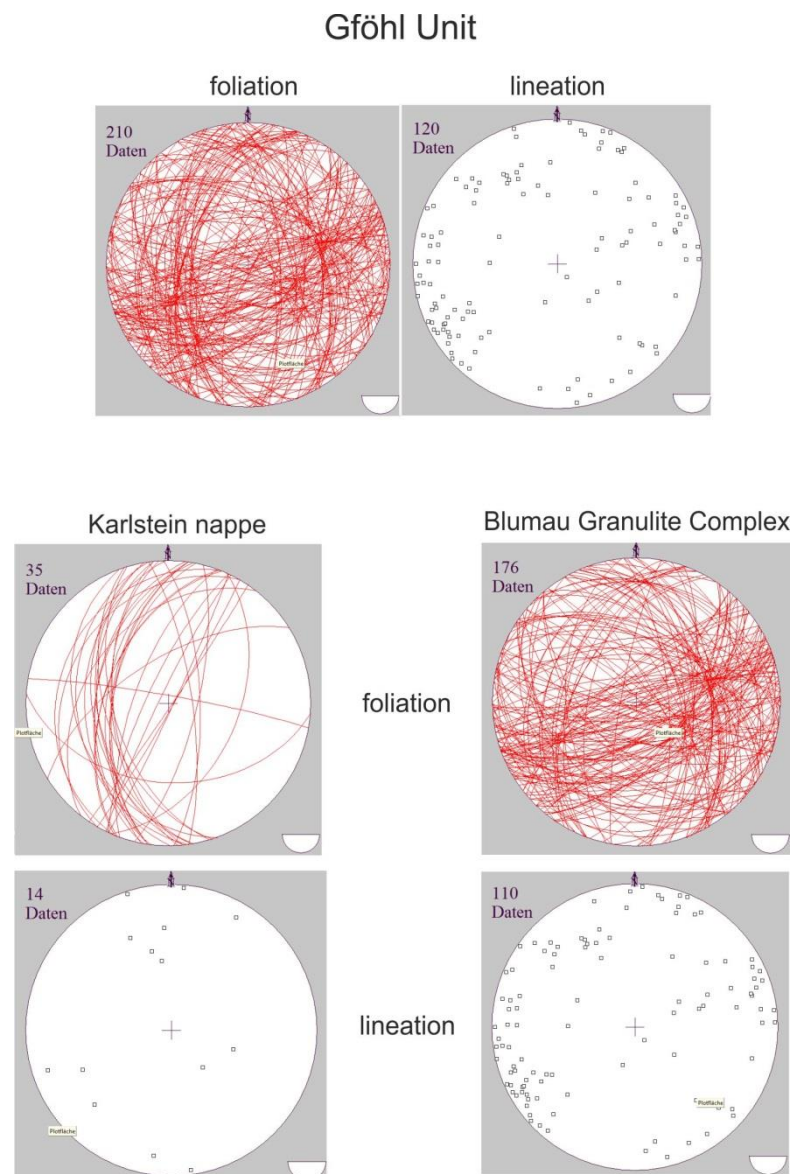
Figure 45   Foliation and lineation of the Gföhl Unit (all sampled granulites). In the upper part of the picture the structural data of all of the collected samples is displayed.

The foliation data from the Karlstein Schuppe have a strong preference to westerly dip direction. The Blumau Granulite Complex has three strong dipping directions. These are as followed: WSW - ENE trends dominate the interior of the Blumau Granulite Complex and suggest folding along W-E axes. Steep N-S dipping foliations are concentrated on the margins of the Blumau Granulite Complex. These different data may be caused by different evolutionary phases. The interior has a synformic structure with internal N-S folds and W-E coaxial shearing flow as indicated by foliation data and observations in thin sections (figure 46). Structures along margins overprint earlier formed fabrics and may be related to final emplacement of granulites.
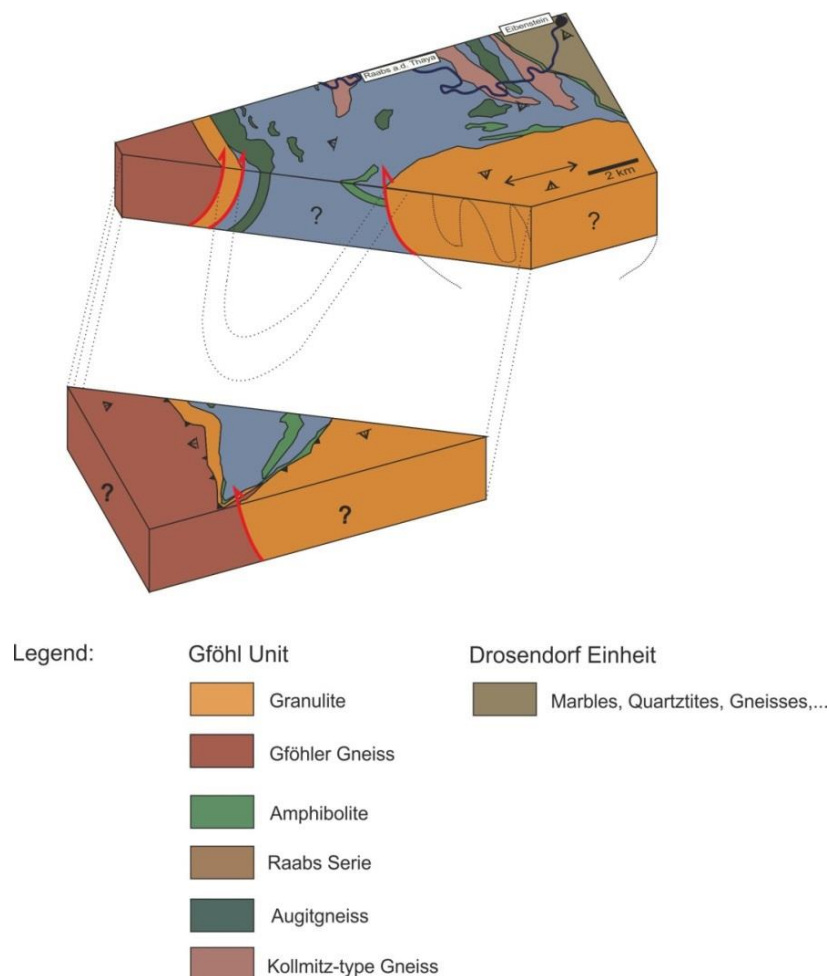
Figure 46 3D-Modell of the lithotectonic units found in the field area of the master thesis. The structures of the granulites are indicated by punctuated lines. Especially the Blumau granulite body in the south has a synform-like shape with internal W-E trending N-S directed folds. The Karlstein Schuppe is characterised by W-directed dipping with steep inclination. Maybe there is also a curved connection between the granulites derived from the Blumau complex and the granulites of the Karlstein Schuppe. Unfortunately, the direct contact between these two bodies is not exposed in the field.

6.2.1. Microstructures

A distinction between the typical HT-granulites (figure 47), LT-granulites and mylonitic granulites has also been made in this chapter. Individual deformation stages exhibit different senses of shear (figure 48).

An example for a HT-granulite which has been overprinted by semi-brittle to brittle faults is shown below.
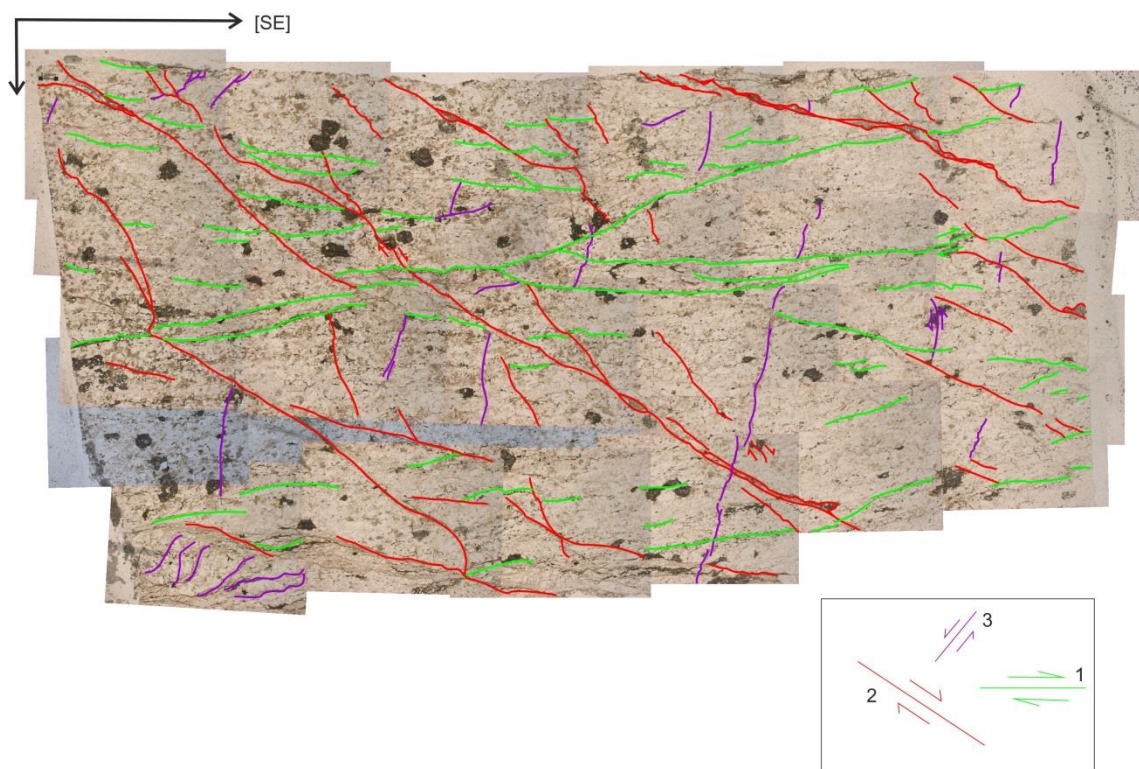
Figure 47 Thin section of a HT-granulite (ML 8) with marked fractures of different fracture systems. In the lower right section of this picture an overview of this fracture sets is shown. The numbers above the strike-slip systems indicate the chronology (1 is the oldest and 3 the youngest).

The "typical" HT-granulites with small garnets and disc-shaped quartzes generally have symmetric structures and only depict in few cases hints for non-coaxial deformation with shear sense indicators. Sometimes, the garnets have strain shadows containing biotite and/or chlorite and may indicate the direction flow during retrogression. These structures are associated with, partly oblique brittle fractures in garnet, another hint for increasing non-coaxiality during the retrograde metamorphic imprint. Fractures in thin sections of granulites are quite common and may indicate small as well as younger shear systems.

The LT-granulites are characterised by "augen"-structures build up by larger feldspar grains with frequent brittle bookshelf structures and recrystallized small quartz grains in shear zones and strain shadows. Also the garnets show those brittle bookshelf structures with strain shadows made of biotite and chlorite. These mineral assemblages and appearances help to determine the shear sense direction of the last deformation event overprinting the rock. Especially the mylonitic shear bands are sometimes easy targets for defining the direction of deformational flow.
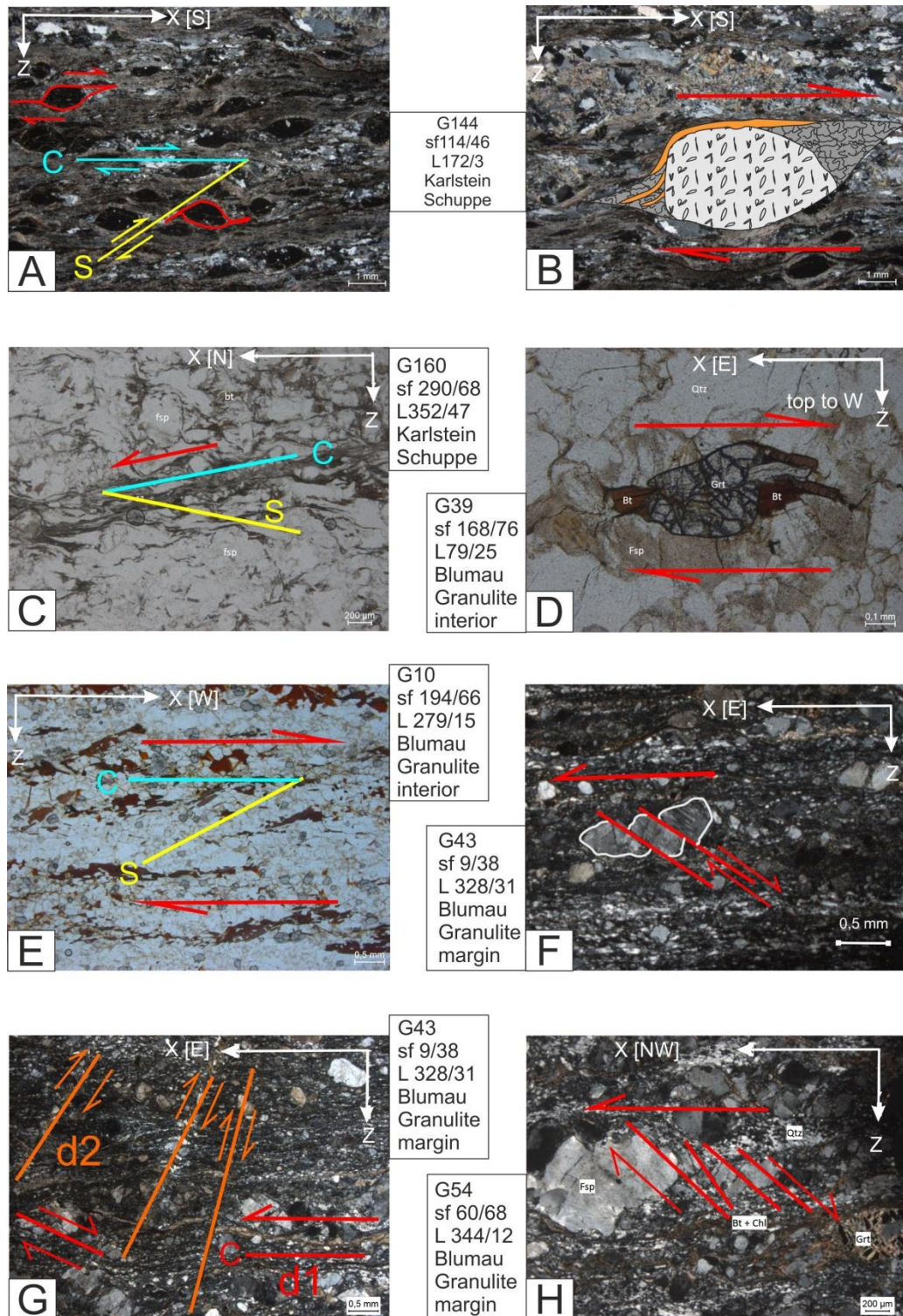
Figure 48 Thin section overview with focus on the kinematics. The figure A and B show a LT-granulite with mylonitized shear bands of biotite, quartz and feldspar. The garnets and feldspar make typical "augen"-structures with strain shadows. Also a SC-texture is seen in this sample and suggests a dextral shear sense with a top to south direction. The figure C (L-T granulite) displays a SC-structure with a sinistral deformational flow. The picture D (HT-granulite) presents a garnet with biotite minerals as strain shadows under dextral deformation and top to west flow. The picture E (HT-granulite) is characterised by SC-structure made by biotite minerals and indicates a dextral, top to west deformational flow. The picture F and G (LT-granulite) exhibit a typical bookshelf-structure of feldspar. The displacements within the separated feldspar hint a sinistral (top to E) shear sense direction. Especially in the picture G a chronology of different deformation events (d1 and d2) can be detected. The last picture H (LT-granulite) shows brittle feldspar with sinistral top to NW shear sense direction.

By analysing the shear sense directions observed from the minerals, a strongly preferred direction is not detected. The shear senses are heterogeneous and vary from site to site.

The granulites from the Karlstein Schuppe have N- or S-orientated strike-slip dominated flow directions. The difference of the orientations may be caused by a strike-slip zone in the Karlstein Schuppe.

The Blumau Granulite Complex displays internal N-S trending folds with W-E coaxial flow. This is also observed in the samples. Only around the boundaries of this granulitic body, the thin sections show different flow directions. This could be caused by the emplacement of the Blumau Granulite Complex onto the lithostratigraphic lower units, such as the Raabs Serie or the Drosendorf Unit.

6.3.   Deformation and metamorphic reactions

Metamorphic events are indicated by distinct mineral assemblages occurring in rocks. These mineral assemblages develop at specific temperature and pressure conditions and are used as kind of markers for metamorphic conditions.

The granulites have experienced the highest deformation conditions occurring in the field area of this master thesis. Nevertheless, younger and colder events as well as strong shearing-induced deformation events caused complete overprinting of some of the sampled granulites.

6.3.1. Metamorphic mineral assemblages and reactions

The granulites as representative HT/HP - (maybe also UHT/UHP) rocks have experienced lower-crustal metamorphic conditions during their formation (Schulmann et al., 2009; figure 49).

G155, G140	Grt -> Pl + Hbl	Decompression; Ca. 650 – 750°C; 7-13 kbar (?)
ML 9, ML 10, ML11, ML 12, G147	Ky -> Sil	Decompression; Ca. 600 – 750°C, 6-10 kbar (?)
ML 5, G54, G147, G159	Grt -> Chl	Ca. 300 – 550 °C, 3-6kbar (?)
ML 4, G7, G54, G134, G147, G160, G158, G159	Bt -> Chl	Ca. 550 – 300°C; 3-6 kbar (?)
ML 5	Ms growth	Ca. 550 – 300°C; 3-6 kbar (?)
ML 5, G7, G39, G137, G160, G158	Plagioclase -> Saussuritization	Ca. 300°C; 2-6 kbar (?)

Representatives of decompression reactions are garnets with plagioclase rims as well as kyanites to sillimanite which got overprinted by lower temperature deformations. Furthermore, retrograde deformations are shown by appearance of sillimanite, chlorite, brittle mineral reactions, appearances of biotite, and saussuritization of

feldspar. High stress/strain dominated deformations are characterised by completely mylonitized mineral grains and stress lamella appearing in the minerals such as feldspar. Garnets are replaced by symplectitic reactions to plagioclase and hornblende and indicate retrograde metamorphic reactions.

The mineral reaction assemblages hint to a HP-event (grt, ky) that was replaced by lower pressure minerals (sil, bt) and retrograde minerals (chl, mica, saussuritization).

| Symplectitic reaction of garnet which decays due to retrograde metamorphic reactions to plagioclase and hornblende (G140). | Weißstein with biotite: transformation of kyanite (core) to sillimanite (rim; G10). |
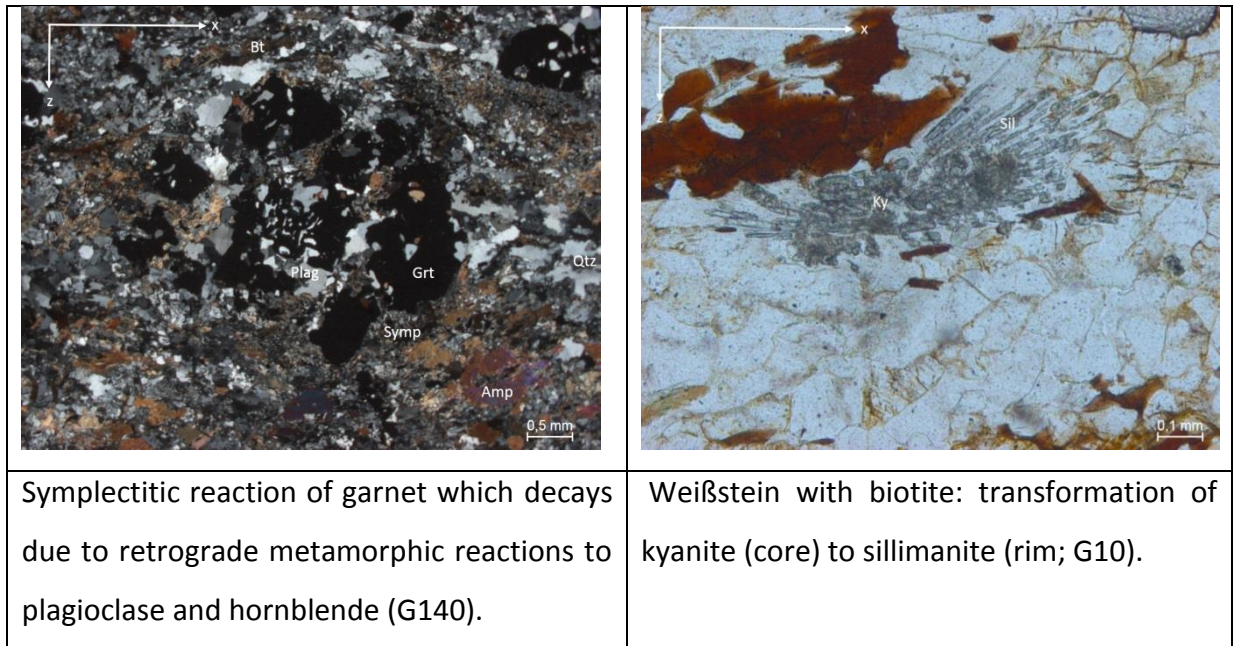
Figure 49 Metamorphic reactions in the thin sections.

6.4.   Rheology of Quartz

A table has been created which summarizes the rheology of different deformation mechanism of quartz observed in the thin sections (figure 50). Different mechanism of recrystallization with changing temperatures determine the type of recrystallization. BLG, undulatory extinction and stress twinning are shown as characteristic features of LT-mechanism in quartz. The other granulite samples display high to very HT-mechanism like unimodal polygonal quartz grains (GBM), disc – shaped quartzes, chessboard pattern and also GBAR.

Quartz	BLG U= undulatory extinction	SGR	GBM amoeboid - polygonal	Diffusion Disc quartz D Chessboard pattern Ch
ML 3		X	XX	Ch
ML 4		X	XX	Ch D
ML 5			X	D
ML 8	X		XX	D
ML 9			XX	D
G 7		X	XX	Ch D
G 10		X	XX	D
G 35		X	XX	D
G 39			XX	
G 54	XX			
G 24		X	XX	Ch D
G 51			XX	
G 137	XX	X	XX	Ch D
G 134			XX	Ch D
G 133			X	D
G 151		X	XX	D

The HT- event in the granulites is characterised by disc-shaped and elongated quartzes as well as grain boundary migration recrystallization. This is mostly seen in the typical HT-granulites, the so-called "Weißstein"-granulites.

A later and colder deformation overprinted some of these HT-temperature textures and big disc-shaped quartzes decayed due to grain boundary migration followed by subgrain rotation recrystallization and bulging recrystallization. Also younger and maybe even colder deformation has caused crystallization of quartz veins with bulging features and which crosscut the matrix. Additionally, bulging is characteristic for occurring quite common in small shear zones.

A big and relict quartz grain disintegrates because of SGR and BLG to smaller grains (G158).	Polygonal GBM occurs in the elongated quartz grains and in the minerals below (G154).
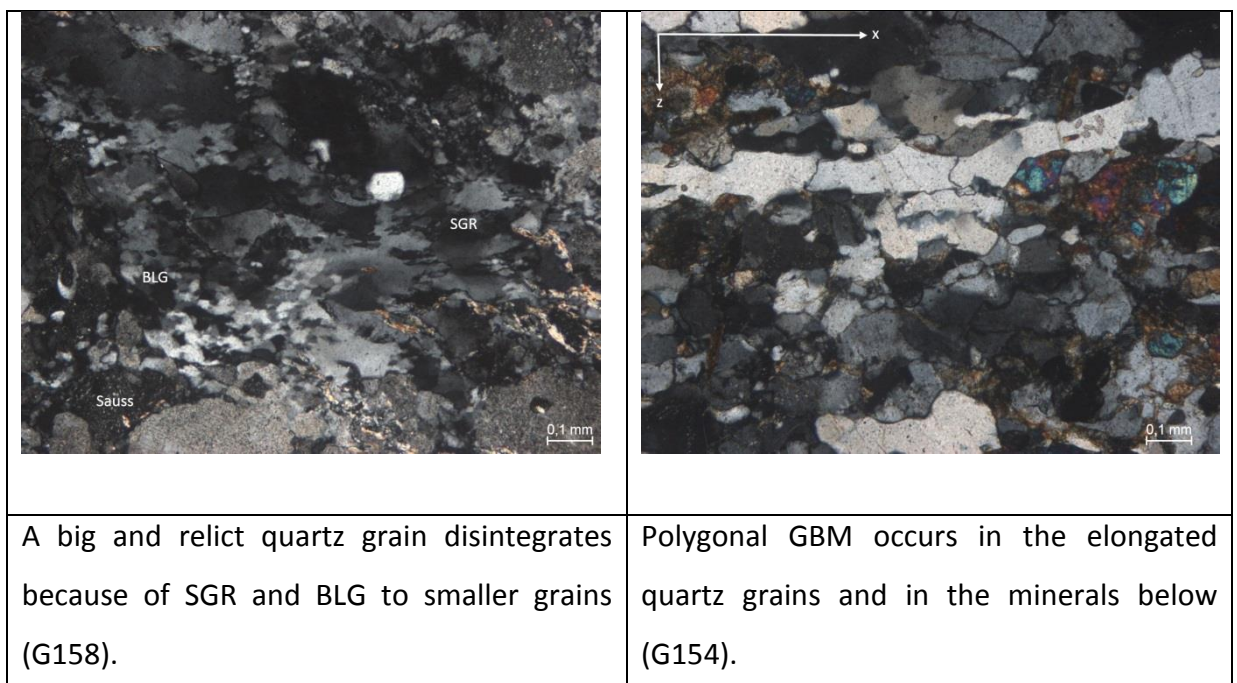
Figure 50 Dynamic recrystallizations of quartz in the thin sections.

6.4.1. Textures of LPO Quartz

Textures of quartz were obtained on different granulite samples taken from the Blumau Granulite Complex (BG) and from the Karlstein granulite Schuppe (KG). Defined lattice glide systems in quartz grains correlate with specific temperatures (Kruhl, 1998). Therefore, temperature ranges can be distinguished based on the appearance of the LPO girdles measured on quartz.
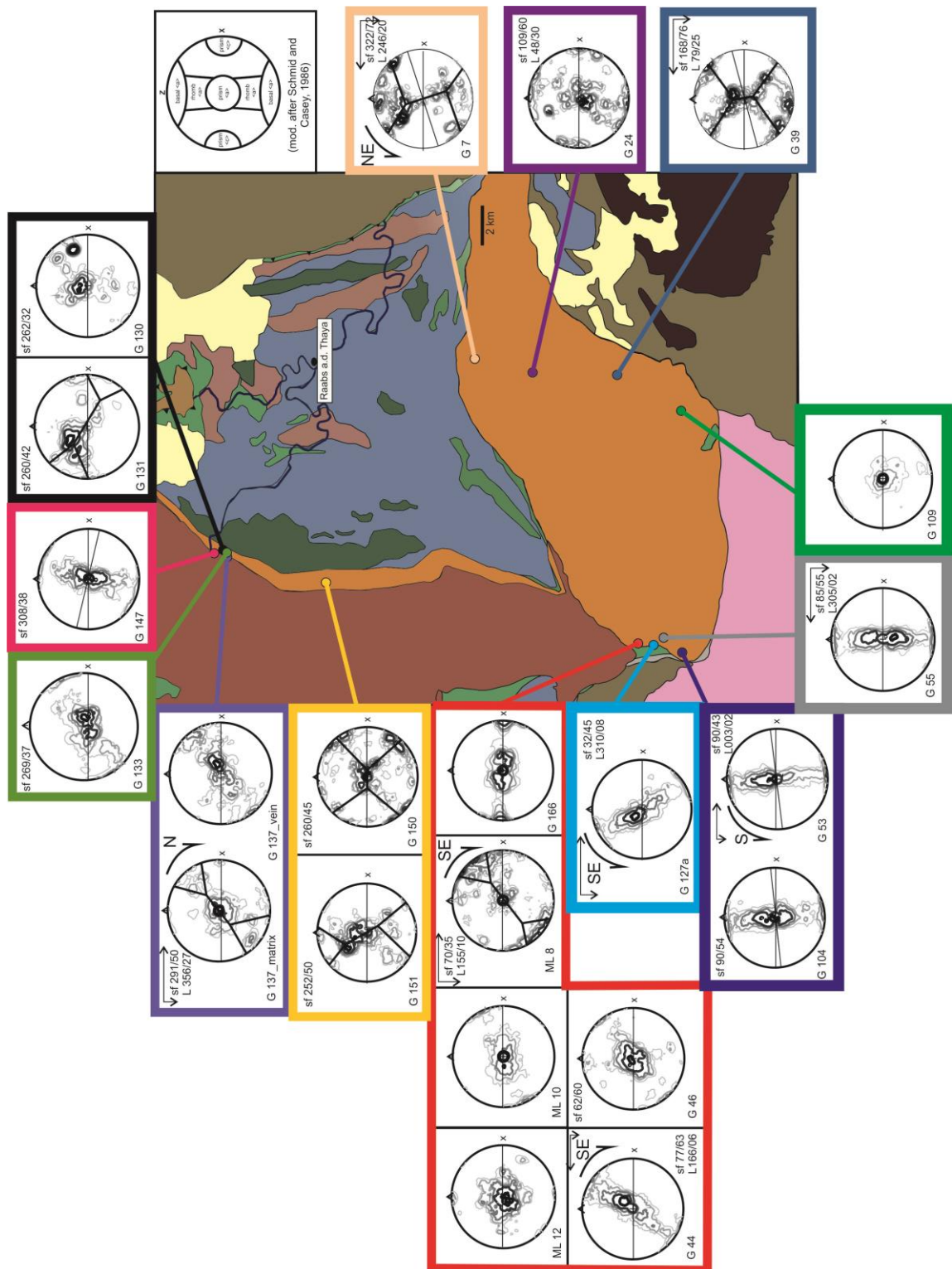
Figure 51 Geological overview map with sample points and studied LPO patterns of quartz. For legend see figure 10. Different colours indicate different groups of sampling points as shown by the frames and lines which point to the origin of the sample.

The figure 51 depicts LPO – patterns investigated on quartz in granulites. Especially, in the near of lithotectonic boundaries, LPO – single girdles or girdles with small opening angles can be detected and indicate very low deformation temperatures. A second type of LPO – pattern topology which is exhibited, is the prism <a> slip in quartz. They can be seen in the near of lithotectonic margins but also in the middle of the granulite nappes. Only the LPO – girdles with wide opening angles are distributed only within the granulite nappe bodies.

Internal parts of the Blumau Granulite Complex display either pronounced prism <a> glide (G109, G24) or symmetric cross girdles with wide opening angles (G39, G7). The western margin of the Blumau Granulite Complex exhibits overprinted fabrics with very high temperature deformation seen in prism <a> and prism <c> glide systems (G166, ML10, G46, ML12, ML10, G55) overprinted by mylonites with oblique single girdles and combined rhomb <a> and prism <a> glide. Shear senses along this western margin are oblique normal displacement to S or SE.

Conspicuous on the Karlstein Schuppe is that the LPO patterns seem to be distorted. This suggests that previously formed fabrics were folded and/or tilted. All the patterns from the Karlstein Schuppe display similar glide systems, although more pronounced shearing during retrogression is observed here.

Sample	Lithology	Quartz C-Axes Opening angle	Temperature
ML 8	Blumau Granulite Complex	89°	700°C
G 7	Blumau Granulite Complex	122°	>800°C
G 39	Blumau Granulite Complex	115°	>800°C
G 131	Karlstein Schuppe	70°	550°C
G 137_matrix	Karlstein Schuppe	70°	550°C
G 147	Karlstein Schuppe	81°	650°C
G 150	Karlstein Schuppe	90°	710°C
G 151	Karlstein Schuppe	82°	670°C

The results of the c-axis opening angle measurements of the granulite samples are shown in the table above. Based on a slight temperature difference, a differentiation between granulites of different origins can be made (figure 52). The granulites taken from the Blumau Granulite Complex show wider opening angles varying between 89° and 122° degree and indicate temperatures of about 700°C to more than 800°C. The granulites derived from the Karlstein Schuppe depict narrower c-axes opening angles than the granulites descended from the Blumau Granulite Complex. Opening angles of about 70° to 90° are detected and temperatures of 550°C to 710°C are assumed for the Karlstein Schuppe.

sample	Lithology	Opening angle β	Rf
G 39	Blumau Granulite Complex	15°	5 - 10
G 53	Blumau Granulite Complex	7°	5 – 10
G 7	Blumau Granulite Complex	18°	5 - 10
G 104	Blumau Granulite Complex	6°	5 - 10
G 147	Karlstein Schuppe	13°	5 - 10

For the determination of the deformation flow which was active in the granulites, a plot has been drawn which enables a correlation between finite strain Rf, mean kinematic vorticity Wm and the angle β. A deformation strain Rf of 5 – 10 is assumed, because of the low to middle displacements observed in the granulites (figure 52).
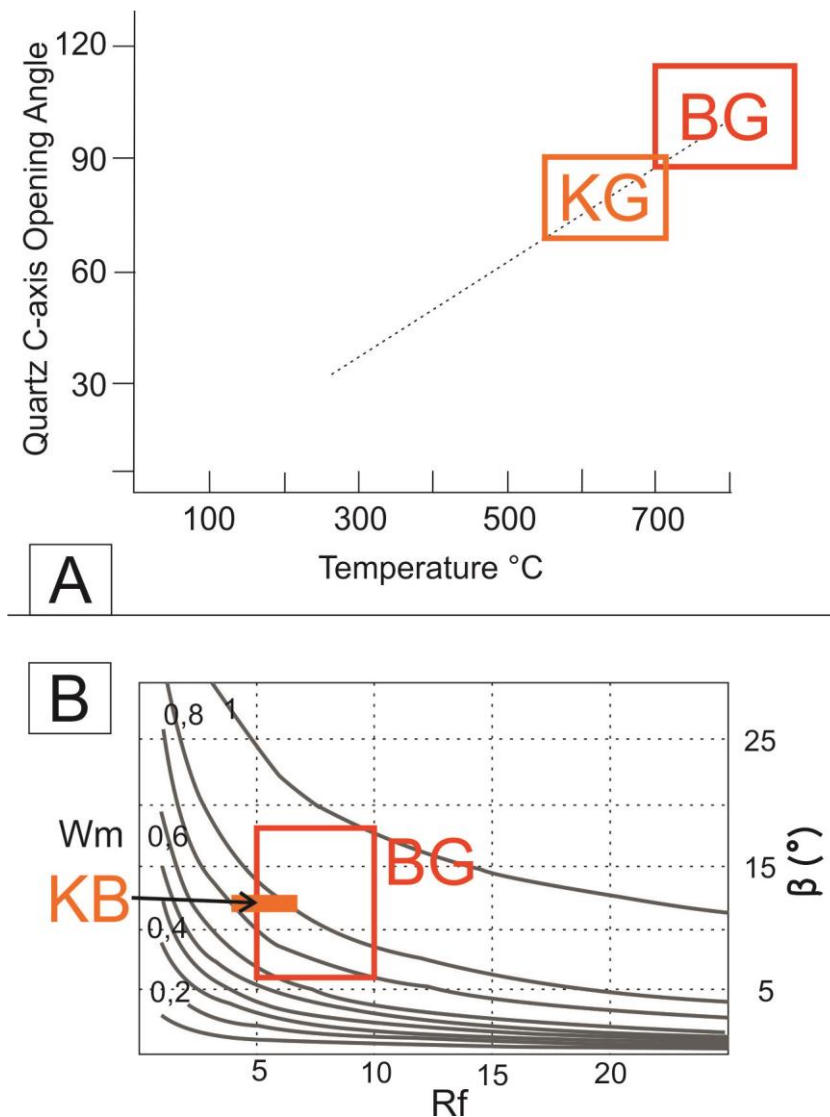
Figure 52 A: Diagram quartz c-axis opening angle vs temperature. The textures of quartz can be used as a geothermometer. B: Diagram finite strain Rf vs angle β for different kinematic vorticity numbers. The main statement of this diagram is the occurrence of simple shear or pure shear for difference samples at varying strains (modified after Grasemann et al., 1999). A differentiation between the granulites origin of location has been made: BG (Blumau Granulite Complex); KB (granulites sampled in the Karlstein Schuppe)

The vorticity for the granulites, which are separated because of their different origin, can be interpreted directly from the diagram. The Blumau Granulite Complex (BG) is characterised by strong changing of β angles (6° - 18°). However, for different Rf (5-10) a trend from pure shear (Wm around 0,4) to simple shear (0,9 < Wm < 1) is indicated. From the Karlstein Schuppe derived granulites, only one sample has been studied in this way. This sample shows a strong preference to simple-shear enhanced deformational flow.

6.5.   Summary of granulites

The granulites are rocks characterised by a complicated and interesting past. The origin of the granulites lies deep in the lower-crust (Kotoková, 2007). Three different metamorphic events overprinted these HP/HT-stones and gave them their appearance of today (Faryad et al., 2010; Friedl et al., 2011). During their exhumation to the surface, the granulites were overprinted by a retrograde deformation. The exact exhumation type is still a matter of debate (as an example Schulmann et al., 2009).

The evolution of the granulites derived from the Karlstein Schuppe and from the Blumau Granulite Complex after their exhumation to upper crustal levels has been different. The Karlstein granulites have suffered strongly under overall NW-SE trending shear zone belts and have a general west-orientated dip direction. Also strike-slip zones play an important role.

The granulites of the Blumau body exhibit a wide variety of foliation data, but a preference of steep W-E trending foliation is indicated. This is clearly in correlation with the internal N-S folds as observed from the interior of this granulitic body. On the margins of the Blumau Granulite Complex, the samples display different foliation data like a typical synform geologic body.

However, both the Blumau granulites as well as the Karlstein granulites exhibit colder characteristics. After their evolution under high – to medium high pressure conditions, younger brittle fractures and shear zones developed and crosscut the samples. In the near of shear zones some of the granulites have developed to mylonites and depict cataclastic features.

A chronology of deformation events is suggested based on the data observed from the granulite samples (modelled after Hasalova et al., 2008; Racek et al., 2006).

1) The during chapter 1 mentioned UHP event or eclogite-facies metamorphism is not preserved in any of the samples

2) The oldest event preserved is a granulite facies metamorphism dominant with coaxial W-E flow, which is clearly indicated by wide opening angles of quartz c-axes, HT minerals such as sillimanite, and typical HT-textures of quartz such as GBM and GBAR. Kinematic is characterized by W-E coaxial flow.

3) This penetrative fabric is folded in internal parts of the Blumau body with W-E trending axes and vertical axial planes.

4) Later a low-temperature overprint with partly ultramylonite features occurred. Concentration of shear zones is found along the Blumau Granulite Complex margins and Karlstein Schuppe. This is indicated by retrograde mineral crystallization and low-temperature characteristics of quartz such as tight opening angles of quartz c-axes and the appearances of BLG as well as SGR. Shear senses are identified as strike slip zones around Karlstein. The Blumau Granulite Complex depicts a combined strike slip and top to east flow on the western margin of Blumau body as well as strike slip zones in the south.

5) The last and coldest event identified in the samples has cataclastic features which are related to young fault patterns as later displayed on cross sections (chapter 7).

Deformation events	Structures and mineralogy	Plate tectonics
D1	Relict foliation	
D2	growth of garnet and kyanite	Compression, thickening of crust, maybe evolution of N-S folds within the Blumau body
D3	N-S flow Retrograde overprint, decay of garnet, growth of biotite, sillimanite	Exhumation of HP-rocks, emplacement on lower lithostratigraphic units, emplacement of Blumau body and Karlstein as today, activation of strike-slip zones (like Karlstein boundary); influence of tectonic bedding by the indenter of Brunia and ongoing exhumation
D4	shear zone developments	Brittle fractures developments; maybe Variscan shear zone development (?)

7. Results and Interpretation

All of those different lithotectonic units, the Drosendorf Unit, the Raabs Serie as well as the Gföhl Unit located in the south-eastern Bohemian Massif, have experienced a polyphase deformation history.

Summaries of traces of experienced metamorphic conditions and deformation patterns were shown at the end of the respective lithotectonic units (see chapter 4.5, 5.5 and 6.5).

Despite their different past and protolithic formations, the gained results in this master thesis of the Drosendorf Unit, the Raabs Serie and the Gföhl Unit are now analysed together. But before the data results of these particular units can be discussed and interpreted, a geological map with the kinematics is shown and the locations of the lithotectonic units in the field area are studied.

7.1. Cross-sections

Several W-E and NW-SE cross-sections were drawn (figure 53). The Moldanubian units are thrusted eastwards onto the Brunia terrane. The Ostrong Unit is overlain by the strongly folded Drosendorf Unit. The Dobra gneiss at the base of the Drosendorf Unit is exposed in the south of the field area. The Drosendorf Unit exhibits antiformic characteristics and folds as well as thrust planes.

The Raabs Serie displays folds with both antiformic and synformic features. The Gföhl Unit depicts discordant contact boundaries and usually appears as synformic basin within the other lithotectonic nappes. Later plutonic intrusions cross-cut the previously stacked lithotectonic units.

An interpretation of all of the cross-sections was made in figure 53 and a cross-section from NW to SE of the field area is interpreted in figure 54.
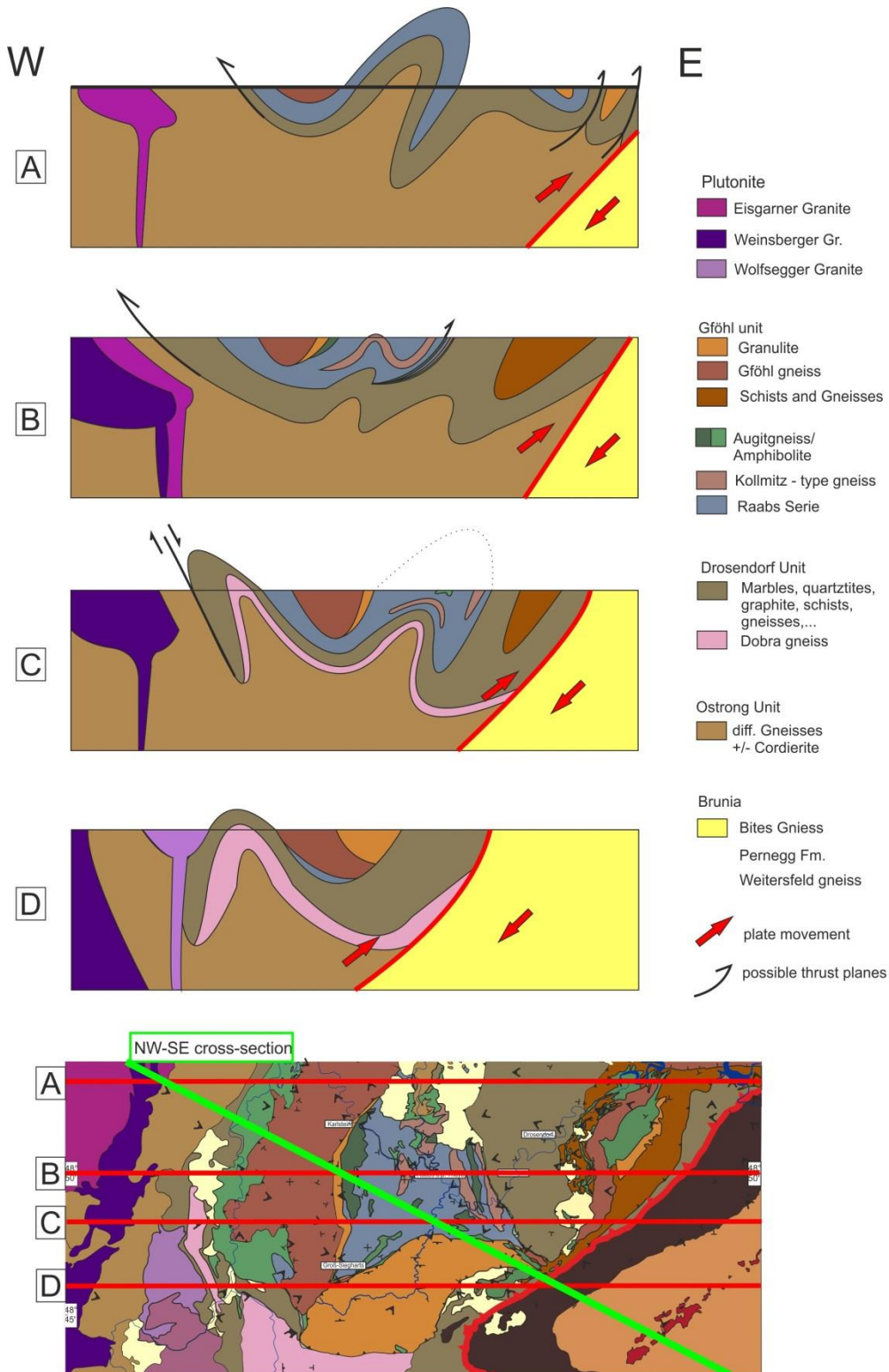
Figure 53 Four cross-sections (A, B, C and D) were created following a line drawn from west to east. The geological map at the bottom of this figure displays the locations of the cross-sections as indicated by the red lines. The curved indenter of Brunia in the geological map has been summarized to Brunia (yellow in the cross-sections).

In the cross-sections, the tectonostratigraphy is as followed: from bottom to top, the Ostrong Unit, the Drosendorf Unit, and the Gföhl Unit with the Raabs Serie at its bottom. The Drosendorf Unit lies strongly folded above the Ostrong Unit. As exhibited in the cross-sections, the Raabs Serie may also be folded. Striking is the discordant contact of the Gföhl Unit and the Raabs Unit to the lower lithotectonic units. They form synformic basins in the Drosendorf Unit which has an antiformic character.

113
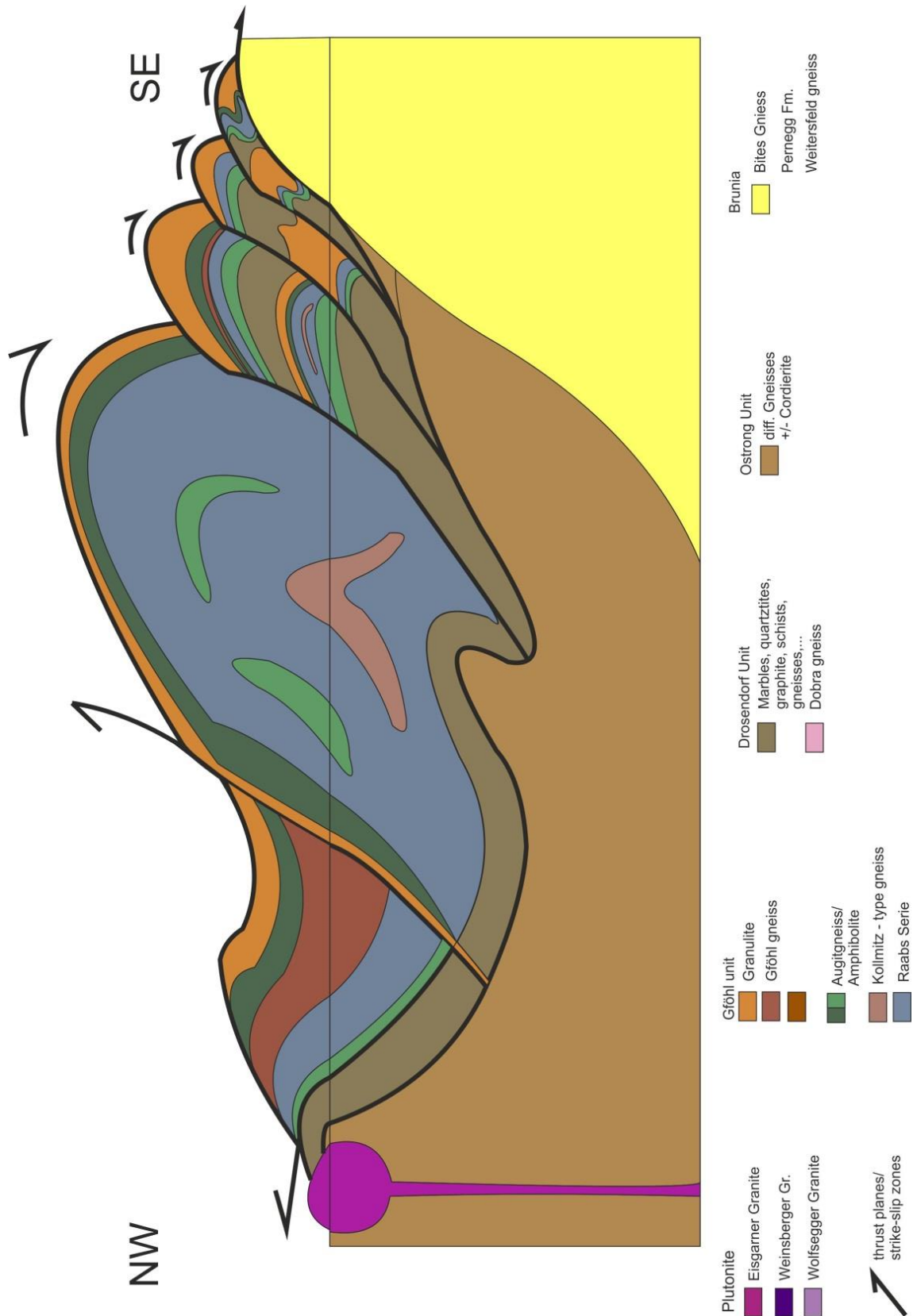
Figure 54 Cross-section from NW-SE drawn across the green line of the geological map in figure 53. Several thrust planes might be the cause of the repeated layering of the Gföhl Unit as well as the Drosendorf Unit in the eastern area of the field area. A later plutonic intrusion crosscuts the nappe stacking on the left side.

The chronological steps of the different deformation mechanism which have enabled the appearance of the cross-section in figure 54 is tried to solve. Especially, the thrust movement onto Brunia in the east has constructed several thrust planes with duplex structures as a subsequent result.

Before balancing the whole cross-section of figure 54, the thrust planes at the contact to Brunia are interpreted (figure 55).
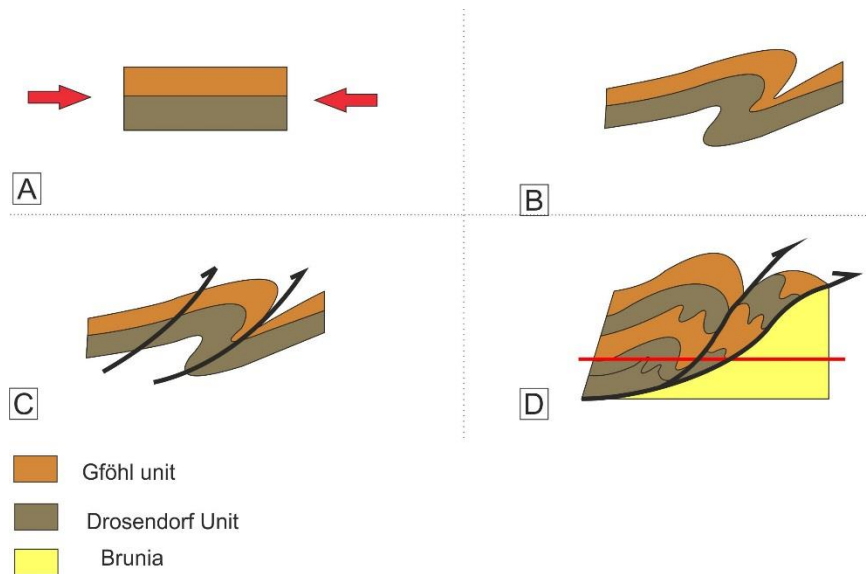
Figure 55 Solving the deformation sequence of the duplex structures in the east near the contact to Brunia. A compressional force may cause folding of layered nappes (A, B). Thrust planes develop in the folds and cause duplex structures (C). Ongoing compressional force may cause the development of another set of thrust planes (D), like the thrusting of the Moldanubian units onto Brunia.

A simplified balancing process is created which might have caused the nappe stacking observed in the field area of today (figure 56).

The first step is to bring the nappes on the left side to "down fold" (figure 56 A; indicated by the red thrust plane). The steep inclination of the Karlstein Schuppe is caused by a strike-slip zone between the Karlstein Schuppe and the Gföhl gneiss.

After bringing the units left to the Karlstein Schuppe and the units on the right side onto the same level, folds are restored that appear for instance in the Raabs Serie (Figure 56, B).

Finally, the duplex structure of the Moldanubian units in the east of the field area near the contact to Brunia is solved with the same mechanism as suggested in figure 55 (Figure 56 C, D and E).
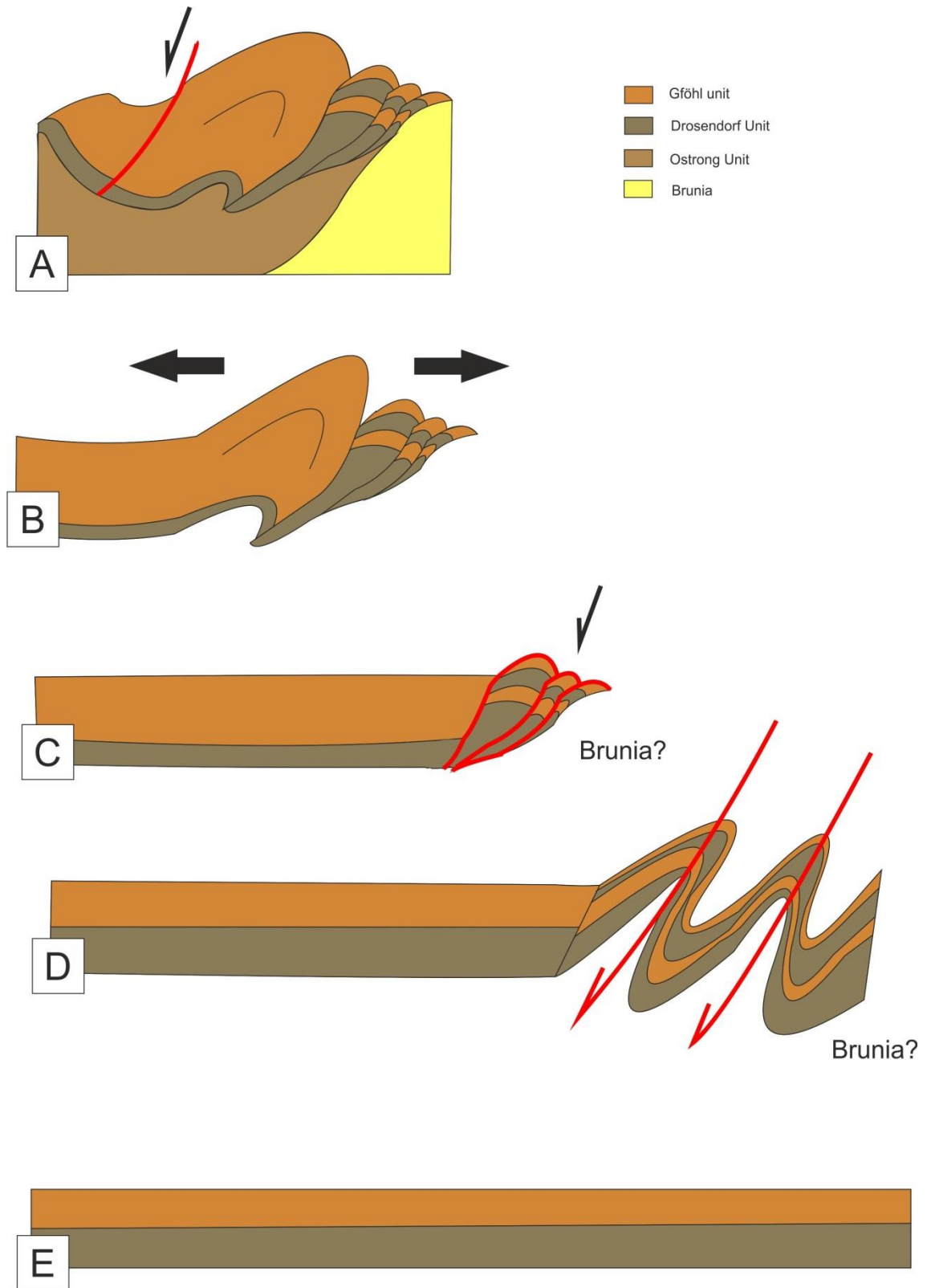
Figure 56 Cross-section balancing.

The tectonostratigraphy of the Moldanubian units as introduced in chapter 1 is proven here as still the same without changing the locations of the lithotectonic units. The uppermost unit is the Gföhl Unit with the granulites on top and the Raabs Serie at its base, followed by the Drosendorf Unit and the Ostrong Unit.

The deformation sequence described in figure 56 takes a previously layering of the Gföhl Unit onto the Drosendorf Unit for granted. How the Drosendorf Unit was thrusted onto the Ostrong Unit as well as the thrusting of the Gföhl Unit on to the Drosendorf Unit is unclear but may be caused by an earlier deformation event such as during the subduction of the Rheic Ocean.

7.2.   Kinematic interpretation

The HT-metamorphic event which has been observed in the Drosendorf Unit, the Raabs Serie as well as the Gföhl Unit possible took place before the nappe stacking or during the Moldanubian nappe stacking (figure 57). This would suggest that the HT/LP metamorphic event which occurred around 340 Ma (Finger et al., 2007; Friedl et al., 2004) is the cause for these HT-characteristics as shown by the wide opening angles of quartz c-axes and the occurrences of GBM, chessboard pattern and the findings of sillimanite in the HT-granulites.

Two distinct kinematic categories based on the temperature regime influencing the deformation in the SE-Bohemian Massif are defined. In figure 58 the kinematic flow of the HT-event of different units is shown in form of white arrows. However, little is known about the kinematics of this HT-event. The LT event is characterized by localized distributed shear zones which developed prior to NW and NE trending faults such as the major Diendorf or Pfahl faults of the Bohemian Massif. This LT-kinematics is displayed in figure 59.
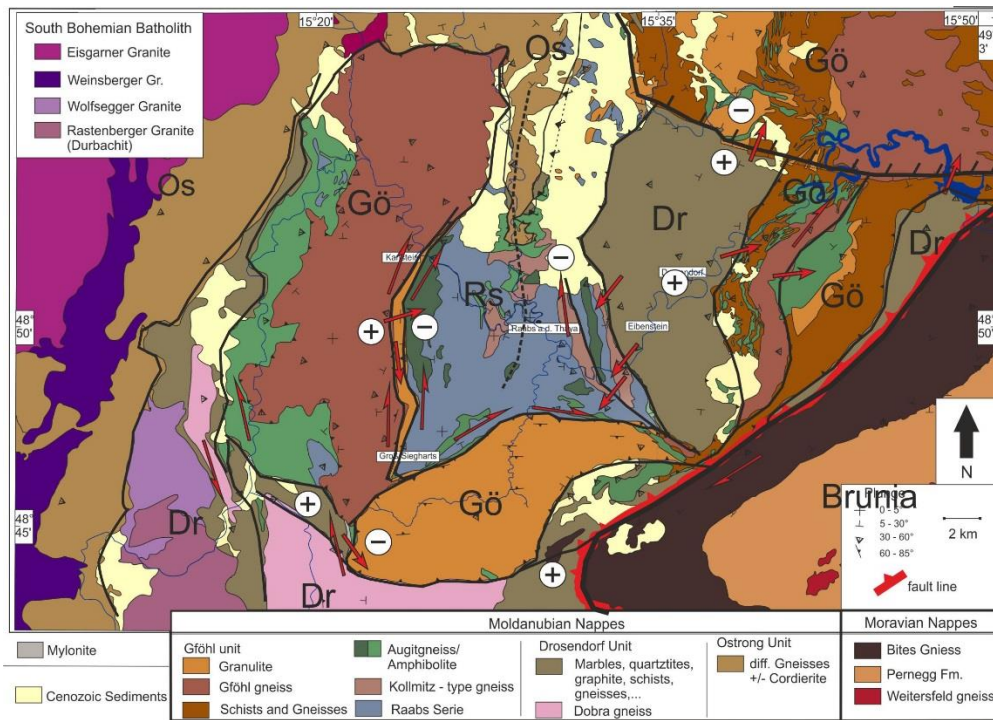
Figure 57 Overview of the lithotectonic locations and labelling for the following kinematic maps (figure 58 and 59).

Structures are a combination of strike-slip, thrust faults and normal faults responsible for the actual distribution of rocks. Simplified, structures can be grouped into dextral strike slip along the Brunia margin with associated strike-slip duplexes resulting in duplication of units along this margin. Secondly, a shear system branches away from the W-E trending upper margin of Brunia (Bittesch Gneiss) north of Horn, defines the south margin of the Blumau Granulite and bends northward parallel to the Karlstein Schuppe as well as Gföhl gneiss. This boundary arises in highly discordant contact between the granulite nappe and the Drosendorf Unit to the south (figure 58, 59).
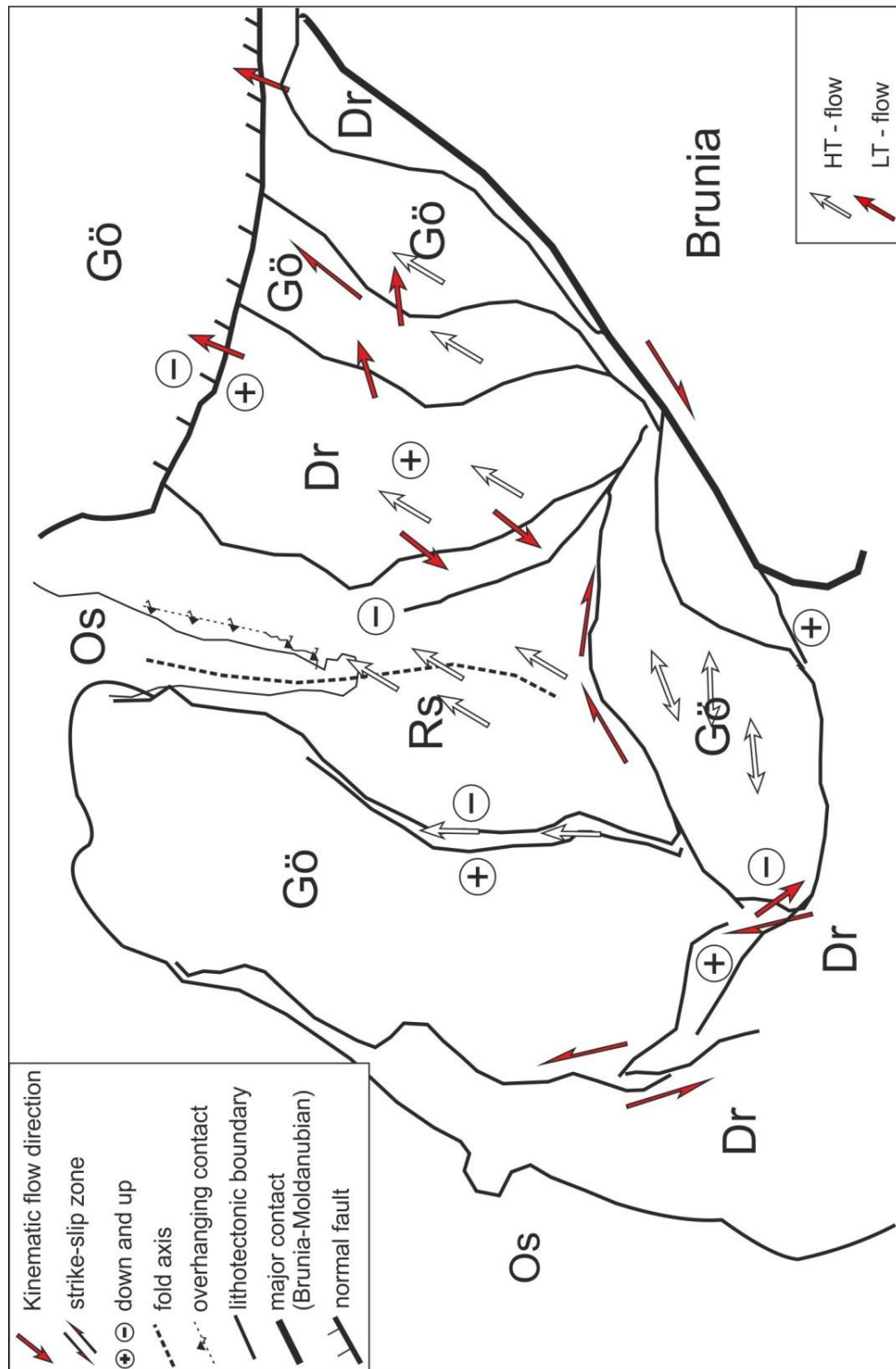
Figure 58 Kinematics of the different deformation events which happened in the field area. The kinematic flow direction of the HT-event is colored in white arrows. The plus symbol indicates uplift and the minus symbol means sinking. The red arrows characterizes the LT-event. The Blumau Granulite Complex shows W-E coaxial flow, whereas all of the other units display NE-flow during the HT-event. The punctuated line in the middle of the Raabs Serie indicates a big fold axis which is drawn in figure 54. Gö (Gföhl Unit), Dr (Drosendorf Unit), Rs (Raabs Serie belonging to the Gföhl Unit) and Os (Ostrong Unit).
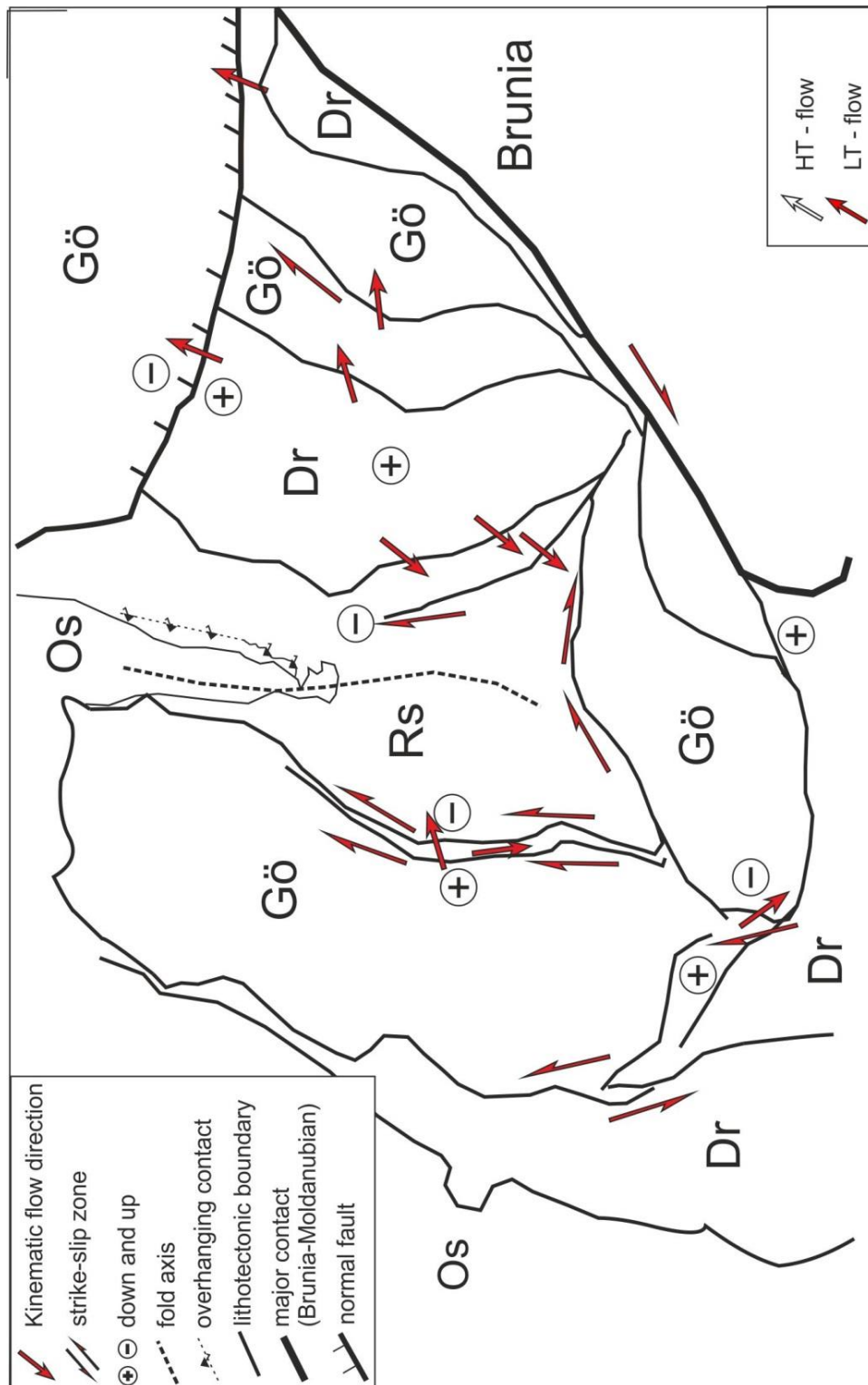
Figure 59 Kinematics of the different deformation events which happened in the field area. The kinematic flow direction of the LT-event is colored in red arrows. The plus symbol indicates uplift and the minus symbol means sinking. Strike-slip zones are frequent during this event. Especially around the Karlstein Schuppe, the Kollmitz-type gneiss in the Raabs Serie, the northern margin of the Blumau Granulite Complex and at the contact to Brunia are several strike-slip zones. The punctuated line in the middle of the Raabs Serie indicate a big fold axis which is drawn in figure 54. Gö (Gföhl Unit), Dr (Drosendorf Unit), Rs (Raabs Serie Unit) and Os (Ostrong Unit).

The kinematic flow during the HT-metamorphic event is generally north-east directed for all units of the field area. This may be related to thrusting onto Brunia during the Variscan orogeny around 340 Ma (Finger et al., 2007). The Blumau Granulite Complex is characterized by W-E coaxial flow, which may also be a kinematic indicator for an older HT-metamorphic event.

The LT-event which is characterized by bulging of quartzes, cataclastic mineral reactions, small opening angles of quartz c-axes and retrograde mineral alterations can be observed in all of the units. The kinematic flow of this LT-event is shown in figure 59. Striking is the frequent occurrence of strike-slip zones around lithotectonic nappes. The eastern border of the Gföhl Unit exhibits sinistral movement whereas the Karlstein Schuppe, the Kollmitz-type gneiss, the norther margin of the Blumau Granulite Complex display dextral shear sense. The writer of this thesis suggests that the entrapment of plutonic intrusions such as the Southern Bohemian Pluton (SBP) as cause of later LT-adjustments of those lithotectonic units. Furthermore, the indenter of Brunia in the east may be a trigger for shearing and deformation of the Moldanubian nappes in the field area.

On larger scale the shear systems of the PMZ (Přibyslav Mylonite Zone west of the Gföhl gneiss in the field area, see Žák et al., 2014, figure 62) and the Moravian Thrust (in the east) determine the geometry of nappes. The thickened Moravian "promontory" forms an arc in the east. Shear zones branch away from this arc and continue northwards along the PMZ. This arises in an overall oblique corridor with extensional steps to the southwestern part of the Blumau Granulite Complex and a compressional step to the north of the St. Leonhard Granulite. North of the promontory strike slip and normal faults developed (see figure 60).
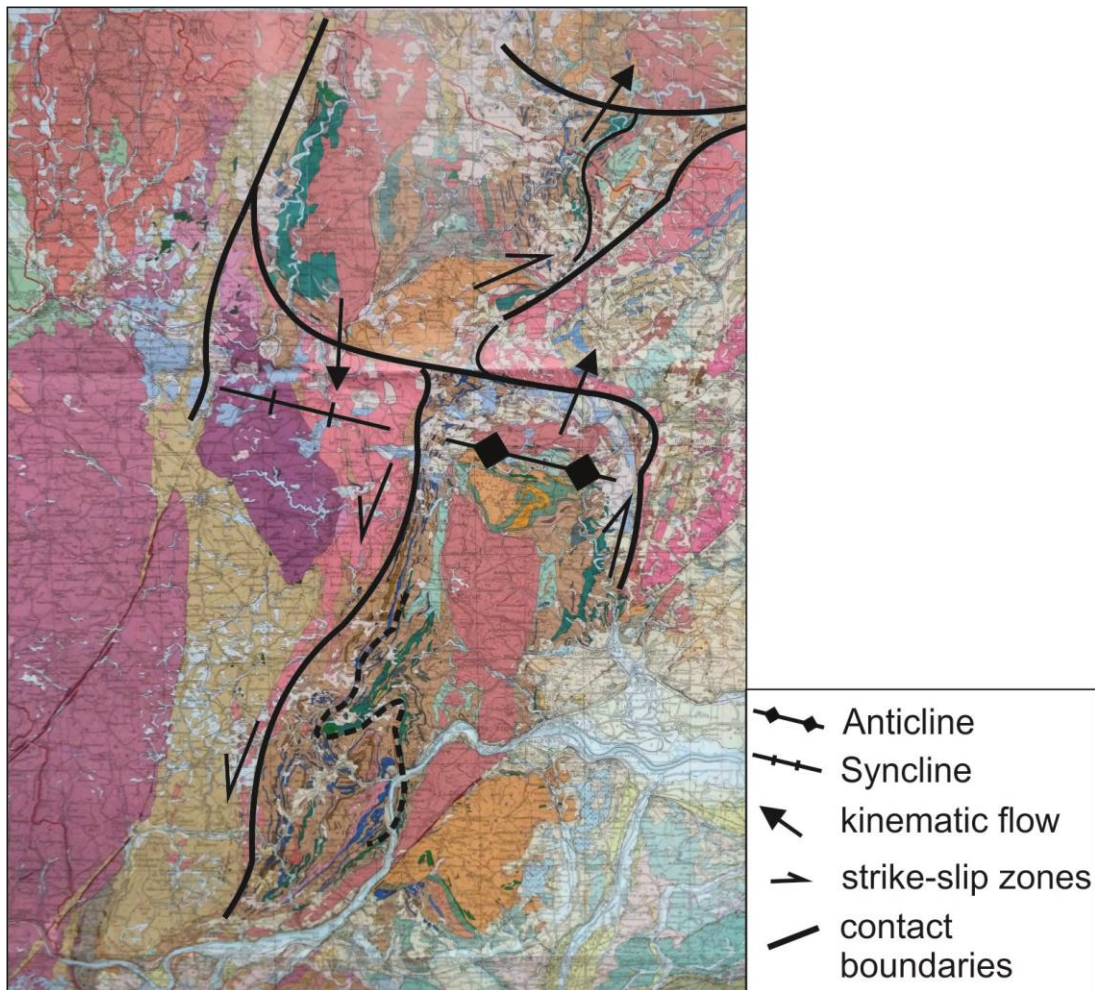
Figure 60 Kinematic study of the SE-Bohemian Massif. Major strike-slip zones of a LT-deformation event influence the movement of the lithotectonic units. The indenter of Brunia is characterised by a dextral strike-slip zone whereas sinistral strike-slip zones crosscut the Moldanubian unit. Extension or compression may be the cause of exhumation of high-grade deformed rocks. The dextral strike-slip zone in the west is called PMZ (Žák et al., 2014). The geological map is redrawn after Geologische Karte Niederösterreich-Niederösterreich Nord by G. Fuchs, A. Matura, R. Roetzel and S. Scharbert © Geologische Bundesanstalt Wien, 2002.

Older structures include the assembly of major nappe complexes including Ostrong Unit, Drosendorf Unit, Raabs Serie and Gföhl Unit. They assembled likely during general north transport but their distribution has been obscured by the above mentioned structures.

As a rule, the basal Ostrong Unit is concordantly overlain, although sometimes tectonically reduced by the Drosendorf Unit. The Gföhl Unit including the Raabs Serie, in contrast, cuts the previously assembled nappes. Examples for this are seen to the north of the Karlstein Schuppe where Gföhl Units overlay different nappes. Hence, it has to be concluded that the emplacement of granulite nappes is, at least in the area considered, a comparably young process.

7.3.　　Kinematics of the Bohemian Massif

In this chapter, the kinematic structures of the whole Bohemian Massif and the tectonostratigraphic sequence of the Moldanubian units is studied and summarized. The metamorphic processes which influenced the Moldanubian units from the beginning of the Variscan orogeny until post-Variscan times are discussed and interpreted with focus on the tectonostratigraphic and the deformation events in the field area. The UHP-event around 370 Ma caused the eclogite-facies metamorphism of the granulites (Faryad et al., 2015) and is maybe the first metamorphic event occurring in the granulites of the field area. However, this event is not preserved in the samples. This HP (UHP) event is in connection with the subduction of the Saxothuringian Ocean north-east (in today's coordinates) of the Tepla-Barrandian at the Tepla-Suture (figure 61).
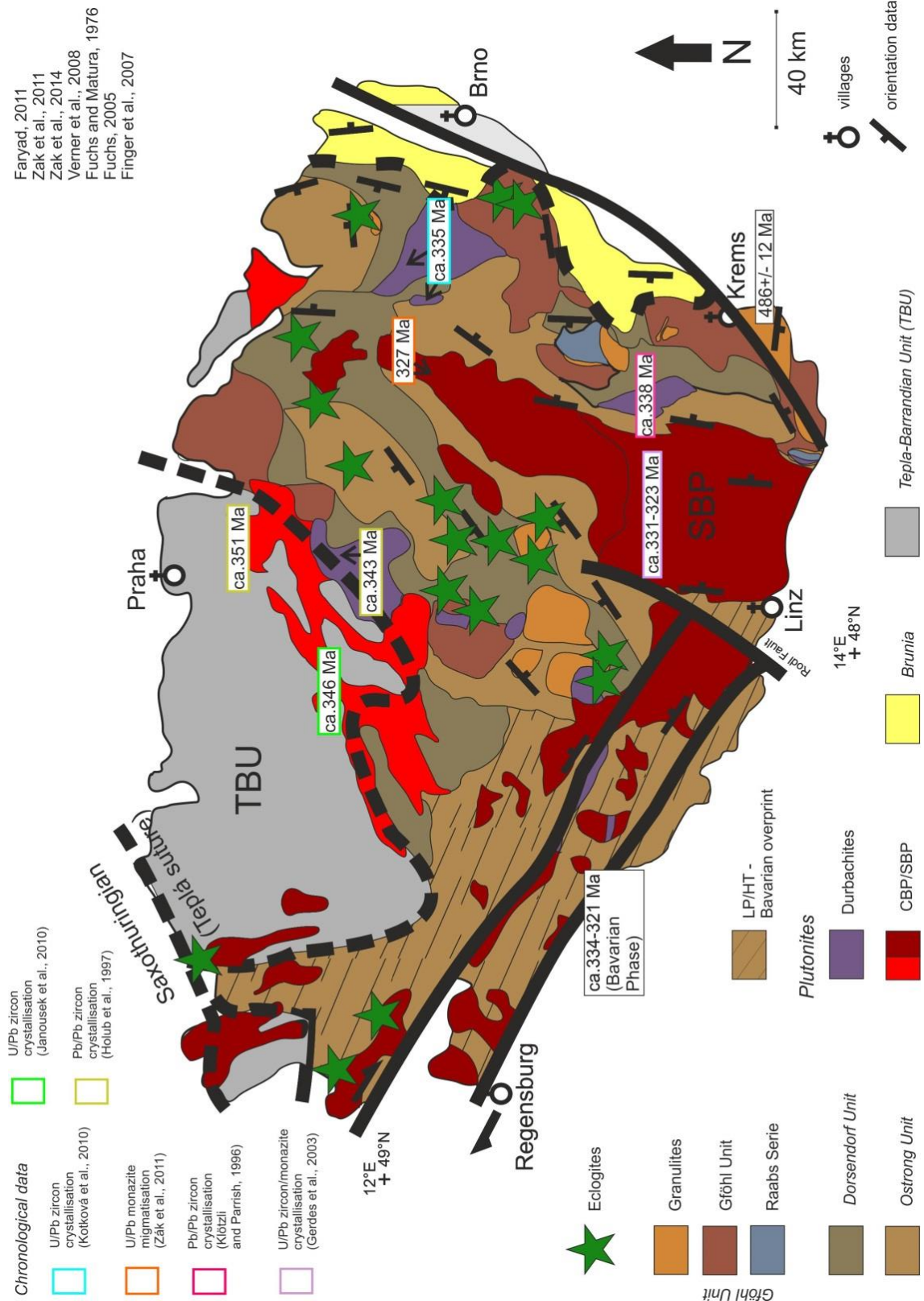
Figure 61 Simplified geological map with chronological data and major fault zones. Eclogites are indicated with green stars. The orientation data of the foliation is also shown (modified and created after Faryad, 2011; Žák et al, 2011 and 2014; Verner et al., 2008; Fuchs and Matura, 1976; Fuchs, 2005 and Finger et al., 2007)
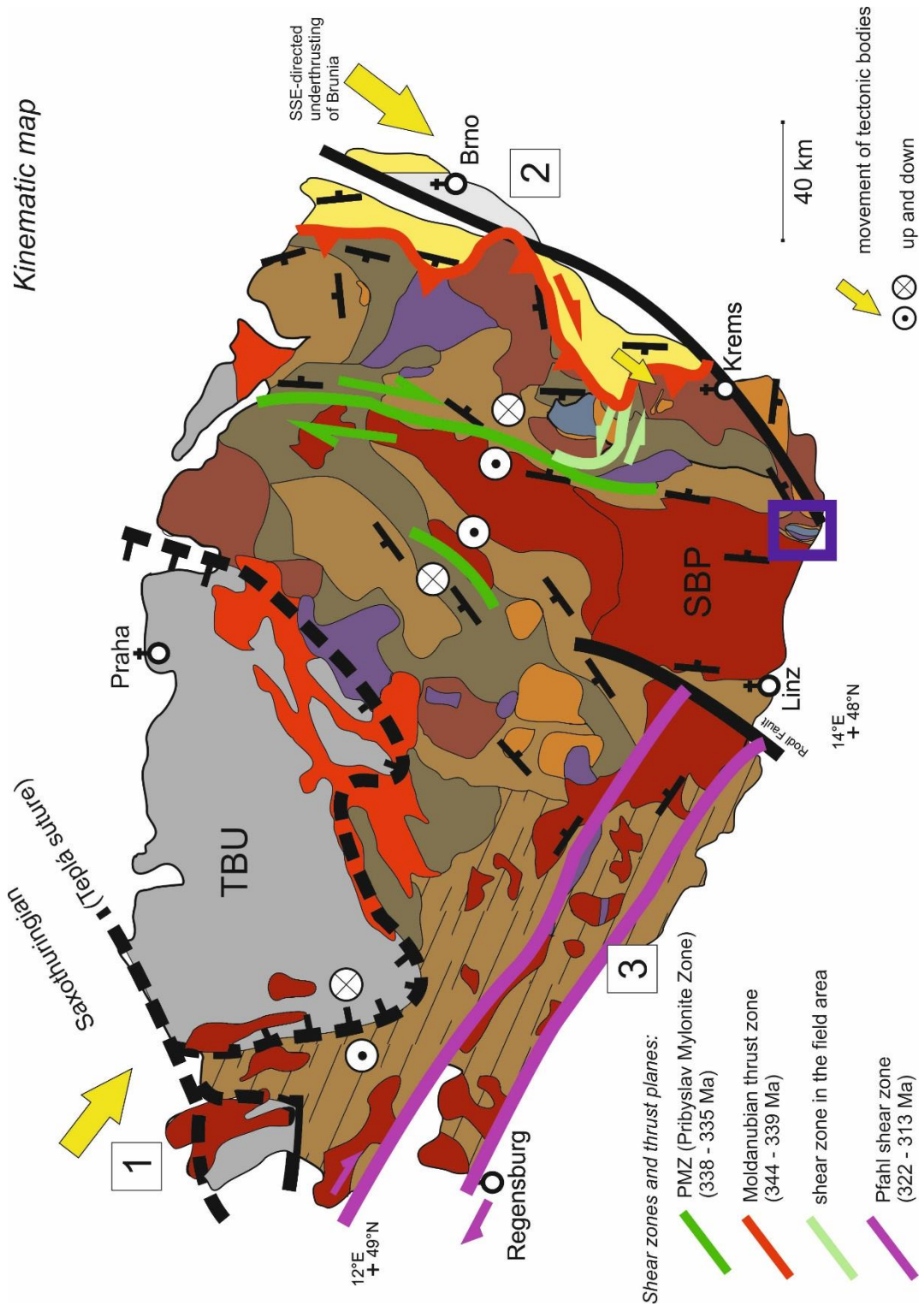
Figure 62 Kinematic map of the Bohemian Massif. The shear zones are highlighted with light colours (modified and created after Faryad, 2011; Žák et al, 2011 and 2014; Verner et al., 2008; Fuchs and Matura, 1976; Fuchs, 2005 and Finger et al., 2007). Number 1 indicates the subduction of the Saxothuringian Ocean and the eclogite-facies metamorphism of the granulites derived from the Gföhl Unit around 370 Ma (Faryad et al., 2015). Number 2 is the dominant HT/LP-metamorphic event around 340 Ma which included the underthrusting of Brunia and the nappe stacking of the Moldanubian nappes (Finger et al., 2007). Number 3 is the HT/LP event (Bavarian Phase) and the development of numerous shear zones throughout the Bohemian Massif (Finger et al., 2007; Žák et al., 2014). The blue frame in the south of the Bohemian Massif indicates the area of Strudengau.

The granulite-facies metamorphism that gave the granitic protolithes its granulitic features occurred in lower-crustal levels (Schulmann et al., 2009; Friedl et al., 2011) and were exhumed along suture zones (Babuška and Plomerová, 2013). However, the real locations of tectonic zones are still a matter of debate. In figure 61 eclogites as indicators for HP-rocks are shown in the geological map (Faryad, 2011). Those HP-rocks may be the traces of hidden tectonic suture zones (Farayd, 2011). The vast amount of eclogites south-east of the Tepla-Barrandian may be the Gföhl suture zone which play a dominant role in the model after Babuška and Plomerová, 2013. Another evidence for a subduction zone between the Tepla-Barrandian in the north as well as the Moldanubian unit in the south is the emplacement of voluminous calc-alkaline magmatic bodies (such as the Central Bohemian Plutonic Complex- CBP; Žák et al., 2014).

In figure 62, the subduction of the Saxothuringian Ocean and the sinking of the Moldanubian unit beneath the Tepla-Barrandian is indicated with number 1.

Around 340 Ma the subduction of the Brunia terrane under the Moldanubian unit takes place (in figure 62 marked with number 2; Finger et al., 2007; Žák et al., 2014). During this time, also the HT-metamorphism overprinted all of the Moldanubian nappes in this master thesis field area. If, the Ostrong Unit, the Drosendorf Unit as well as the Gföhl Unit were already stacked above each other during that time or were stacked during the SE-directed underthrusting of Brunia, is still unknown. Maybe chronological dating of contact zones between the lithotectonic units will give more information about this question.

The number 3 in figure 62 displays shear zone formations as well as the entrapment of voluminous S-type granitic plutons (340-310 Ma; Neubauer and Handler, 2000; Žák et al., 2014). The ongoing collision between Laurussia and Gondwana as well as melting of sinking Brunia crust enabled shear zone formations and plutonic body intrusions into crust (Neubauer and Handler, 2000). Also the shear zone evolutions with strike-slip characteristics in the master thesis field area may have developed during this time. The HT/LP Bavarian phase (Finger et al., 2007) did not reach to the field area and only low-temperature deformation overprinted the samples.

The LT-deformation may be caused by reorganisation of lithotectonic bodies during the emplacement of the South Bohemian Pluton. Also the indenter of Brunia reacted

as a rigid backstop throughout the Variscan orogeny and during the post-Variscan times. Additionally the uplift and sinking of the lithotectonic units enabled the juxtaposition of lower-metamorphosed rocks next to high-grade nappes.

The writer of this master thesis favours a model where the Drosendorf Unit was thrusted on to the Ostrong Unit shortly after the subduction of the Rheic Ocean. The basis of this assumption is still made on the model after Finger and Steyrer (1995). The Gföhl Unit could have been incorporated into the Raabs Serie during the ocean floor subduction and then thrusted onto the Drosendorf Unit as well as the Ostrong Unit. Of course, is this a very simplified plate tectonic model consideration and further interesting studies should be made.

7.4.   Tectonostratigraphic of the Moldanubian units

It is generally agreed that the Gföhl Unit and especially the granulites are building the top of the tectonostratigraphic of the Moldanubian units (Fuchs, 1976; Friedl et al., 2004). At its base, the Raabs Serie can be found, followed by the Drosendorf Unit as well as the Ostrong Unit (Racek et al., 2006). This is proven by the succession of the lithotectonic units in the field area of this master thesis. But, apparently, is this not seen everywhere in the Moldanubian unit of the Bohemian Massif.

The Strudengau area in lower Austria near Krems (blue frame in figure 62) has a different tectonostratigraphic succession. In figure 63 a simplified geological map with a W-E trending cross-section is demonstrated. Striking is the lack of a Drosendorf Unit which would lie beneath the Gföhl Unit including the Raabs Serie. In this area, it also appears that the granulites do not build the top of the tectonostratigraphy. The Raabs Serie has experienced a compressional event which enabled the Raabs Series' synformic bowl shape. The granulites at the border of the Raabs Serie could have been folded during the previously mentioned compressional force or be influenced by shear zones at the contact to the Ostrong Unit. The Drosendorf Unit may not be exposed at the surface or do not show up because of other tectonic processes.
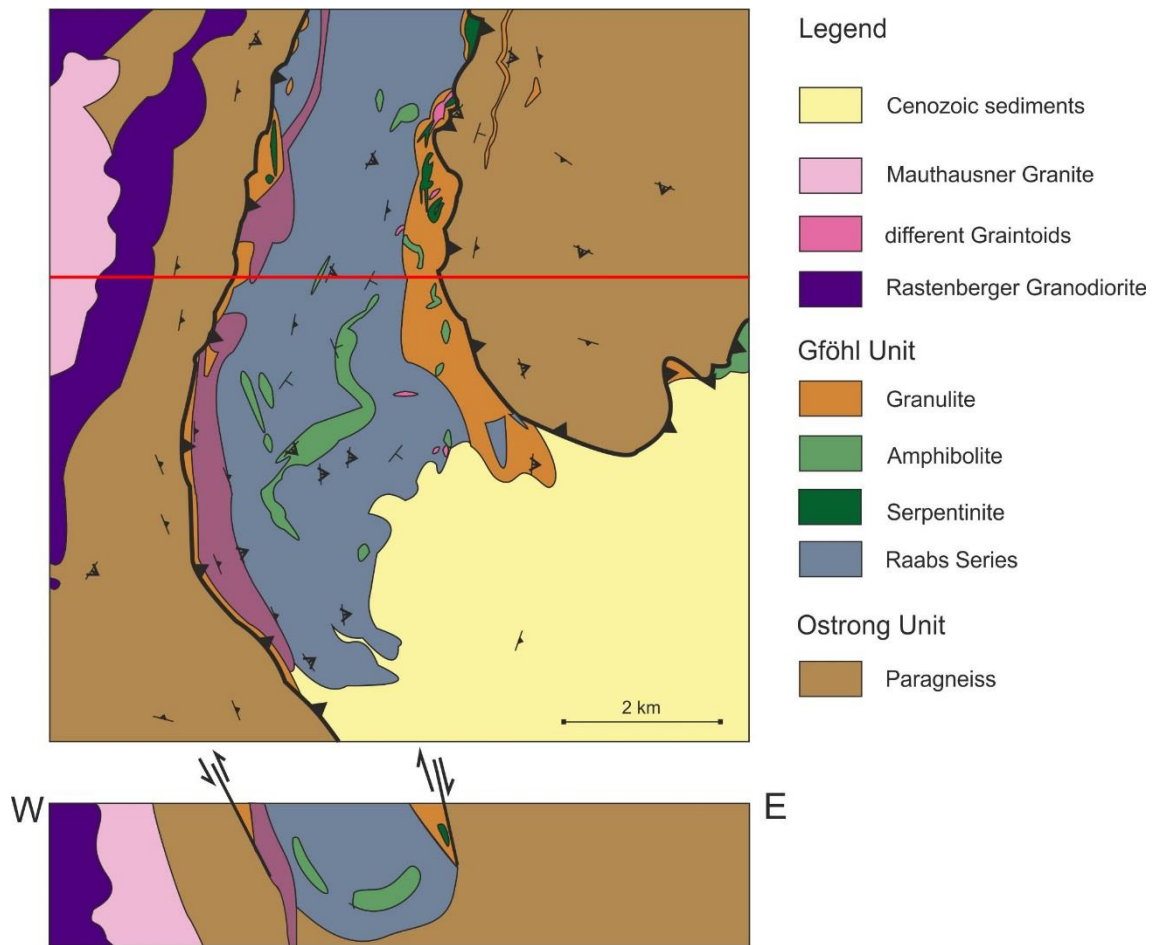
Figure 63 Simplified geological map of Strudengau with a cross-section drawn below (modified and redrawn after Fuchs, 2005)

All of this considerations display strongly that more analyses and investigations with a special focus on the kinematics as well as the younger and colder deformation processes should be made.

8. Conclusions

The observations which have been made during this master thesis are now summarized into several concluding points:

- An old eclogite facies metamorphic overprint may have influenced the granulites of the Gföhl Unit but is not seen in the samples
- Granulite facies – metamorphism changed the granitic protolithes to granulites
- A HT- metamorphic deformation influenced all of the Moldanubian units in the field area. This is proven by HT-mineral assemblages, HT-rheological features of quartz and feldspar as well as wide opening angles of quartz c-axes. Kinematic flow is directed to NE.
- A LT-metamorphic event can also be observed in the field area. Retrograde mineral alterations, small opening angles of quartz c-axes and LT-characteristics of quartz such as bulging is shown by the samples. The kinematic shear sense is influenced by strike-slip zones near to the Karlstein Schuppe, the Kollmitz-type gneiss of the Raabs Serie, at the northern margin of the Blumau Granulite Complex as well as around the indenter of Brunia. Flow to N/NE as well as S/SW directions are common.
- An additional later low-temperature deformation is also possible which has caused smaller shear zones and cataclastic features in the samples.

The different metamorphic events and deformation stages which influenced the lithotectonic units in the field area are summarized in a table below.

	High temperature	High temperature	Low temperature	Low temperature
Unit	D1	D2	D3	D4
Drosendorf Unit	Top N-NW (coaxial) stretching intrafolial folds	Top NE shear folding	Localized shear Duplex formation (top E)	
	GBM and disc quartz ca. 650-ca.800°C <c> glide	GBM 550-600°	350-400°C Subgrain rotation. Basal and rhomb <a>	
Raabs Serie	N-S coaxial stretch	Top NW-NE folding	W-E convergence, Folding and Shearing (Kollmitz-type gneiss)	Localized shear
	Migmatic, Disc and chessboard quartz c.750°C (800°C?)	GBM	GBM to SGR 450-600°C	Bulging c.400°C
Gföhl Unit Granulites	W-E coaxial stretch	N-S compression	Marginal mylonites	Marginal cataclasite
	Disc chessboard quartz Prism <c> 800°C		Combined strike-slip (Karlstein) and c.550-450°C	c. 300°

The HT-metamorphism might have caused the tectonostratigraphic that is seen today, but the younger structures have overprinted those and reorganized the geological bodies throughout the Bohemian Massif. Further studies about this low-temperature deformation should be made and may help to understand today's appearance of the Bohemian Massif with its interesting and different geological units.

References

Geological maps

Geographical overview of the field area of the master thesis (Land Niederösterreich, BEV, downloaded on the 21th November, 2016; © Land Niederösterreich; http://www.noe.gv.at/Land-Zukunft/Karten-Geoinformation.html)

Sheet number 7 Gross-Siegharts by O.Thiele © Geologische Bundesanstalt Wien, 1987

Sheet number 8 Geras by R. Roetzel and G. Fuchs © Geologische Bundesanstalt Wien, 2001

Sheet number 20 by G. Fuchs and E. Kupka © Geologische Bundesanstalt Wien, 1984

Geologische Karte Niederösterreich-Niederösterreich Nord by G. Fuchs, A. Matura, R. Roetzel and S. Scharbert © Geologische Bundesanstalt Wien, 2002

Literature

Anczkiewicz, R., Szczepánski, J., Mazur, S., Storey, C., Crowley, Q., Villa, I.M., Thirlwall, M.F. and Jeffries, T.E., 2007. Lu-Hf geochronology and trace element distribution in garnet: Implications for uplift and exhumation of ultra-high pressure granulites in the Sudetes, SW Poland. Lithos, v. 95, p. 363 – 380

Babuška, V. and Plomerová, J., 2013. Boundaries of mantle–lithosphere domains in the Bohemian Massif as extinct exhumation channels for high-pressure rocks. Gondwana Research, v. 23, p. 973 – 987

Büttner, S. and Kruhl, J.H., 1997. The evolution of a late-Variscan high-T/low-P region: the southeastern margin of the Bohemian massif. Geologische Rundschau, v. 86, p. 21 – 38

Carswell, D.A. and Jamtveit, B., 1990. Variscan Sm-Nd ages for the high-pressure metamorphism in the Moldanubian Zone of the Bohemian Massif, Lower Austria. Neues Jahrbuch für Mineralogie-Abhandlungen, v.162, issue 1, p. 69 – 78

Cooke, R.A., O'Brien, P.J. and Carswell, D.A., 2000. Garnet zoning and the identification of equilibrium mineral compositions in high-pressure-temperature granulites from the Moldanubian Zone, Austria. Journal of metamorphic Geology, v. 18, p. 551 – 569

Faryad, S.W., Nahodilová, R. and Dolejš, D., 2010. Incipient eclogite facies metamorphism in the Moldanubian granulites revealed by mineral inclusions in garnet. Lithos, v. 114, p. 54 – 69

Faryad, S.W., 2011. Distribution and Geological Position of High-/Ultrahigh-Pressure Units Within the European Variscan Belt: A Review. In: *Ultrahigh-Pressure Metamorphism: 25 Years After The Discovery Of Coesite And Diamond* (eds Dobrzhinetskaya, L., Faryad, S.W., Wallis, S. and Cuthbert, S.), p. 361 – 397, Elsevier

Faryad, S.W., Kachlík, V., Sláma, J. and Hoinkes, G., 2015. Implication of corona formation in a metatroctolite to the granulite facies overprint of HP-UHP rocks in the Moldanubian Zone (Bohemian Massif). Journal of Metamorphic Geology, v. 33, p. 295 – 310

Finger, F. and von Quadt, A, 1995. U/Pb ages of zircons from a plagiogranite-gneiss in the south-eastern Bohemian Massif, Austria – further evidence for an important early Paleozoic rifting episode in the eastern Variscides. Schweizerische Mineralogische und Petrographische Mitteilungen, v. 75, p. 265 – 270

Finger, F. and Steyrer, H. P., 1995. A tectonic model for the eastern Variscides: indications from a chemical study of amphibolites in the south-eastern Bohemian Massif. Geologica Carpathica, Bratislava, v. 46, issue 3, p. 137 – 150

Finger, F., Gerdes, A., Janoušek, V., René, M. and Riegler G., 2007. Resolving the Variscan evolution of the Moldanubian sector of the Bohemian Massif: the significance of the Bavarian and the Moravo-Moldanubian tectonometamorphic phases. Journal of Geosciences, v. 52, p. 9 – 28

Finger, F. and Schubert, G., 2015. Die Böhmische Masse in Österreich: Was gibt es Neues? Abhandlungen der Geologischen Bundesanstalt, Wien, Bd 64, p. 167 – 179

Franke, W., 2000. The mid-European segment of the Variscides; tectonostratigraphic units, terrane boundaries and plate tectonic evolution. In: Franke W, Haak V, Oncken O, Tanner D (eds) Orogenic processes: quantification and modelling in the Variscan Belt. Geol Soc Spec Publ, v. 179, p. 35 – 61

Franěk, J., Schulmann, K. and Lexa, O., 2006. Kinematic and rheological model of exhumation of high pressure granulites in the Variscan orogenic root: example of the Blanský les granulite, Bohemian Massif, Czech Republic. Mineralogy and Petrology, v. 86, p. 253 – 276

Friedl, G., von Quadt, A., Ochsner, A. and Finger F., 1993. Timing of the Variscan Orogeny in the Southern Bohemian Massif (NE-Austria) deduced from new U-Pb zircon and monazite dating. Terra Abstracts, v. 5, p. 235 – 236

Friedl, G., Finger, F., Paquette, J.-L., von Quadt, A., McNaughton, N.J. and Fletcher, I.R., 2004. Pre-Variscan geological events in the Austrian part of the Bohemian Massif deduced from the U-Pb zircon ages. International Journal of Earth Sciences, v.93, p. 802 – 823

Friedl, G., Cooke, R.A., Finger, F., McNaughton, N.J. and Fletcher, I.R., 2011. Timing of Variscan HP-HT metamorphism in the Moldanubian Zone of the Bohemian Massif: U-Pb SHRIMP dating on multiply zoned zircons from a granulite from the Dunkelsteiner Wald Massif, Lower Austria. Mineralogy and Petrology, v. 102, p. 63 – 75

Fritz, H. and Neubauer, F., 1993. Kinematics of crustal stacking and dispersion in the south-eastern Bohemian Massif. Geologische Rundschau, v. 82, p. 556 – 565

Fritz, H., 1994. The Raabs Series, a Variscan Ophiolite in the SE – Bohemian Massif: a key for the tectonic interpretation. Journal of the Czech Geological Society, 39/1, p. 32 – 33

Fritz, H., 1995. The Raabs Series: A Probable Variscan Suture in the SE Bohemian Massif. Jahrbuch der Geologischen Bundesanstalt, Wien, Bd. 138, Heft 4, p. 639 – 653

Fritz, H., Dallmeyer, R.D. and Neubauer, F., 1996. Thick-skinned versus thin-skinned thrusting: rheology controlled thrust propagation in the Variscan collisional belt (the southeastern Bohemian Massif, Czech Republic – Austria). Tectonics, v. 15, p. 1389 – 1413

Fritz, H., Tenczer, V., Hauzenberger, C. A., Wallbrecher, E., Hoinkes, G., Muhongo, S., and Mogessie, A., 2005. Central Tanzanian tectonic map: A step forward to decipher Proterozoic structural events in the East African Orogen. Tectonics, v. 24, TC6013, p. 1 – 26

Fuchs, G., 1976. Zur Entwicklung der Böhmischen Masse. Jahrbuch der Geologischen Bundesanstalt, v. 119, p. 45 – 61

Fuchs, G. and Matura, A., 1976. Zur Geologie des Kristallins der südlichen Böhmischen Masse. Jahrbuch der Geologischen Bundesanstalt, v. 119, p. 1 – 43

Fuchs, G. and Scharbert, H. G., 1979. Kleinere Granulitvorkommen im niederösterreichischen Moldanubikum und ihre Bedeutung für die Granulitgenese. Verh. Geol. B.-A., v. 2, p. 29 – 49

Fuchs, G., 1991. Das Bild der Böhmischen Masse im Umbruch. Jahrbuch der Geologischen Bundesanstalt, v. 134, p. 701 – 710

Fuchs, G., 2005. Der geologische Bau der Böhmischen Masse im Bereich des Strudengaus (Niederösterreich). Jahrbuch der Geologischen Bundesanstalt, v. 145, number 3+4, p. 283 – 291

Gebauer, D. and Friedl, G., 1994. A 1.38 Ga protolith age for the Dobra orthogneiss (Moldanubian zone of the southern Bohemian Massif, NE-Austria): Evidence from the ion-microprobe (SHRIMP) dating of zircon. J. Czech. Geol. Soc., v. 39/1, p. 34 – 35

Gerdes, A., Friedl, G., Parrish, R.R. and Finger, F., 2003. High-resolution geochronology of Variscan granite emplacement – the South Bohemian Batholith. Journal of the Czech Geological Society, v. 48, Issue 1-2, p. 53 – 54

Grasemann, B., Fritz, H. and Vannay, J.-C., 1999. Quantitative kinematic flow analysis from the Main Central Thrust Zone (NW-Himalaya, India): implications for a decelerating strain path and the extrusion of orogenic wedges. Journal of Structural Geology, v. 21, p. 837 – 853

Guy, A., Edel, J.-B., Schulmann, K., Tomek, C. and Lexa, O., 2011. A geophysical model of the Variscan orogenic root (Bohemian Massif): Implications for modern collisional orogens. Lithos, v. 124, p. 144 – 157

Hasalová, P., Schulmann, K., Lexa, O., Štípská, P., Hrouda, F., Ulrich, S., Haloda, J. and Týcová, P., 2008. Origin of migmatites by deformation-enhanced melt infiltration of orthogneiss: a new model based on quantitative microstructural analysis. Journal of metamorphic Geology, v. 26, p. 29 – 53

Holub, F.V., Cocherie, A. and Rossi, P., 1997. Radiometric dating of granitic rocks from the Central Bohemian Plutonic Complex (Czech Republic): constraints on the chronology of thermal and tectonic events along the Moldanubian-Barrandian boundary. Comptes Rendus de l'Académie des Sciences-Series IIA-Earth and Planetary Science,v. 325, number 1, p. 19 – 26

Janoušek, V., Wiegand, B. A. and Žák, J., 2010. Dating the onset of Variscan crustal exhumation in the core of the Bohemian Massif: new U-Pb single zircon ages from the high-K calc-alkaline granodiorites of the Blatná suite, Central Bohemian Plutonic Complex. Journal of the Geological Society, v. 167, p. 347 – 360

Kossmat, F., 1927 Gliederung des varistischen Gebirgsbaues. Abhandlungen des Sächsischen Geologischen Landesamtes, v.1, p. 1 – 39

Klötzli, U.S. and Parrish, R.R., 1996. Zircon U/Pb and Pb/Pb geochronology of the Rastenberg granodiorite, South Bohemian Massif, Austria. Mineralogy and Petrology, v. 58, Issue, 3, p. 197 – 214

Klötzli, U., Frank, W., Scharbert, S. and Thöni, M., 1999. Evolution of the SE Bohemian Massif Based on Geochronological Data – A Review. Jahrbuch der Geologischen Bundesanstalt, v. 141, Heft 4, p. 377 – 394

Košler, J., Konopásek, J., Sláma, J. and Vrána, S., 2014. U-Pb zircon provenance of Moldanubian metasediments in the Bohemian Massif. Journal of the Geological Society, London, v. 171, p. 83 – 95

Kotková, J., 2007. High-pressure granulites of the Bohemian Massif: recent advances and open questions. Journal of Geosciences, v. 52, p. 45 – 71

Kotková, J., Schaltegger, U. and Leichmann, J., 2010. Two types of ultrapotassic plutonic rocks in the Bohemian Massif – Coeval intrusions at different crustal levels. Lithos, v. 115, p. 163 – 176

Kroner, U. and Romer, R. L., 2013. Two plates – Many subduction zones: The Variscan orogeny reconsidered. Gondwana Research, v. 24, p. 298 – 329

Kruhl, J.H., 1996. Prism- and basal-plane parallel subgrain boundaries in quartz: a microstructural geothermobarometer. J. metamorphic Geol., v. 14, p. 581 – 589

Kruhl, J.H., 1998. Reply: Prism- and basal-plane parallel subgrain boundaries in quartz: a microstructural geothermometer. Journal of metamorphic Geology, v. 16, p. 141 – 146

Law, R.D., Searle, M.P. and Simpson, R.L., 2004. Strain, deformation temperatures and vorticity of flow at the top of the Greater Himalayan Slab, Everest Massif, Tibet. Journal of the Geological Society, v. 161, p. 305 – 320

Law, R.D., 2014. Deformation thermometry based on quartz c-axis fabrics and recrystallization microstructures: A review. Journal of Structural Geology, v. 66, p. 129 – 161

Mainprice, D., Bouchez, J.-L., Blumenfeld, P. and Tubià, J. M., 1986. Dominant c slip in naturally deformed quartz: Implications for dramatic plastic softening at high temperature. Geology, v. 14, p. 819 – 822

Matte, Ph., Maluski, H., Rajlich, P. and Franke, W., 1990. Terrane boundaries in the Bohemian Massif: Result of large-scale Variscan shearing. Tectonophysics, v. 177, p. 151 – 170

Neubauer, F. and Handler, R., 2000. Variscan orogeny in the Eastern Alps and Bohemian Massif: How do these units correlate? Mitt. Österr. Geol. Ges., v. 92, p. 35 – 59

Nance, R.D., Gutiérrez-Alonso, G., Keppie, J.D., Linnemann, U., Murphy, J.B., Quesada, C., Strachan, R.A. and Woodcock, N.H., 2009. Evolution of the Rheic Ocean. Gondwana Research, v. 17, 2-3, p. 194 – 222

O'Brien, P.J. and Carswell, D.A., 1993. Tectonometamorphic evolution of the Bohemian Massif: evidence from high pressure metamorphic rocks. International Journal of Earth Sciences, v. 82, Issue 3, p. 531 – 555

Okudaira, T., Takeshita, T. and Toriumi, M., 1998. Prism- and basal-plane parallel subgrain boundaries in quartz: a microstructural geothermobarometer. Journal of metamorphic Geology, v. 16, p. 141 – 146

Passchier, C.W. and Trouw, R.A.J., 2005. Microtectonics. Second edition, Springer-Verlag Berlin Heidelberg

Perraki, M. and Faryad, S.W., 2014. First finding of microdiamond, coesite and other UHP phases in felsic granulites in the Moldanubian Zone: Implications for deep subduction and revised geodynamic model for Variscan Orogeny in the Bohemian Massif. Lithos, v. 202 – 203, p. 157 – 166

Petrakakis, K., 1997. Evolution of Moldanubian rocks in Austria: review and synthesis. Journal of metamorphic Geology, v. 15, p. 203 – 222

Racek, M., Štípská, P., Pitra, P., Schulmann, K. and Lexa, O., 2006. Metamorphic record of burial and exhumation of orogenic lower and middle crust: a new tectonothermal model for the Drosendorf window (Bohemian Massif, Austria). Mineralogy and Petrology, v. 86, p. 221 – 251

Roberts, M.P. and Finger, F., 1997. Do U-Pb zircon ages from granulites reflect peak metamorphic conditions? Geology, v. 25, No. 4, p. 319 – 322

Schmid, S.M. and Casey, M., 1986. Complete Fabric Analysis of Some Commonly Observed Quartz C-Axis Patterns, in Mineral and Rock Deformation: Laboratory Studies: The Paterson Volume (eds B.E. Hobbs and H.C. Heard), American Geophysical Union

Schulmann, K., 1990. Fabric and kinematic study of the Bites orthogneiss (southwestern Moravia): result of large-scale northeastward shearing parallel to the Moldanubian/Moravian boundary. Tectonophysics, v. 177, p. 229 – 244

Schulmann, K., Lobkowicz, M., Melka, R. and Fritz, H., 1995. Structure of the allochthonous Moravo-Silesian units. In: Pre-Permian Geology of Central and Eastern Europe (eds Dallmeyer, R. D., Franke, W., and Weber, K.,), Springer, Berlin,p. 530 – 540

Schulmann, K., Kroner, A., Heger, E., Wendt, I., Konopásek, J., Lexa, O. and Stípská, P., 2005. Chronological constraints on the preorogenic history, burial and exhumation of deep-seated rocks along the eastern margin of the Variscan Orogen, Bohemian Massif, Czech Republic. Am. J. Sci. v. 305, p.407 – 448

Schulmann, K., Konopásek, J., Janoušek, V., Lexa, O., Lardeaux, J.-M., Edel, J.-B., Štípská, P. and Ulrich, S., 2009. An Andean type Palaeozoic convergence in the Bohemian Massif. C.R. Geoscience, v. 341, p. 266 – 286

Stampfli, G. M. and Borel, G.D., 2002. A plate tectonic model for the Paleozoic and Mesozoic constrained by dynamic plate boundaries and restored synthetic oceanic isochrons. Earth and Planetary Science Letters, v. 196, p. 17 – 33

Stampfli, G. M., von Raumer, J. and Wilhelm, C., 2011. The distribution of Gondwana-derived terranes in the early Paleozoic, in: eds: Gutiérrez-Marco, J.C., Rábano, I. and García-Bellido, D. (eds.), Ordovican World

Stipp, M., Stünitz, H., Heilbronner, R. and Schmid, S.M., 2002. The eastern Tonale fault zone: a 'natural laboratory' for crystal plastic deformation of quartz over a temperature range from 250 to 700°C. Journal of Structural Geology, v.24, p. 1861 – 1884

Verner, K., Žák, J., Nahodilová, R. and Holub, F.V., 2008. Magmatic fabrics and emplacement of the cone-sheet-bearing Knížecí Stolec durbachitic pluton (Moldanubian Unit, Bohemian Massif): implications for mid-crustal reworking of granulitic lower crust in the Central European Variscides. International Journal of Earth Sciences, v. 97, p. 19 – 33

Von Raumer, J.F., Finger, F., Veselá, P. and Stampfli, G., 2013. Durbachites-Vaugnerites – a geodynamic marker in the central European Variscan orogen. Terra Nova, v. 0, p. 1 – 11

Wilson, C.J.L., Russel-Head, D.S., Kunze, K. and Viola, G., 2007. The analysis of quartz c-axis fabrics using a modified optical microscope. Journal of Microscopy, v. 227, p. 30 – 41

Žák, J., Verner, K., Finger, F., Faryad, S.W., Chlupáčová, M. and Veselovský, F., 2011. The generation of voluminous S-type granites in the Moldanubian unit, Bohemian Massif, by rapid isothermal exhumation of the metapelitic middle crust. Lithos, v. 121, p. 25 – 40

Žák, J., Verner, K., Janoušek, V., Holub, F.V., Kachlík, V., Finger, F., Hajná, J., Tomek, F., Vondrovic, L. and Trubač, J., 2014. A plate-kinematic model for the assembly of the Bohemian Massif constrained by structural relationships around granitoide plutons. Geological Society of London, Special Publications, v. 405, p. 169 – 196

Appendix

List of samples

Sample	N Coordinates	E Coordinates	sf azimut	sf dip	Lst azim	Lst dip
G1	48°48´19´´	15°29´15´´	322	76	240	22
G2 (unten)	48°48´19´´	15°29´15´´				
G3	48°48´19´´	15°29´15´´	314	83	234	14
G4(unten)	48°48´05´´	15°29´10´´	165	88	254	16
	48°48´05´´	15°29´10´´	150	60		
	48°48´05´´	15°29´10´´	160	66		
	48°48´05´´	15°29´10´´	161	50		
	48°48´05´´	15°29´10´´	158	85	246	2
G5(unten)	48°48´02´´	15°29´06´´	318	72	234	6
	48°48´02´´	15°29´06´´	134	88	224	4
G6	48°48´02´´	15°29´06´´	149	69	63	7
G7	48°48´01´´	15°29´18´´	109	60	48	30
G8	48°48´01´´	15°29´18´´	138	50	228	2
	48°48´01´´	15°29´18´´	134	52	224	4
	48°48´01´´	15°29´18´´	158	66	198	65
G9	48°48´01´´	15°29´04´´	175	15	245	4
	48°48´01´´	15°29´04´´	153	72		
	48°48´01´´	15°29´04´´	158	82	242	10
	48°48´01´´	15°29´04´´	153	48	240	4
	48°47´53´´	15°29´01´´	152	50	68	9
	48°47´53´´	15°29´01´´	129	60	30	7
	48°47´53´´	15°29´01´´	188	74		
	48°47´53´´	15°29´01´´	190	65		
	48°47´53´´	15°29´01´´	130	55		
	48°47´53´´	15°29´01´´	160	65	70	5
	48°47´53´´	15°29´01´´	125	60		
	48°47´53´´	15°29´01´´	157	60		
G10	48°47´49´´	15°28´49´´	194	66	279	15
	48°47´49´´	15°28´49´´	200	80	282	5
	48°47´49´´	15°28´49´´	196	85		
	48°47´49´´	15°28´49´´	148	70		
	48°47´43´´	15°28´56´´	280	80	145	80
G11	48°47´38´´	15°28´54´´	179	65		
G12	48°47´32´´	15°28´43´´	180	20	278	10
	48°47´32´´	15°28´43´´	194	23	250	10
	48°47´32´´	15°28´43´´	189	25	240	8
	48°47´32´´	15°28´43´´	194	42	271	10
	48°47´25´´	15°28´36´´	171	55	257	1
	48°47´25´´	15°28´36´´	178	38	270	2
	48°47´25´´	15°28´36´´	186	56	271	16
G13	48°47´22´´	15°28´33´´	174	64	265	4
G14	48°47´15´´	15°28´30´´	140	60	54	20

G15	**48°47´15´´**	**15°28´30´´**	**162**	**61**	**75**	**14**
G16(unten)	**48°47´15´´**	**15°28´30´´**	**160**	**60**	**72**	**10**
G17(unten)	**48°47´15´´**	**15°28´30´´**	**200**	**67**		
	48°47´15´´	**15°28´30´´**	330	85	66	4
	48°47´15´´	**15°28´30´´**	2	56	82	10
	48°47´06´´	**15°28´37´´**	148	55		
	48°47´06´´	**15°28´37´´**	172	55	83	2
G18(unten)	**48°46´57´´**	**15°28´33´´**	**171**	**68**	**88**	**10**
	48°46´57´´	**15°28´33´´**	160	80		
G19	**48°46´56´´**	**15°28´23´´**	**160**	**87**	**242**	**3**
G20	**48°46´56´´**	**15°28´23´´**				
	48°46´56´´	**15°28´23´´**	161	68		
G21	**48°46´56´´**	**15°28´23´´**				
G22	**48°46´41´´**	**15°28´41´´**	**340**	**86**	**250**	**10**
G23	**48°46´41´´**	**15°28´41´´**	**320**	**70**	**230**	**4**
G24	**48°46´41´´**	**15°28´41´´**	**322**	**72**	**246**	**20**
G25	**48°46´41´´**	**15°28´41´´**				
G26	**48°46´41´´**	**15°28´41´´**				
G112	**48°46´41´´**	**15°28´41´´**	**356**	**74**		
G113	**48°46´41´´**	**15°28´41´´**	**179**	**80**		
G114	**48°46´41´´**	**15°28´41´´**	**160**	**85**		
G115	**48°46´41´´**	**15°28´41´´**	**164**	**74**		
G116	**48°46´41´´**	**15°28´41´´**				
G117	**48°46´41´´**	**15°28´41´´**	**355**	**50**		
G118(unten)	**48°46´41´´**	**15°28´41´´**	**132**	**75**		
	48°46´41´´	**15°28´41´´**	328	78	238	10
	48°46´41´´	**15°28´41´´**	348	78	261	10
G27	**48°46´39´´**	**15°28´45´´**				
G28	**48°46´39´´**	**15°28´45´´**	178	88		
G29	**48°46´39´´**	**15°28´45´´**				
G30	**48°46´39´´**	**15°28´45´´**				
G31(unten)	**48°46´39´´**	**15°28´45´´**				
G32	**48°46´39´´**	**15°28´45´´**				
G33	**48°46´39´´**	**15°28´45´´**				
	48°46´29´´	**15°28´43´´**	264	46		
	48°46´29´´	**15°28´43´´**	230	60		
G34	**48°46´22´´**	**15°29´04´´**	**192**	**87**	**285**	**15**
G35	**48°46´23´´**	**15°28´35´´**	**154**	**88**	**244**	**14**
	48°46´23´´	**15°28´35´´**	170	75	252	10
G36	**48°46´21´´**	**15°28´35´´**	156	90	250	7
G37	**48°46´31´´**	**15°28´27´´**	**353**	**78**	**262**	**6**
	48°46´31´´	**15°28´27´´**	178	78	88	2
	48°46´31´´	**15°28´27´´**	192	80	105	14
G38	**48°46´13´´**	**15°28´27´´**	**155**	**76**	**242**	**11**
	48°46´13´´	**15°28´27´´**	340	76	242	11
G39	**48°45´25´´**	**15°29´21´´**	**168**	**76**	**79**	**25**

G40	**48°45´25´´**	**15°29´21´´**				
G41	**48°45´25´´**	**15°29´21´´**	**52**	**75**	**146**	**9**
G42	**48°45´25´´**	**15°29´21´´**				
	48°45´25´´	**15°29´21´´**	199	58	282	10
	48°45´25´´	**15°29´21´´**	60	78		
	48°45´25´´	**15°29´21´´**	52	80	312	22
	48°45´25´´	**15°29´21´´**	162	80	68	25
G57	**48°45´25´´**	**15°29´21´´**	**70**	**15**	**132**	**7**
G58	**48°45´25´´**	**15°29´21´´**	**42**	**18**	**130**	**10**
G43	**48°44´45´´**	**15°21´15´´**	**9**	**38**	**328**	**31**
G44(unten)	**48°44´45´´**	**15°21´15´´**	**77**	**63**	**166**	**6**
G45	**48°44´45´´**	**15°21´15´´**	**25**	**60**		
G46	**48°44´45´´**	**15°21´15´´**	**62**	**60**		
G47(unten)	**48°44´45´´**	**15°21´15´´**	**46**	**44**	**340**	**25**
G48(unten)	**48°44´45´´**	**15°21´15´´**	**66**	**30**		
	48°44´45´´	**15°21´15´´**	62	48	134	17
	48°44´45´´	**15°21´15´´**	11	15	306	26
	48°44´45´´	**15°21´15´´**	62	48	134	17
	48°44´45´´	**15°21´15´´**	31	48	329	25
	48°44´45´´	**15°21´15´´**	24	50	310	16
	48°44´45´´	**15°21´15´´**	66	45	134	19
	48°44´45´´	**15°21´15´´**	19	50	295	5
	48°44´45´´	**15°21´15´´**	60	45		
G165	**48°44´45´´**	**15°21´15´´**				
G166	**48°44´45´´**	**15°21´15´´**				
G49	**48°44´28´´**	**15°21´20´´**	**20**	**16**	**293**	**2**
G50	**48°44´28´´**	**15°21´20´´**	**298**	**52**	**334**	**42**
	48°44´28´´	**15°21´20´´**	295	34	335	32
	48°44´28´´	**15°21´20´´**	290	34	330	27
	48°44´28´´	**15°21´20´´**	66	44		
G51	**48°44´06´´**	**15°20´50´´**	**104**	**55**	**28**	**10**
G52	**48°44´06´´**	**15°20´50´´**	**99**	**25**	**20**	**10**
G115	**48°44´06´´**	**15°20´50´´**	**340**	**54**	**28**	**40**
G126	**48°44´06´´**	**15°20´50´´**	**29**	**45**	**315**	**15**
G127	**48°44´06´´**	**15°20´50´´**	**32**	**45**	**310**	**8**
G128	**48°44´06´´**	**15°20´50´´**	**50**	**45**		
G53	**48°43´42´´**	**15°20´14´´**	**90**	**43**	**3**	**2**
G54	**48°43´42´´**	**15°20´14´´**	**60**	**68**	**344**	**32**
G104	**48°43´42´´**	**15°20´14´´**	**90**	**54**		
G105	**48°43´42´´**	**15°20´14´´**	**80**	**44**	**356**	**15**
G55(unten)	**48°44´02´´**	**15°20´59´´**	**85**	**55**	**305**	**2**
G56(unten)	**48°44´02´´**	**15°20´59´´**	**86**	**60**	**358**	**5**
G106	**48°44´02´´**	**15°20´59´´**	**68**	**38**		
G107(unten)	**48°44´02´´**	**15°20´59´´**	**79**	**44**		
	48°44´02´´	**15°20´59´´**	64	44	342	7
	48°44´02´´	**15°20´59´´**	88	42	10	6

143

	48°44′02″	15°20′59″	33	52	330	30
	48°44′02″	15°20′59″	35	55	170	17
	48°44′02″	15°20′59″	35	55	175	12
	48°44′02″	15°20′59″	70	62	60	58
	48°44′02″	15°20′59″	10	65	70	64
G59(unten)	48°43′55″	15°24′13″	360	60	74	48
G60(unten)	48°43′55″	15°24′13″	350	82	73	45
	48°43′55″	15°24′13″	15	60	66	40
	48°43′55″	15°24′13″	348	85		
G61(unten)	48°43′58″	15°29′16″				
G108	48°43′58″	15°29′16″				
G109	48°43′58″	15°29′16″				
G62	48°43′56″	15°29′08″				
G63(unten)	48°43′56″	15°29′08″	214	45		
G64(unten)	48°43′56″	15°29′08″	209	7		
G65	48°44′42″	15°29′27″				
G66	48°44′42″	15°29′27″				
G67	48°44′34″	15°29′43″	304	25	220	5
G68	48°44′34″	15°29′43″	295	25		
G69(unten)	48°45′25″	15°29′21″	282	60		
G70	48°45′25″	15°29′21″	40	88	316	20
	48°45′25″	15°29′21″	40	80		
	48°45′25″	15°29′21″	35	82		
	48°45′25″	15°29′21″	218	60		
	48°45′25″	15°29′21″	50	88		
G71	48°45′24″	15°29′19″	165	45		
G72	48°45′24″	15°29′19″	345	88	74	14
	48°45′24″	15°29′19″	130	84		
	48°45′24″	15°29′19″	344	82	262	2
G73	48°46′33″	15°25′37″	165	46		
G74	48°46′33″	15°25′37″	158	10		
G75	48°46′33″	15°25′37″				
G76	48°46′33″	15°25′37″				
G77	48°46′33″	15°25′37″				
G78(unten)	48°47′27″	15°24′43″	124	58		
G79	48°47′27″	15°24′43″	141	65	225	30
G80	48°47′27″	15°24′43″				
G81	48°47′27″	15°24′43″				
G82	48°47′27″	15°24′43″				
G83	48°47′27″	15°24′43″	134	72		
G84	48°47′27″	15°24′43″	130	85	44	20
G86	48°46′41″	15°24′30″	154	66	236	9
G87	48°46′41″	15°24′30″				
	48°46′41″	15°24′30″	145	70	60	5
G88(unten)	48°46′41″	15°24′30″	156	46		
G89	48°46′41″	15°24′30″	138	60		

G110(unten)	48°46′41′′	15°24′30′′	125	45		
G111	48°46′41′′	15°24′30′′	129	59		
G90	48°46′21′′	15°32′19′′	290	44	12	8
G91	48°46′21′′	15°32′19′′	291	42		
	48°46′21′′	15°32′19′′	290	50	19	3
	48°46′21′′	15°32′19′′	300	52	20	14
	48°46′21′′	15°32′19′′	280	46	22	2
G92	48°47′15′′	15°33′44′′				
G93(unten)	48°47′27′′	15°34′54′′	216	41		
G94	48°47′27′′	15°34′54′′	221	35		
G95	48°47′27′′	15°34′54′′	202	85	125	60
G119	48°47′16′′	15°34′29′′	150	44	223	15
	48°47′16′′	15°34′29′′	214	85	140	30
G96	48°47′16′′	15°34′29′′	335	75	271	48
G98	48°47′16′′	15°34′29′′	20	86	295	50
G100/101	48°47′16′′	15°34′29′′				
G102	48°47′16′′	15°34′29′′				
G103	48°47′16′′	15°34′29′′				
G120	48°47′16′′	15°34′29′′	227	25		
G121(unten)	48°47′16′′	15°34′29′′	163	33		
G122	48°47′16′′	15°34′29′′	230	35		
G123	48°47′16′′	15°34′29′′	348	84		
G124	48°47′16′′	15°34′29′′	230	57		
G162	48°47′22′′	15°35′00′′		242	27	
	48°47′22′′	15°35′00′′	240	30	240	30
G163	48°47′22′′	15°35′00′′	196	25		
G64	48°47′22′′	15°35′00′′	175	35		

Karlstein Schuppe

G129(unten)	48°52′44′′	15°24′28′′	264	45		
G130(unten)	48°52′35′′	15°24′27′′	262	32		
G131(unten)	48°52′35′′	15°24′27′′	260	42		
G132	48°52′32′′	15°24′22′′	292	50	226	24
G133(unten)	48°52′33′′	15°24′21′′	269	37		
G134	48°52′34′′	15°24′11′′	277	44	336	28
G135(unten)	48°52′34′′	15°24′11′′	184	40		
G136(unten)	48°52′34′′	15°24′11′′	280	44		
G137	48°52′34′′	15°24′11′′	291	50	356	27
G138	48°52′34′′	15°24′11′′	278	55		
G139	48°52′46′′	15°24′18′′	278	54		
G140	48°52′46′′	15°24′18′′	281	55		
G141	48°52′46′′	15°24′18′′	250	31		
G142	48°52′52′′	15°24′14′′	328	62		
G143	48°52′52′′	15°24′14′′	115	87		
G144	48°52′52′′	15°24′14′′	114	46	172	3

	48°52′52′′	15°24′14′′	10	85	107	50
	48°52′52′′	15°24′14′′	120	87	140	60
G145(unten)	48°52′55′′	15°24′12′′	296	84		
G146	48°52′55′′	15°24′12′′	124	88		
G147	48°52′57′′	15°24′15′′	308	38		
G148	48°50′07′′	15°23′39′′				
G14	48°50′03′′	15°23′40′′	278	54	5	2
G150(unten)	48°50′35′′	15°23′43′′		260	45	
G151	48°50′35′′	15°23′43′′	252	50		
G152	48°50′35′′	15°23′43′′	253	55	342	2
G153	48°50′35′′	15°23′43′′	264	55		
G154	48°50′35′′	15°23′43′′	266	54	188	12
G155	48°50′35′′	15°23′43′′				
G156	48°50′35′′	15°23′43′′				
G157(unten)	48°47′0335′′	15°23′05′′	88	70		
G158(unten)	48°47′0335′′	15°23′05′′	82	75		
G159	48°47′0335′′	15°23′05′′	104	72		
G160	48°47′0335′′	15°23′05′′	290	68	352	47
G161	48°47′0335′′	15°23′05′′	295	76	346	40

Raabs Serie

	48°50′27′′	15°30′01′′	205	15	205	15
	48°50′27′′	15°30′01′′	240	27	205	26
	48°50′27′′	15°30′01′′	245	28	206	27
	48°50′27′′	15°30′01′′	225	28	205	28
R51	48°50′27′′	15°30′01′′				
R52	48°50′27′′	15°30′01′′				
R53	48°50′27′′	15°30′01′′				
	48°50′04′′	15°30′12′′	280	25		
	48°50′04′′	15°30′12′′	284	34		
	48°50′04′′	15°30′12′′	280	50		
	48°49′43′′	15°29′51′′	296	30	230	10
R54	48°49′43′′	15°29′51′′	220	30		
	48°49′46′′	15°30′26′′	285	35		
R55(unten)	48°49′49′′	15°30′26′′	262	15		
R56(unten)	48°49′49′′	15°30′26′′	285	19		
R57	48°50′04′′	15°30′12′′	289	50		
R58(unten)	48°49′59′′	15°30′14′′	288	28		
R59)unten)	48°49′59′′	15°30′14′′	202	20		
R60	48°50′01′′	15°30′11′′				
R61	48°50′01′′	15°30′10′′	262	46		
R62	48°50′02′′	15°30′10′′	250	38		
R63	48°50′02′′	15°30′09′′				
R64	48°49′54′′	15°30′05′′	298	22		
R65	48°49′54′′	15°30′05′′	246	22		

	48°51´55´´	**15°28´23´´**	10	26	60	20
	48°51´55´´	**15°28´23´´**	20	20	70	15
R76	**48°51´55´´**	**15°28´23´´**	**45**	**25**		
R77(unten)	**48°51´55´´**	**15°28´23´´**	**62**	**20**		
R79(unten)	**48°52´48´´**	**15°28´56´´**	**10**	**28**		
R80	**48°52´48´´**	**15°28´56´´**			**268**	**20**
R81	**48°52´48´´**	**15°28´56´´**			**268**	**22**
R83	**48°52´54´´**	**15°29´00´´**	**358**	**20**		
R85(unten)	**48°52´03´´**	**15°28´50´´**	**350**	**34**		
	48°52´03´´	**15°28´50´´**	345	35		
	48°52´03´´	**15°28´50´´**	328	45		
R91(unten)	**48°52´03´´**	**15°28´50´´**	**88**	**16**		
	48°52´03´´	**15°28´50´´**	104	13	20	5
	48°52´03´´	**15°28´50´´**			45	2
	48°52´03´´	**15°28´50´´**			52	3
R92	**48°52´03´´**	**15°28´50´´**			61	2
R93(unten)	**48°52´03´´**	**15°28´50´´**	**42**	**15**		
R94(unten)	**48°52´03´´**	**15°28´50´´**	**98**	**10**		
R95	**48°52´03´´**	**15°28´50´´**				
R96	**48°52´03´´**	**15°28´50´´**	**132**	**24**		
R97	**48°52´03´´**	**15°28´50´´**	**142**	**15**		
	48°52´03´´	**15°28´50´´**			66	2
	48°52´03´´	**15°28´50´´**			72	6
	48°52´44´´	**15°28´44´´**	82	15	26	10
R101	**48°53´26´´**	**15°28´32´´**	331	48	250	4
R102(unten)	**48°53´26´´**	**15°28´32´´**	340	30		
	48°53´26´´	**15°28´32´´**	300	40	250	10
R104	**48°53´26´´**	**15°28´32´´**	322	26		
R105	**48°53´26´´**	**15°28´32´´**	360	20		
R108(unten)	**48°53´26´´**	**15°28´32´´**	322	45		
R110	**48°53´40´´**	**15°28´38´´**	2	26		
R111	**48°53´40´´**	**15°28´38´´**	329	22		
	48°53´40´´	**15°28´38´´**				
R120	**48°49´18´´**	**15°32´10´´**	**251**	**27**	**236**	**26**
	48°49´24´´	**15°32´11´´**	238	45	220	38
R121	**48°49´32´´**	**15°32´04´´**	**208**	**32**	**302**	**88**
	48°49´32´´	**15°32´04´´**	282	85	196	36
	48°49´32´´	**15°32´04´´**	112	85	198	35
R122(unten)	**48°49´33´´**	**15°32´12´´**	**238**	**48**	**306**	**45**
R123(unten)	**48°49´33´´**	**15°32´15´´**	**176**	**32**		
R124	**48°49´33´´**	**15°32´15´´**	**196**	**34**	**196**	**34**
	48°49´41´´	**15°33´11´´**	234	32	209	**27**
R125(unten)	**48°49´31´´**	**15°33´29´´**	**253**	**16**	**208**	**15**
R126(unten)	**48°49´33´´**	**15°33´39´´**	**243**	**40**		
R127	**48°49´33´´**	**15°33´39´´**	**255**	**55**		
B47	**48°49´33´´**	**15°33´39´´**	**360**	**60**		

R130	48°49´33´´	15°33´39´´	242	42			
R128(unten)	48°49´33´´	15°33´39´´	239	34			
B41	48°49´37´´	15°33´48´´	230	47	230	47	
B42(unten)	48°49´37´´	15°33´48´´	226	28			
B43	48°49´37´´	15°33´48´´	246	33			
B45(unten)	48°49´36´´	15°33´46´´	267	30			
B46(unten)	48°49´33´´	15°33´42´´	255	45			
	48°51´11´´	15°29´47´´					
R131	48°51´11´´	15°29´47´´	279	16			
R132	48°51´11´´	15°29´47´´	306	10			
R133(unten)	48°51´11´´	15°29´47´´	274	5			
R134(unten)	48°51´11´´	15°29´47´´	272	20			
R135(unten)	48°51´11´´	15°29´47´´	275	10			
R136	48°51´11´´	15°29´47´´					
R137(unten)	48°50´51´´	15°28´30´´	88	24			
R139(unten)	48°50´51´´	15°28´30´´	60	36			
R140	48°50´51´´	15°28´30´´					
R141	48°50´51´´	15°28´30´´		100	23		
R142	48°50´51´´	15°28´30´´	116	38			
R143(unten)	48°50´48´´	15°27´50´´	96	24			
R144(unten)	48°50´48´´	15°27´50´´	12	40			
	48°50´48´´	15°27´50´´	100	55	20	50	

ML-samples

sample	Coordinates N (WGS84)	Coordinates E (WGS84)	Lithology	Nappe system	sf_dipdir	sf_dip	L_dipdir	L_dip
ML 1	48,854483	15,576833	Biotit - Gneiss	Drosendorf Unit	225	28	180	40
ML 2	48,844133	15,578067	Quartzite	Drosendorf Unit	240	46	290	34
ML 3	48,82135	15,535483	Orthogneiss	Kollmitz-type Gneiss	235	66		
ML 4	48,87725	15,4086	Orthogneiss	Raabs Serie	274	52	190	5
ML 5	48,935717	15,398367	Granulite	Gföhler Gneiss	278	51	246	30
ML 6	48,935717	15,398367	Serpentinite	Gföhler Gneiss	300	25	30	10
ML 7	48,904817	15,443267	Orthogneiss	Gföhler Gneiss	292	20	252	10
ML 8	48,741233	15,3572	Mylonite	Mylonitzone	70	35	155	10
ML 9	48,741233	15,3572	Mylonite	Mylonitzone	85	70		
ML 10	48,741233	15,3572	Mylonite	Mylonitzone				
ML 11	48,741233	15,3572	Mylonite	Mylonitzone				
ML 12	48,741233	15,3572	Mylonite	Mylonitzone				
ML 13	48,828217	15,55705	Orthogneiss	Kollmitz-type Gneiss				
ML 14	48,830967	15,56425	Biotit Gneiss	Drosendorf Unit	220	40		
ML 15	48,831867	15,56547	Biotit Gneiss	Drosendorf Unit	228	40	250	30
ML 16	48,831867	15,56547	Quartzite	Drosendorf Unit	240	40	244	40
ML 17	48,84412	15,57822	Quartzite	Drosendorf Unit	250	40	292	40
ML 18	48,82992	15,53702	Orthogneiss	Kollmitz-type Gneiss				
ML 19	48,82992	15,53667	Orthogneiss	Kollmitz-type Gneiss	210	35	190	40
ML 20	48,82758	15,52917	Orthogneiss	Kollmitz-type Gneiss	224	30	220	30
Ml 21	48,82207	15,53217	Orthogneiss	Kollmitz-type Gneiss	250	40	200	20
ML 22	48,83644	15,39242	Granulite	Karlsteiner Schuppe				
ML 23	48,85258	15,498	Biotit Gneiss	Raabs Serie	204	15	200	12
ML 24	48,85172	15,497017	Biotit Gneiss	Raabs Serie	294	15	204	5
ML 25	48,85132	15,49602	Biotit Gneiss	Raabs Serie	150	15	130	10
ML 26	48,85132	15,49602	Biotit Gneiss	Raabs Serie	284	24	350	5